# DEVELOPING ION MOBILITY-MASS SPECTROMETRY TECHNIQUES TO INCREASE SENSITIVITY AND RESOLUTION FOR CARBOHYDRATE MIXTURE ANALYSIS

A Ph.D. Dissertation
Presented to
The Academic Faculty

by

Kristin R. McKenna

In Partial Fulfillment
of the Requirements for the Degree
Doctorate of Philosophy in the
School of Chemistry and Biochemistry

Georgia Institute of Technology
December 2021

# DEVELOPING ION MOBILITY-MASS SPECTROMETRY TECHNIQUES TO INCREASE SENSITIVITY AND RESOLUTION FOR CARBOHYDRATE MIXTURE ANALYSIS

Approved by:


Dr. Facundo M. Fernández, Advisor
School of Chemistry and Biochemistry
*Georgia Institute of Technology*

Dr. Charles Liotta
School of Chemistry and Biochemistry
*Georgia Institute of Technology*

Dr. Ronghu Wu
School of Chemistry and Biochemistry
*Georgia Institute of Technology*

Dr. Ramanarayanan Krishnamurthy
Department of Chemistry
*The Scripps Research Institute*

Dr. Amanda Stockton
School of Chemistry and Biochemistry
*Georgia Institute of Technology*



Date Approved: August 12, 2021

*Dedicated to my late grandmother and dear friend, Janet Martin*

**ACKNOWLEDGEMENTS**

I would like to start by expressing my gratitude my advisor, Dr. Facundo Fernández. Without his guidance and support, this thesis would not have been possible. Additionally, my committee members: Dr. Charlie Liotta, Dr. Ram Krishnamurthy, Dr. Amanda Stockton, and Dr. Ronghu Wu were instrumental in shaping my thesis research and giving me outside perspectives. Drs. Liotta and Krishnamurthy provided the organic chemistry and origins of life knowledge to ground the applications of my analytically-geared work, and Drs. Stockton and Wu helped direct the more analytical portions and gave insight from outside the field of origins of life chemistry. Several other members of the Center for Chemical Evolution were great supporters, collaborators, and mentors throughout my thesis research and concurrent outreach initiatives including Dr. Jay Forsythe, Dr. Chiamaka Obianyor, Dr. Christine Conwell, Shantel Floyd, Dr. Zhao Li, Dr. Li Li, and Christopher Parsons, Dr. Martha Grover, and Dr. Nick Hud. Throughout all of the Center and Polysaccharide subgroup meetings, I became a much better scientist and presenter from the feedback from these amazing people. Dr. Brian Clowers and Dr. Kelsey Morrison were instrumental in the development of the frequency modulated ion mobility methodology. Dr. Andy Baker from Waters Corp. was a very helpful collaborator who taught me the capabilities of the prototype cyclic ion mobility instrument.

Other members of the Fernández lab (both past and present) were always willing to help me when I ran into difficult problems that they are more experienced with, provide feedback on my presentations, or just discuss interesting science including Dr. Anyin Li, Dr. David Gaul, Dr. Danning Huang, Dr. Molly Hopper, Dr. Stephen Zambrzycki, Dr. Xiaoling Zang, Carter Asef, Markace Rainey, Alex Van Grouw, Dmitry Leontyev, Xin Ma, Samyukta Sah, Dr. Joel Keelor, Dr. Eric Parker, Eric Gier, and Dr. Scott Hogan. I truly appreciate the supportive environment everyone in the lab worked to create and uphold.

I would also like to thank my family and friends for their endless support. After a difficult day in lab, I could always rely on my mom, Karen, my dad, Reggie Sr., and my grandparents, Janet and Ken Martin for uplifting phone calls. My brothers, Ryan and Reggie Jr., Reggie's wife, Amanda, and their children, Tara and Reggie III were all great sources of laughs and connection. Aunt Kristina, Uncle Al, my cousins Anthony and Matthew, and their girlfriends Amanda and Alex have been amazingly supportive especially through the most difficult times. I would also like to thank my friends, Nicole and Beth Reynolds, Ashley Clarke, Julia Pinholster, Kathleen McDonald, Kylie Yao, Jesson Lim, Christopher Evangelista, Ted He, George Solter, Parag Kapadia, Becca Kruse, and especially my partner, Tori Lam, for all the support and good times throughout my graduate school experience.

**TABLE OF CONTENTS**

## LIST OF TABLES AND SCHEMES

Page

## LIST OF FIGURES

Page

## LIST OF SYMBOLS

| | |
|---|---|
| $k_b$ | Boltzmann constant |
| $e$ | Electron charge |
| $E$ | Electric field |
| $\mu$ | Reduced mass |
| $L$ | Length |
| $N$ | Number density of a gas |
| $V$ (kV, eV) | Voltage (kilovolts, electron volts) |
| Hz (kHz) | Hertz (kilohertz) |
| $[M+H]^+$ | Protonated Ion |
| $[M-H]^-$ | Deprotonated Ion |
| $K$ | Ion Mobility Coefficient |
| $M$ ($\mu M$, $mM$) | Molar concentration (micromolar, millimolar) |
| $m$ | Mass |
| $z$ | Charge |
| $R_p$ | Resolving power |
| $R_{pp}$ | Peak-to-peak resolution |
| $t_d$ | Drift time |
| $\Delta t_d$ | Full Width Half Maximum of the Drift Time |
| $\Omega$, CCS | Collision Cross Section |
| $^{13}C$ | Carbon-13 |
| $^{1}H$ | Hydrogen-1 |
| Å | Angstrom |
| Da | Dalton |

## LIST OF ABBREVIATIONS

| | |
|---|---|
| 3C5NBA | 3-carboxy-5-nitrophenylboronic acid |
| ATD | Arrival Time Distribution |
| BN gate | Bradbury-Nielsen gate |
| CE | Capillary Electrophoresis |
| CID | Collision Induced Dissociation |
| cIM | Cyclic Ion Mobility |
| DC | Direct Current |
| DTIM | Drift Tube Ion Mobility |
| ESI | Electrospray Ionization |
| FAIMS | High-Field Asymmetric Waveform Ion Mobility Spectrometry |
| FEP | Fluorinated Ethylene Propylene |
| FTIM | Fourier Transform Ion Mobility |
| FY | Fragment Ion Yield |
| HDMS | High Definition Mass Spectrometer |
| IM-MS | Ion Mobility-Mass Spectrometry |
| $IMS^n$ | Tandem Ion Mobility Spectrometry |
| LC (HPLC, UPLC) | Liquid Chromatography (High Performance, Ultra Performance) |
| MIT | Maximum Injection Time |
| MS | Mass Spectrometry |
| MS/MS | Tandem Mass Spectrometry |
| nESI | Nanoelectrospray Ionization |
| NMR | Nuclear Magnetic Resonance |
| PMP | 1-phenyl-3-methyl-5-pyrazolone |

| | |
|---|---|
| Q | Quadrupole Mass Spectrometer |
| RNA | Ribonucleic Acid |
| SNR | Signal-to-Noise Ratio |
| TENG | Triboelectric Nanogenerator |
| TOF MS | Time-of-Flight Mass Spectrometry |
| TWIMS | Traveling Wave Ion Mobility Spectrometry |

## SUMMARY

Carbohydrates are the most abundant class of biomolecules by mass with a diverse array of biological roles including cell wall structure,[1-2] adhesion and signaling of cells,[3-4] metabolism,[5-6] and protein modification.[7-8] They most likely played crucial roles in the origin of life, including their extant functions as well as assisting in the co-solubility of other biomolecules of differing polarities. Many analytical techniques have been applied for carbohydrate analysis, and ion mobility-tandem mass spectrometry is one of the most rapid and sensitive techniques available for these analyses.[9-12] Ion mobility separates ions in the gas phase by their collision cross section, which is related to the size, shape, and charge of the ion in addition to external factors, such as temperature and pressure. Mass spectrometry can be coupled to ion mobility to analyze the mass-to-charge ratio (*m/z*) of these ions.

The work presented in this thesis aims to apply ion mobility and/or tandem mass spectrometry for the analysis and characterization of model prebiotic carbohydrate polymerization reaction mixtures as well as mono- and disaccharide derivatives and noncovalent complexes. **Chapter 1** includes the introduction to the problems historically associated with carbohydrate isomer analysis, different types of ion mobility spectrometry, how these ion mobility-mass spectrometry methods can be applied to carbohydrate analysis, and how analytical methodology in the field of origins of life chemistry have developed over time. Some issues with carbohydrate analysis arise due to the large number of isobaric species, or molecules with the same *m/z* can be produced from a single monomer. This includes various regio- and stereoisomers. **Chapter 2** presents collaborative work in which tandem mass spectrometry was used to analyze model prebiotic glucose oligomerization reactions developed by Dr. Zhao Li and 3-carboxy-5-nitrophenylboronic acid (3C5NBA) mono- and disaccharide derivatives from a reaction developed by Dr. Li Li. Tandem mass spectrometry was used to identify the regio- and stereochemistry of the products of these reactions. In **Chapter 3**, the 3C5NBA derivatives analyzed in **Chapter 2** are further investigated using cyclic ion mobility-tandem mass spectrometry. Cyclic ion mobility-tandem

mass spectrometry distinguished all four monosaccharide and eight disaccharide isomers analyzed. Tandem ion mobility combined with tandem mass spectrometry allowed for even deeper structural characterization than tandem mass spectrometry alone.

Noncovalent shift reagents were used in place of covalent derivatization in **Chapter 4**. This is due to the nearly instantaneous timescale for binding that could be done either pre- or post-LC separation as well as the ability to bind to multiple oligomers with fewer products than the 3C5NBA derivatization reaction. Organic acids were used as noncovalent shift reagents, and a combination of L-malic acid and N-methyl-D-aspartic acid could be used to distinguish eight disaccharide isomers by their collision cross sections. However, this would not be applicable to very complex mixtures, so high resolution atmospheric pressure drift tube ion mobility was necessary. This improved separations at the cost of sensitivity. To solve this issue of low sensitivity, a Fourier transform-based frequency modulation ion mobility method was developed in **Chapter 5**. This method was analyzed for the optimal ion mobility and mass spectrometry parameters. This was followed by the conclusions that could be drawn from this work and potential future directions to advance the fields of carbohydrate analysis both in general and within the field of prebiotic chemistry in **Chapter 6**. **Appendix A** details the potential for triboelectric nanogenerator ionization to improve the sensitivity of carbohydrate analysis by ion mobility-mass spectrometry.

# CHAPTER 1. Carbohydrate Analysis by Ion Mobility Spectrometry

## 1.1. Abstract

Emerging technologies within the field of ion mobility-mass spectrometry have been applied to carbohydrates to distinguish isomeric species. There are a high number of isobaric species possible for different lengths of oligo- and polysaccharides, with various monosaccharides able to form different regio- and stereoisomers. Mass spectrometry analysis of carbohydrates has historically been hindered by the low ionization efficiency of this class of molecules. This effect is lessened by nanoelectrospray when compared to traditional (micro)electrospray. Advancements in ion mobility techniques have also improved the potential to analyze isobaric carbohydrates. These advancements include cyclic ion mobility spectrometry that increases the path length of the ion mobility cell to be tailored to the analytes. Additionally, atmospheric drift tube ion mobility, which has high resolving power as an ion mobility technique, has been altered with various types of multiplexing techniques to alleviate the historically low sensitivity of the technique. These advanced analytical methods have been applied to more efficiently and accurately identify model prebiotic reaction products, including both protein analogs and carbohydrates.

## 1.2. Carbohydrate Isomer Analysis

Carbohydrates are the most abundant class of biomolecules on Earth by mass and are ubiquitous across all known forms of life. There is a diverse array of structure and functions within this class of molecules. The roles of carbohydrates include involvement in metabolic processes,[5] protein modification,[4, 7-8] and cell wall structures.[1] In conjunction with these diverse functions, sugars have a large array of potential structures. This included different lengths of oligo- and polysaccharides, which would have different mass-to-charge ratios (*m/z*) and be differentiated by mass spectrometry. However, within one *m/z*, there are many possible isobaric carbohydrate structures with varying regio- and stereochemistry as well as different monomeric unit composition.

There have been many analytical methods developed for the analysis of isobaric carbohydrates including nuclear magnetic resonance (NMR) spectroscopy, tandem mass spectrometry, liquid chromatography, and capillary electrophoresis. Many analytical methods have been developed for oligosaccharide characterization. Liquid chromatography (LC), for example, has been extensively used for oligosaccharide separations, with its major advantages being high specificity for derivatized carbohydrates and the capability to perform quantitative analysis.[13-15] LC can be used in conjunction with tandem mass spectrometry (MS/MS) to further increase specificity with similar or lower experiment times. MS/MS can also be used as a standalone technique to decrease the time required to analyze oligosaccharides, as MS/MS does not rely as heavily on derivatization and is much faster than LC. While MS/MS can efficiently distinguish relatively pure disaccharide samples, it can have limited success for the characterization of lower abundance components in complex mixtures of isobaric carbohydrates due to precursor ion co-selection, requiring additional information from another complementary technique such as NMR spectroscopy or LC for full characterization of these complex mixtures.[16-17]

### 1.3. Ionization of Carbohydrates for Ion Mobility and Mass Spectrometric Analyses

#### *1.3.1. Electrospray Ionization*

Electrospray ionization (ESI) of neutral carbohydrates has historically been diminished by ionization suppression due to the low ionization efficiency of this class of biomolecules.[18] This generally necessitates derivatization reactions, chromatographic separations, or both for the analysis of complex oligosaccharide mixtures. In negative mode ESI, oligosaccharides are often detected as their $[M-H]^-$ ions or depending on the other components of the solution, as adducts of chloride, nitrite, or other ions. In particular, chloride and nitrite adducts were found to be more stable than the $[M-H]^-$ ions by Harvey *et al.* and producing around twice the signal detected.[19] In positive mode, oligosaccharides are generally detected as their $[M+Na]^+$ ions. The formation of $[M+Na]^+$ ions occurs at high cone voltages, which can

cause in source fragmentation, so these two factors must be balanced.[19] Longer chains of oligosaccharides tend to ionize less well and are thereby more difficult to detect.[20] This effect is lessened when using nanoelectrospray (nESI) instead of standard microelectrospray.[21-22]

### *1.3.2. Triboelectric Nanogenerator Ionization*

Across all IM-MS techniques, carbohydrate analysis is made more difficult by the low ionization yields of this class of molecules.[23-24] A systematic study of ESI and triboelectric nanogenerator (TENG) ionization, a technique that was first reported as an ion source for MS by Li *et al.* in 2017,[25] is necessary to attempt to address this problem. TENG involves the use of two electrodes with mechanical motion of another triboelectric layer to generate charge, which can be applied through an electrode in a sample solution to ionize molecules for MS analysis.[25] TENG has previously been shown to have unique properties relative to ESI and nESI, including the promotion of oxidation reactions for lipid bonds[26] and nanoliter sample volume requirements.[27] Ionization suppression has not yet been systematically investigated for a TENG ion source, so in addition to the knowledge of carbohydrate ion suppression gained, this work will further characterize TENG ion sources in general.

## 1.4.Ion Mobility Spectrometry Separations

Ion mobility spectrometry- first developed as "plasma chromatography" by Cohen *et al.*- involves the gas-phase separations of ions under an electric field in a neutral buffer gas.[28] There are several types of ion mobility, two of which will be involved in this thesis work- drift tube ion mobility and traveling wave ion mobility. Ion mobility techniques generally separate ions on the basis of their collision cross section (CCS or Ω), a two-dimensional projection of the three-dimensional ion related to the size, shape, and compactness of the ion as well as the buffer gas used and external factors such as the temperature (T) and pressure (P) of the experiment. The equation below describes Ω for a drift tube ion mobility experiment with a constant electric field, where *z* represents the charge of the ion, *e*

is the charge of a single electron, $k_b$ is Boltzmann's constant, $E$ is the electric field strength, $t_d$ represents the drift time of the ion, $L$ is the length of the drift cell, and $\mu$ is the reduced mass of the ion and the buffer gas.

$$\Omega\ (\text{Å}^2) = \left(\frac{760}{P}\right)\left(\frac{273}{T}\right)\frac{(18\pi)^{1/2}}{16N}\frac{ze}{(k_bT)^{1/2}}\frac{E * t_d}{L * \mu^{1/2}}$$

### *1.4.1. Drift Tube Ion Mobility*

Atmospheric pressure drift tube ion mobility-mass spectrometry (DTIM-MS) of oligosaccharides offers a relatively high resolving power,[29] but generally suffers from low duty cycle, defined as the ratio of ions detected to those produced in the source. This occurs because ions can only pass through when the gates are open, and to have reasonably useful resolution, the gates will each be open for approximately 1% of the duration of each scan. Therefore, ions that pass through both gates will only be approximately 0.01% of the ions produced. In order to reach the necessary sensitivity for the analysis of realistic mixtures, some type of IM multiplexing approach is often necessary to increase duty cycle.

Ion mobility multiplexing involves simultaneously collecting multiple signals that must be deconvoluted in order to obtain an arrival time distribution (ATD). One of the most popular forms of IM multiplexing is based on Hadamard schemes.[30-33] This approach involves pulsing the gate of the drift tube following a pseudorandom sequence and subsequently using the Hadamard transform to obtain the ATD from the raw data.[30, 34] A demonstrated drawback of Hadamard-based IM methods, however, is that they can produce echoes and artifacts that diminish signal-to-noise ratio (SNR) gains, even with the application of algorithms developed to ameliorate this issue.[33, 35]

An alternative approach to ion mobility multiplexing is frequency modulation-based Fourier transform IM (FTIM). This technique involves synchronously opening and closing two ion gates bracketing the IM drift region using a square wave with a linearly increasing frequency. FTIM was first implemented on a standalone IM instrument by Knorr *et al.*[36] and it has been coupled with time-of-flight

(TOF) MS,[37] ion trap MS,[38] and Orbitrap MS.[39] FTIM-Orbitrap MS has been applied to native protein analysis,[39] but its performance for carbohydrate analysis has not yet been characterized in depth.

### *1.4.2. Traveling Wave Ion Mobility*

Traveling wave IM spectrometry (TWIMS) is an IM technique in which the mobility separator is comprised of a series of electrodes enclosed in a gas filled cell. This technique was commercialized by Waters Corporation in 2007 with the Synapt series of TWIM-mass spectrometers.[40] A series of voltage pulses is applied sequentially to each electrode, propelling ions through the device.[41] Ions can "surf" or "roll over" the wave falling back into the preceding wave. Ions of lower mobility undergo more roll over events than higher mobility ions, effectively leading to mobility separation. Drift times ($t_d$) measured in TWIMS can be converted to collision cross section (CCS) using calibration procedures.[42-44] A number of calibrant compounds have been proposed.[45]

### *1.4.3. Cyclic Traveling Wave Ion Mobility*

Since resolving power ($R_p$) of an IM separator can be improved by increasing its length,[46] traveling wave ion mobility has been improved upon by increasing the length of the IM cell. In 2017, Giles *et al.* developed a traveling wave-enabled, cyclic IM (cIM) instrument with multi-pass capabilities.[47] In this instrument, IM resolving power increases as a function of the square root of the number of passes, *n* ($\boldsymbol{R_p \sim 70\sqrt{nz}}$);[47] here 70 is the approximate, single pass resolving power and z is the ion's charge state. Normally, the maximum number of passes is limited by the so called "wrap-around" effect that occurs when the spatial width of the separated ion packets exceeds the length of the cIM device.[48] The cIM control enables selective ejection of ions in a specified range of arrival times from the cIM device that can be followed by activation and/or further separation of product ions ($IMS^n$).[48-49] These functionalities have been used previously for structural studies of carbohydrate[49-50] and protein ions.[51]

Isomeric pentasaccharides, including anomers, have been shown to be able to be separated by the cIM system.[49] Typically, isobaric mono- and disaccharides do not have sufficiently-different CCS values to be separated by commercially-available IM systems. To mitigate this issue, shift reagents — ligands that can bind either covalently or non-covalently to amplify CCS differences between isobaric carbohydrates — have been utilized. Previous examples of shift reagents include alkali and alkaline earth metal cations, and 1-phenyl-3-methyl-5-pyrazolone.[11-12, 52] In recent work, we reported a new shift reagent for carbohydrates, 3-carboxy-5-nitrophenyl boronic acid (3C5NBA) that rapidly reacts with mono- and disaccharides, enhancing their IM separation.[53] Due to the initial promise shown by 3C5NBA, we here evaluate its applicability in combination with high-resolution cIM-MS instrumentation. In addition, we utilized the tandem IMS ($IMS^2$) capability to probe the possibility of interconversion between mobility separated mannose derivatives.

### *1.4.4. Applications of Ion Mobility for Carbohydrate Analysis*

IM is an emerging technique in the field of carbohydrate separations. A study by Williams *et al.*, for example, compared the characterization of sodiated *N*-glycans by DTIM and TWIM-MS with theoretical modelling to investigate the gas-phase properties and conformations of those glycans.[54] Additionally, Morrison *et al*. utilized DTIM-MS/MS to partially resolve five tetrasaccharide isomers as their adducts with several metal cations.[9] Disaccharide isomers are generally much more difficult to separate by IM due to their smaller differences in CCS.[11-12, 55] This creates the need to utilize shift reagents and high-resolution IM in order to successfully distinguish them. Shift reagents are ligands that can covalently or noncovalently modify analytes to amplify their gas-phase CCS differences. The mobility of the analyte is thus “shifted” to less crowded areas of the analytical space, preventing overlaps and interferences. Previously reported shift reagents for disaccharide IM separations include alkali[11] and alkaline earth metal cations,[12,

[54] 1-phenyl-3-methyl-5-pyrazolone,[52] and 3-carboxy-5-nitrophenylboronic acid.[53, 56] Amino acids have previously been shown to have some promise for complexing with monosaccharide isomers to improve separations by Gaye *et al.*[57]

### 1.5. Analytical Methods in the Field of Prebiotic Chemistry

Various analytical techniques have been applied within the field of prebiotic chemistry and the related field of astrochemistry, beginning with paper chromatography with ninhydrin detection for the Miller-Urey experiment in 1953 to analyze amino acid products of a spark discharge reaction mimicking the conditions on the prebiotic Earth.[58] With this technique, only six amino acid products were identified: glycine, alanine, β-alanine, aspartic acid, glutamic acid, α-amino butyric acid, and sarcosine. After this and some related experiments in the 1950s all analyzed by paper chromatography and gravity-driven chromatography with large columns, HPLC instrumentation was developed and, along with fluorescence detection, was applied to derivatized amino acids in a samples from a meteor[59] and the Cretaceous/Tertiary boundary of the Earth's crust.[60] Subsequently, in the 2000s, ultra performance liquid chromatography (UPLC) was developed, which has particles around one third the size of those for HPLC and shorter column lengths.[61] UPLC is often coupled to MS detection for amino acid detection and quantitation, with applications including meteorite analysis.[62] One such meteorite analysis, by Glavin and Dworkin, determined that there was an L-enantiomer enrichment for isovaline on the meterorite Murchison.[62] In addition to amino acids, other organic molecules essential for the origin of life have been studied by UPLC-MS, notably including nucleobases. In a meteorite study, Callahan *et al.* developed a UPLC-MS method for the detection of nucleobases and nucleobase analogs.[63] Three canonical nucleobases: cytosine, guanine, and adenine, were detected in addition to several analogs.

Several samples of Stanley Miller's original experiments were re-analyzed by UPLC in the 2000s and 2010s to gain a more complete view of the spark discharge reaction products than the original paper chromatography analysis could provide. UPLC-MS is both more sensitive and has a

higher separation power than paper chromatography, leading to the identification of more compounds in these product mixtures.[61] By paper chromatography, 7 species were detected: 5 identified amino acids and two unidentified compounds. In 2008, Johnson *et al.*[64] identified 14 amino acids and 5 amines from one of Miller's original samples analyzed by an HPLC-MS method based on that from Glavin and Dworkin.[62] For an altered version of his original experiment, Miller also performed a volcanic spark reaction,[58] in which he detected 5 amino acids, the UPLC-MS analysis by Johnson *et al.* revealed 22 amino acids and 5 amines as products.[64] Another alteration Miller made to his original experiment, deemed the silent discharge reaction, was also found to produce 5 amino acids by paper chromatography[58] and UPLC-MS analysis was able to detect 11 amino acids and an amine.[64]

Model prebiotic polymerization reactions have required the development of novel analytical techniques as well as the application of modern standard analytical techniques. For example, amino acids have been found to polymerize well with a mixture of α-hydroxy acids, and these hybrid products, called depsipeptides, were analyzed by Forsythe *et al.* by UPLC-IM-MS/MS with a custom workup due to their differences from standard peptides and proteins.[65] In terms of carbohydrates, NMR spectroscopy and MS/MS were used to study glucose polymerization reactions and determine the major regiochemistry was a 1→6 linkage.[66] In order to more efficiently and accurately identify complex mixtures of carbohydrates, current work focuses on adding IM separations to this workflow.

# CHAPTER 2. Tandem mass spectrometry to identify model prebiotic carbohydrate mixtures and derivatives

*Adapted from*

Li, L.; McKenna, K. R.; Li, Z.; Yadav, M.; Krishnamurthy, R.; Liotta, C. L.; Fernández, F. M. *Analyst*, **2018**, *143*, 949-955. K.R. McKenna performed IM comparison of 3C5NBA adducts to chloride adducts and MS/MS analysis of 3C5NBA derivatives.

Li, Z.; Li, L.; McKenna, K. R.; Schmidt, M.; Pollet, P.; Gelbaum, L.; Fernández, F. M.; Krishnamurthy, R.; Liotta, C. L. *Orig. Life Evol. Biosph.* **2019,** *49*, 225-240. K.R. McKenna performed MS/MS analysis of the products of the glucose oligomerization reaction.



## 2.1. Abstract

Tandem mass spectrometry (MS/MS) involves the selection of precursor ions by *m/z* followed by fragmentation and detection of the product ions. MS/MS has been extensively applied for the identification of oligo- and polysaccharides with variable success depending upon factors such as mixture complexity and the presence (or absence) of a pre-MS separation method. Here. MS/MS was applied to study the products of acid-catalyzed glucose polymerization reactions designed to mimic potential prebiotic reactions. These results complemented NMR spectroscopy acquired by others to determine the regio- and stereochemistry of these oligosaccharide products. Additionally, MS/MS was used to study the 3-carboxy-5-nitrophenylboronic acid (3C5NBA) derivatives of mono- and disaccharides to characterize the products of the derivatization reaction and identify unique fragments formed by any of the derivatives. In conjunction with IM data, MS/MS could distinguish six out of eight of the 3C5NBA disaccharide derivatives.

## 2.2. Introduction

Monosaccharides and disaccharides play essential roles in all life on earth.[1, 4-5, 7-8] D-glucose, D-galactose, D-mannose and D-fructose serve not only as the basic building blocks of polysaccharides important in energy storage and structural support, but are also involved in post-translational modifications to proteins.[67] Disaccharides are stable, naturally abundant, and can have important biological functions. For example, maltose and cellobiose are common energy storage molecules in plants.[68] Sugars and their oligomers are an important class of biomolecules playing central roles in extant biology. These roles range from participating in metabolic pathways at the monomeric level, to serving as energy-storage units and structural scaffolds in polymers such as cellulose, starch and glycogen.[69] Polysaccharides are one of the three major classes of biopolymers, with the other two being proteins and nucleic acids.[69] While the chemical origins of protein and nucleic acids such as ribonucleic acid (RNA) have been intensely investigated both theoretically and experimentally, oligosaccharides, on the other hand, have received almost no attention except for a small number of review articles and proposals.[70-71] Most of the prebiotic chemistry research involving sugars has been largely limited to the origin of ribose as a building block, and its role as one of the structural units of RNA.[72] Although the formose reaction clearly produces a plethora of hexose and ketose sugars,[73-74] uncertainty regarding the roles of the corresponding oligomers in the origins of life seems to have resulted in their almost complete neglect, with the exception of systematic investigations in chemical etiology of nucleic acid structure by Eschenmoser[75], and studies by Weber in the context of the 'sugar model'.[76]

Given the many possibilities for prebiotic sources and pathways that could produce monosaccharides,[76-80] it was hypothesized that a simple wet-dry cycling reaction[81] of these monosaccharide mixtures mimicking the day-night temperature variations on early earth could produce oligosaccharides. In order to investigate this possibility, we chose glucose as a model compound because it is both one of the most abundant sugars in extant biology[69] and a major

product of the formose reaction.[82] Here, we demonstrate that glucose does indeed condense under model prebiotic (acid catalyzed) conditions driven by cool-wet/hot-dry cycles[83-85] to form oligosaccharides containing up to eight monomeric units (Figure 2.1).

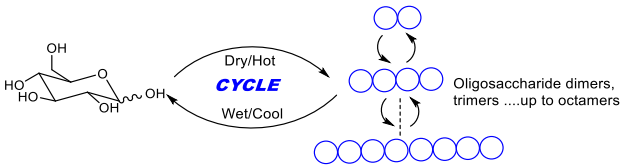


**Figure 2.1.** An illustration of oligosaccharide formation by an acid catalyzed wet/cool-dry/hot cycling reaction of D-(+)-glucose. Each blue circle represents a glucose residue.

Carbohydrate polymers have been also hypothesized to have played a central role in the origin of life in terms of a potential pre-RNA carbohydrate polymer world.[86] In this early-earth scenario, sugar mixtures would have been expected to be highly complex based on the number of glycosidic linkages that can be theoretically formed between any of the non-anomeric hydroxyl groups with either an α- or β-stereochemistry at the anomeric center. Chemical analysis of such complex-mixtures, even at the disaccharide level, would present a major analytical challenge, given the plethora of regio- and stereoisomers that can be formed.

Ion mobility-mass spectrometry (IM-MS) techniques are better suited than mass spectrometry (MS) alone for analysing oligosaccharide mixtures, as they offer the possibility of distinguishing molecular species based on both their molecular shape and their mass-to-charge ratio in the gas phase on the scale of milliseconds. An emerging body of work has shown that IM-MS can be a promising tool to probe carbohydrate linkage, composition, and configuration.[87-89] However, IM-MS separation of small sugar species with similar collision cross sections (CCS), such as mono- and disaccharides, has proved challenging, as the resolving power of the most commonly available commercial instruments is in the range of 40-70.[90-91] Previously reported IM modifications, such as manipulating the electric field in drift tube IM[92] or modifying drift gas

composition,[93] has only provided limited improvements. Labelling of sugar analytes yields amplified differences in CCS, potentially resulting in better resolution for any given IM instrument type. Noncovalent modification by alkali and alkaline earth cations,[94-95] heavy metal acetate ions,[96] chloride and acetate ions,[97] and 1-phenyl-3-methyl-5-pyrazolone (PMP) covalent-labeling[98] have all been shown to improve IM-MS detection and resolution in the literature with varying degrees of success. However, the separations achieved in each of these studies could still be much improved.

Generally, covalently labelling sugars yields more robust, reproducible, and quantitative results for both precursor and product ions in both MS and MS/MS experiments. Suitable labelling reagents must have high selectivity, reactivity, and efficiency under mild, non-destructive conditions. However, many previously-reported labelling reagents do not satisfy all of these criteria. For example, PMP labelling requires reaction at a high temperature (70 $^{o}$C) for several hours.[98] Covalent labelling of sugars with ferrocene boronic acid and 4[(2',6'-diisopropylphenoxy) methyl] phenyl-boronic acid requires organic solvents to dissolve the reagent and a basic pH (7.5-9.0) to allow the reaction to proceed.[99] Sugars, especially monosaccharides, are particularly sensitive to temperature, pH, and solvent composition, all of which can cause isomerization or decomposition prior to detection.[100-101] Progress in this field would greatly benefit from a gentler, aqueous method for covalent derivatization to improve IM-MS detection and identification of mono- and disaccharides.

Here, we report that a commercially-available boronic acid reagent, 3-carboxy-5-nitrophenylboronic acid (3C5NBA), provides facile multi-site derivatization of sugars in aqueous solution at room temperature and unadjusted pH. This reagent, 3C5NBA, bears a carboxylic acid group that aids sugar ionization in negative ion mode and a nitro group that greatly enhances derivatization rate and pH tolerance.[102-103] Derivatization produces isomers with unique CCS

values for each mono- and disaccharide, due to the different possible reaction sites, producing arrival time distributions (ATDs) with distinct patterns. Derivatization with 3C5NBA provides, to our knowledge, the best ion mobility separation of simple sugars reported so far in the literature.

## 2.3. Experimental

### *2.3.1. Materials and Reagents*

Maltose, lactose, lactulose, sucrose, D-(+)-glucose, D-(+) galactose were obtained from Sigma Aldrich (St. Louis, MO). Melibiose was purchased from Fluka, D-mannose was purchased from VWR. Isomaltose, trehalose, cellobiose, D-fructose and the derivatization reagent 3-carboxy-5-nitrophenylboronic acid (3C5NBA) were obtained from TCI (Philadelphia, PA).

### *2.3.2. Polymerization Reactions*

Glucose and glucose disaccharides were oligomerized by Dr. Zhao Li as follows: A 6-dram 22-ml clear glass vial containing 6 mmol (1.081 g) of glucose and 3 mL of 0.01 M HCl (pH = 2) was sonicated at room temperature until the mixture became homogeneous and subsequently heated to 50 $^{o}$C for 7 days in an open vessel. After 7 days, most of the water and essentially all the aqueous HCl had evaporated leaving a viscous residue, which marked the end of the first cycle. A sample of this residue was dissolved in deionized water and analyzed by MS and $^{1}$H and $^{13}$C NMR. Aqueous HCl (0.01 M, 3 mL) was then added to the top of the residue without stirring or shaking. The reaction vessel stood at room temperature for 4-6 hours before it was dried at 50 $^{o}$C for 7 days to complete the second cycle. This procedure was followed for subsequent cycles. Spectral analyses were conducted after each cycle.

### *2.3.3. Mass Spectrometry for Glucose Polymerization Reactions*

Reaction mixtures were diluted in deionized water and directly infused into a Waters SYNAPT G2-S High Definition MS (HDMS) system using electrospray ionization in negative ion mode. Instrument settings were as follows: capillary voltage, 2.0 kV; cone voltage, 30 V; extraction cone voltage, 3.0 V; source temperature, 100 °C; desolvation temperature, 350 °C; cone gas flow, 20.0 L $h^{-1}$; desolvation gas flow 650 L $h^{-1}$; source gas flow, 1.00 mL $min^{-1}$; trap gas flow, 2.0 mL $min^{-1}$; He cell gas flow, 180.0 mL $min^{-1}$; TOF resolution mode (m/Δm= 20,000). For MS/MS experiments, argon was used as the collision gas. The collision energy was set at different values for different precursor ions in the range of 25-40 V. For samples without hydrochloric acid, 2 µL $NH_4Cl$ was added for each mL of sample to enhance ionization efficiency immediately prior to analysis. Monomeric or oligomeric sugars ion species were predominantly detected as their corresponding $[M+Cl]^-$ adducts, with $[M-H]^-$ species detected at a lower abundance.

### *2.3.4. 3C5NBA Derivatization Reactions*

The following methods were developed by Dr. Li Li: Stock solutions of carbohydrate standards (1 mM) were prepared in water. A 1 mM 3C5NBA stock solution was prepared in acetonitrile. This solution was stable for weeks at room temperature. 5 µL of the carbohydrate solution were mixed with 10 µL 3C5NBA in a 1:2 molar ratio and incubated at room temperature for 5 minutes (for disaccharides), or 30 minutes (for monosaccharides), before dilution to 1 mL with deionized water and analysis by IM-MS. A 2 µL of a 0.5% $NH_4Cl$ solution was added to 1 mL of each underivatized sugar standard (5 µM) to favor the formation of chloride adducts to enhance ionization, where applicable.

### *2.3.5. Mass Spectrometry for 3C5NBA Derivatives*

All drift time measurements were performed using a Waters Synapt G2 HDMS ion-mobility mass spectrometer (Waters Corp., Milford, MA) in negative ion mode. Nitrogen was

used as the buffer gas. Ion mobility parameters were optimized to achieve maximum resolution and sensitivity: capillary voltage, 2.8 kV; cone voltage, 40 V; extraction cone voltage, 5.0 V; source temperature, 80 °C; desolvation temperature 150 °C; IMS wave velocity, 500 m $s^{-1}$; IMS wave amplitude, 40 V; transfer wave velocity, 190 $ms^{-1}$; transfer wave amplitude, 4.0 V; trap gas flow, 2 mL $min^{-1}$; helium cell gas flow, 180 mL $min^{-1}$; TOF resolution mode (m/Δm = 20,000). The cone voltage was set to 100 V to eliminate unnecessary non-covalent adduct ion clusters from 3C5NBA at *m/z* 403 and *m/z* 596. For MS/MS experiments, the ions of interest were quadrupole-selected and fragmented in the transfer region following IM separation, as pre-IM collision induced dissociation may lead to considerable heating of the ions and alterations in the mobility profile.[104] The transfer collision energy was varied from 20 to 50 V (nominal) in increments of 5 V for disaccharide derivatives, and from 15 to 40 V in increments of 5 V for monosaccharide derivatives. All major fragment ions were monitored, and the total fragment ion yield calculated.

## 2.4. Results and Discussion

### *2.4.1. Tandem MS Analysis of Disaccharides Formed in the Oligomerization Process*

The disaccharide species formed in the oligosaccharide reaction mixture following 5 wet-dry cycles were selected for MS/MS analysis. The results are shown in Figure 2.2 along with the MS/MS spectra of several disaccharide standards with a variety of regio- and stereo- chemical linkages including: isomaltose (α-(1,6)), gentiobiose (β-(1,6)), maltose (α-(1,4)), cellobiose (β-(1,6)), and trehalose (α-(1,1)-α). As expected, the fragmentation spectrum of the disaccharide precursor ion in the reaction mixture presented a mixture of fragment ions that indicated that the oligomerization process produced several regio- and stereo-isomeric species. The fragment ion at *m/z* 281.10 represented the neutral loss of $C_2H_4O_2$, a diagnostic ion observed for the disaccharides produced in the reaction mixture, as well as all of the standards with the exception of trehalose (1,1-linkage). Comparison of the sample spectrum with the spectra from isomaltose and

gentiobiose indicated the common presence of fragment ions at *m/z* 323.12 and 251.08, again indicating the presence of 1,6-linkages with both α and β stereochemistries in agreement with DEPT-135 $^{13}C$ NMR and HMBC 2D NMR results.[66] The fragment ion at *m/z* 263.10, present in both the sample and also in the maltose and cellobiose standard spectra, indicated the presence of disaccharides with 1,4-linkages. Figure 2.3 shows similar MS/MS analysis on the trisaccharide precursor ion (*m/z* 503.17 ($C_{18}H_{31}O_{16}$, $[M-H]^-$) comparing the observed fragment ions for a 5 wet-dry cycles sample with commercial maltotriose (α-(1,4)-α-(1,4)) and isomaltotriose (α-(1,6)-α-(1,6)) standards. Peaks consistent with these two standard trisaccharides are present in the reaction mixture along with other peaks most likely associated with other trisaccharides.

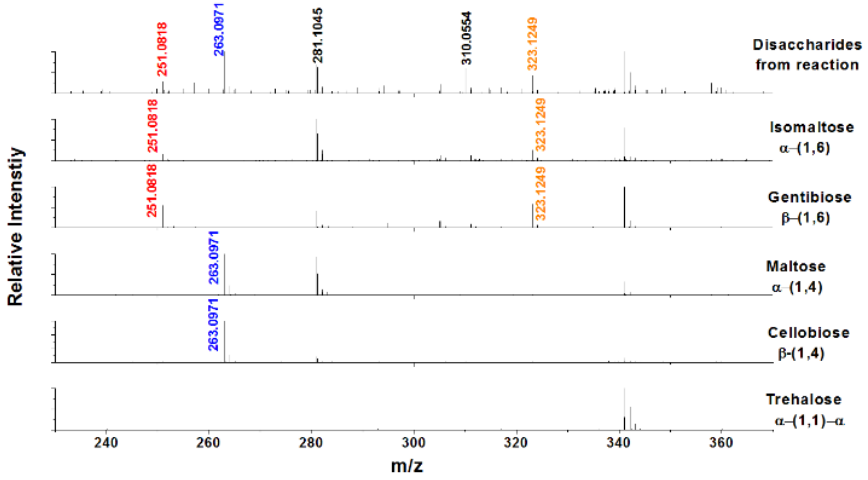


**Figure 2.2.** Tandem MS/MS spectrum (top) of the *m/z* 341.11 ($C_{12}H_{21}O_{11}$, $[M-H]^-$) precursor ion corresponding to the various isobaric glucose disaccharides formed in the reaction mixture of D-glucose after 5 wet-dry (night-day) cycles in 0.01 M HCl at 50 °C, and tandem mass spectra of select glucose disaccharide standards: isomaltose (α-(1,6)), gentiobiose (β-(1,6)), maltose (α-(1,4)), cellobiose (β-(1,6)), and trehalose (α-(1,1)-α). A collision energy of 25V was applied in the transfer cell of the Synapt G2-S mass spectrometer in all cases.

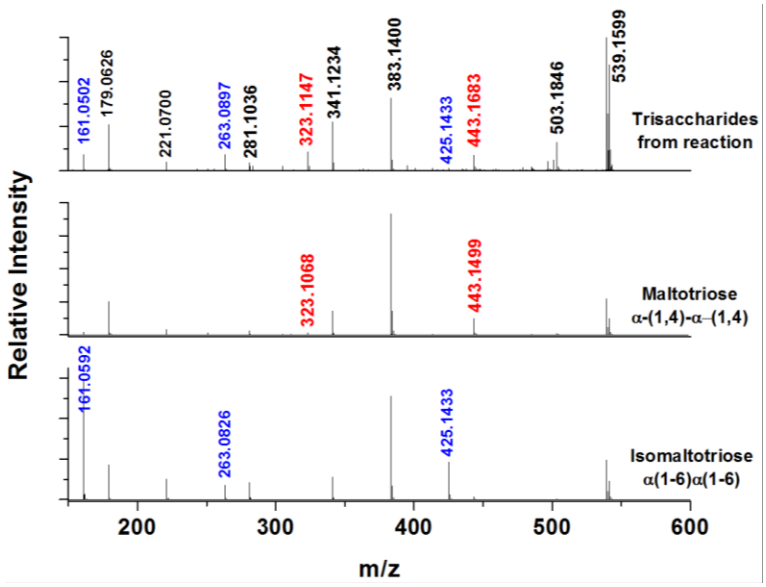


**Figure 2.3.** Tandem MS spectra for trisaccharides formed in the reaction mixture of D-glucose after 5 wet-dry (night-day) cycles in 0.01 M HCl at 50 ºC (top), and tandem mass spectra of two glucose trisaccharide standards including maltotriose (α-(1,4)-α-(1,4)) (middle) and isomaltotriose (α-(1,6)-α-(1,6)) (bottom).

### *2.4.2. Comparison of 3C5NBA derivative separations with chloride adducts*

A number of non-covalent and covalent modifiers have been reported that facilitate the detection and separation of sugar isomers in negative ion mode IM-MS.[97] It has been found that adduct formation with chloride, being able to "bridge" hydrogen bonds in saccharides, is one of the best approaches in terms of isobar resolution.[105] These adducts have also showed exceptionally stability,[106-107] which greatly improves sugar ionization efficiency and detection, as well as their separation by techniques such as high-field asymmetric waveform ion mobility spectrometry (FAIMS).[97]

Shown in Figure 2.4a and c, are the four monosaccharide and seven disaccharide chloride adduct ATDs, which can hardly be distinguished by travelling wave IM-MS experiments under optimized conditions. In contrast, Figure 2.4b and d show overlaid ATD plots obtained for 3C5NBA derivatives, with much improved separation. The best resolution was achieved between lactose and maltose in Figure 2.4d, the drift time showing more than a 1.2 ms difference (R~3.9) between the main signals, approximately 7.5 times better than the 0.16 ms difference (R~1.26) in

drift times observed between the corresponding chloride adducts. The ionization efficiency was also significantly improved. In electrospray ionization, the deprotonated form of most of the disaccharides tested could not be observed directly without derivatization, except for sucrose and trehalose. Most of the detectable signals for underivatized species were either chloride adducts or deprotonated dimers.

Similar to the observations for disaccharides, the electrospray ionization efficiency was also poor for monosaccharide chloride adducts. All species investigated showed very poor drift time peak shapes, as seen in Figure 2.4a. The loose binding of chloride anions to monosaccharides and their aggregation led to dramatic broadening of the peaks in their ATDs, with no separations observed. The covalent shift reagent 3C5NBA, providing more rigid structures, yielded narrower and more symmetric peaks, providing improved separation with an average 2 $Å^2$ CCS difference, see Figure 2.4b.

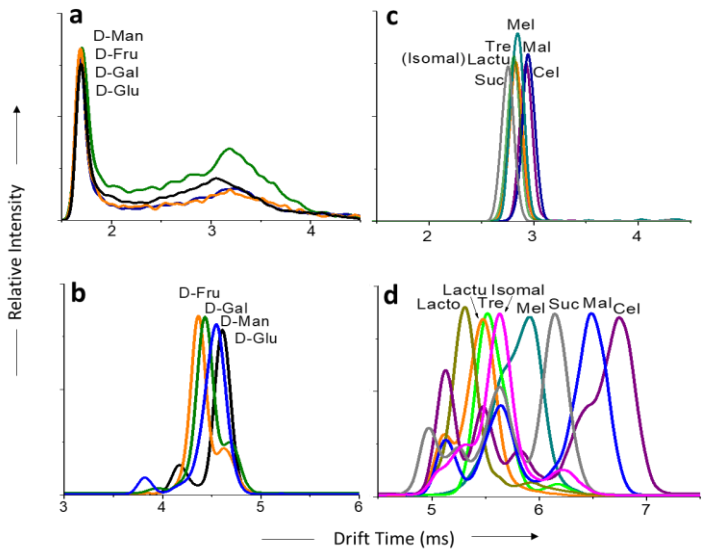


**Figure 2.4.** Overlay of arrival time distributions for chloride adducts of monosaccharides (*m/z* 215.0357) **(a)** and disaccharides (*m/z* 377.0858) **(c)**, compared with the deprotonated doubly 3C5NBA-labelled monosaccharides (*m/z* 529.1012) **(b)** and disaccharides (*m/z* 691.1318) **(d)**.

### *2.4.3. Tandem MS of 3C5NBA derivatives*

Even with the greatly improved IM separations provided by 3C5NBA, mass- and mobility-selected ion activation experiments can be utilized as additional means to confirm identifications (Figure 2.5). For example, trehalose and lactulose derivatives showed drift times of 5.53 ms and 5.48 ms, as shown in Figure 2.4d. Tandem MS experiments, however, showed that trehalose derivatives produced specific fragments at *m/z* 647.1321, 603.1528 and 310.0729, while all other disaccharide derivatives showed negligible fragmentation at these *m/z* values. Even though melibiose showed significant drift time separation from other disaccharides, the cross-ring fragments at *m/z* 480.1078 and 426.0889 in the signature zone (354-691 Da) would provide additional identification information. Besides, isomaltose showed specific fragment at *m/z* 571.0848; sucrose specific fragment *m/z* 441.0958; cellobiose specific fragment *m/z* 511.0756, 456.0919, 396.0721, 190.0341; maltose fragments featured at *m/z* 631.1191, 613.1105, 397.0979 and 190.0341 could all contribute to isomer identification and confirmation. Additionally, with the multi-label pattern of each saccharide derivatives in drift time, each peak resulted in quite different fragments, such as the first peak in maltose at 5.15 ms that produced specific fragment at *m/z* 397.0970 while the peak 2 and 3 at 5.64 ms and 6.51 ms produced unique *m/z* species at 613.1105 and 631.1191. All characteristic fragments are noted in the corresponding MS/MS spectra in Figure 2.5. Among monosaccharides, D-glucose showed a unique fragment at *m/z* 441.1105 (20 V nominal collision energy), D-fructose did not have the common fragments at *m/z* 234.03 and 250.0626 as the rest of the monosaccharides did. The other two monosaccharides, D-mannose and D-galactose, did not produce any specific fragments in this mass region.

In IM-MS, structural stability differences can also be utilized to "energy-resolve" complex ATDs, which allow for better identification of the constituents of an unresolved isomer mixture.[104] We measured the fragment ion yield (FY) of twelve oligosaccharide 3C5NBA derivatives at different collision energies (Figure 2.6). A stepwise increase in activation energy yielded a typical FY sigmoid curve, as shown for the various doubly labelled species. Trehalose, which showed poor ATD resolution with lactulose and

isomaltose, showed a well-resolved FY curve from the other two isomers. At a collision energy of 35 V, the FY for trehalose was 3 times lower than that of lactulose and maltose.

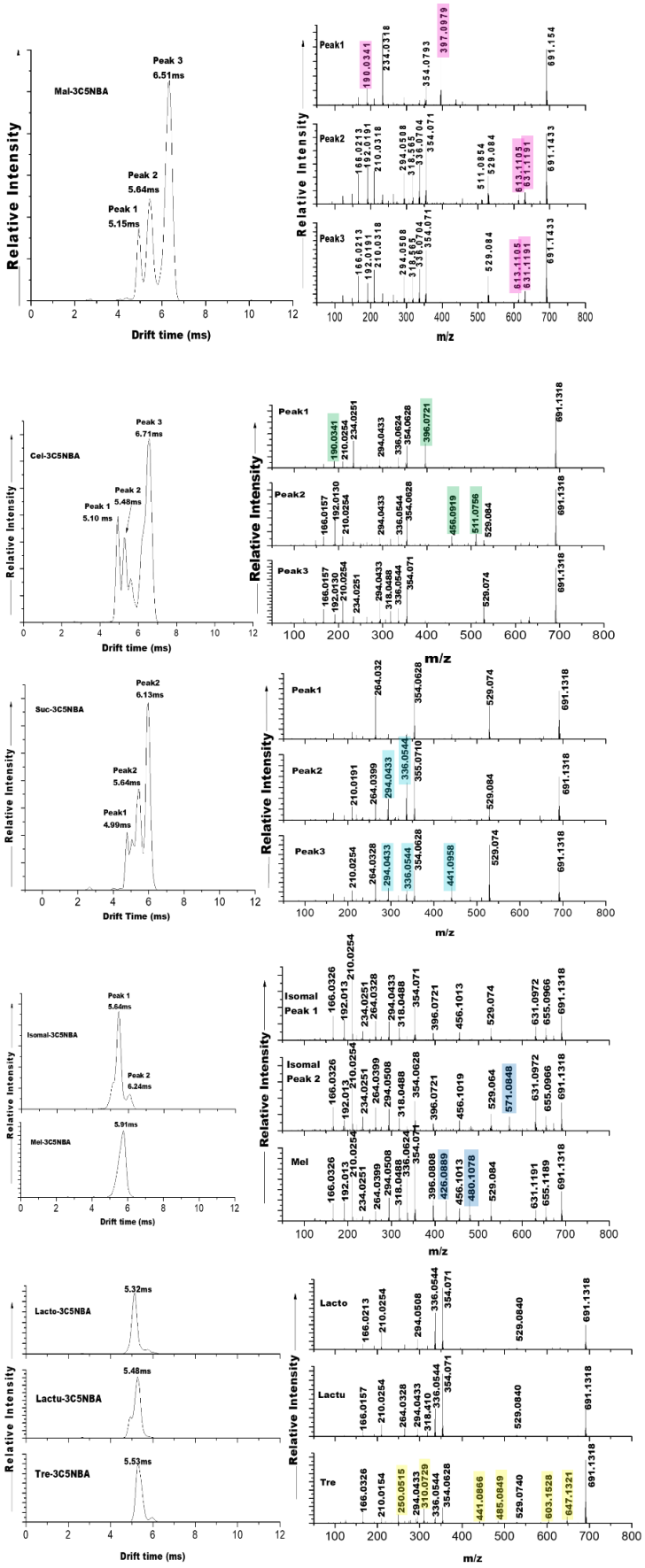
Mal-3C5NBA
Peak 1
5.15ms
Peak 2
5.64ms
Peak 3
6.51ms
Relative Intensity
Drift time (ms)
Peak1
Peak2
Peak3
m/z
Cel-3C5NBA
Peak 1
5.10 ms
Peak 2
5.48ms
Peak 3
6.71ms
Suc-3C5NBA
Peak1
4.99ms
Peak2
5.64ms
Peak2
6.13ms
Drift Time (ms)
Isomal-3C5NBA
Peak 1
5.64ms
Peak 2
6.24ms
Mel-3C5NBA
5.91ms
Isomal
Peak 1
Isomal
Peak 2
Mel
Lacto-3C5NBA
5.32ms
Lactu-3C5NBA
5.48ms
Tre-3C5NBA
5.53ms
Lacto
Lactu
Tre

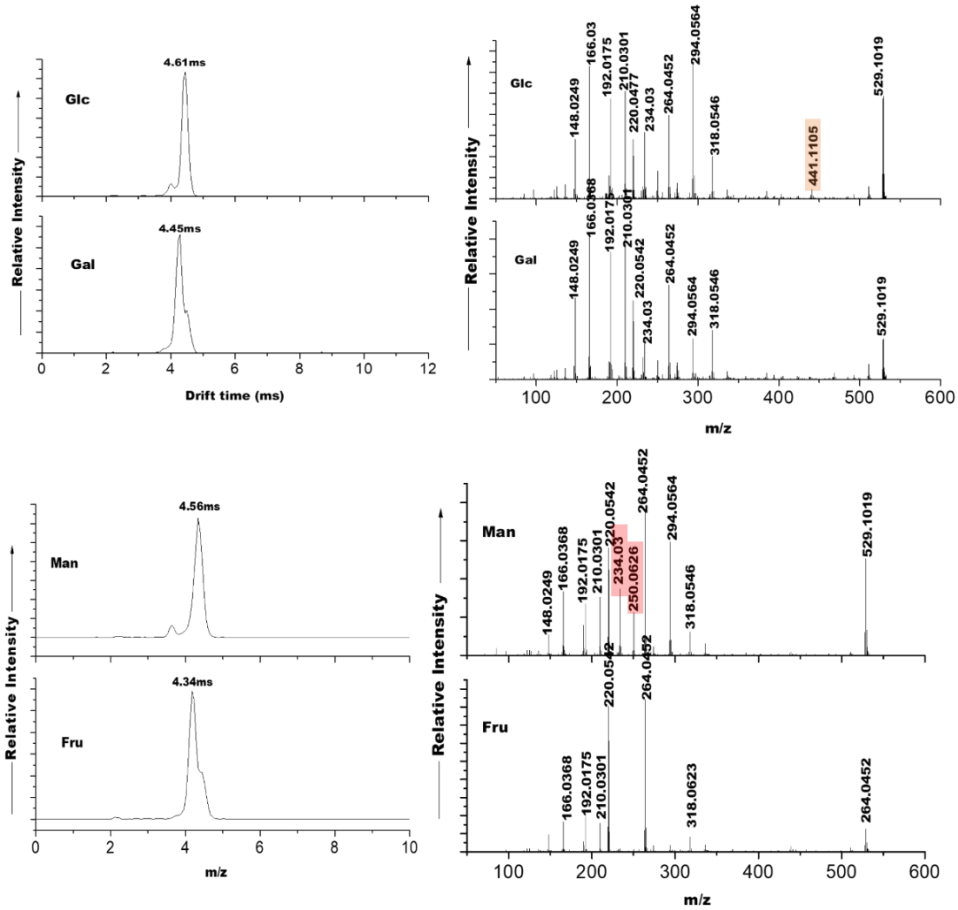


**Figure 2.5.** Fragmentation spectra of mobility-resolved 3C5NBA derivatives of each disaccharide at *m/z* 691.132 (collision energy = 40 V), and monosaccharide at m/z 529.10. All characteristic fragments for each species are highlighted. The disaccharide neutral exact mass is 342.1162 Da, 3C5NBA is 211.0288 and the doubly-labeled neutral product is 692.1316. Abbreviations: maltose (Mal), melibiose (Mel), cellobiose (Cel), isomaltose (Isomal), lactose (Lacto), sucrose (Suc), trehalose (Tre).

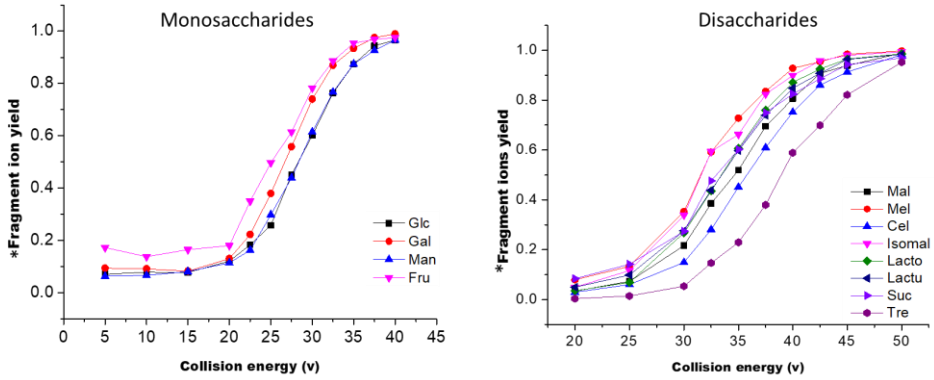


**Figure 2.6.** Energy-resolved ion activation experiments of $[M+2x3C5NBA)-H]^-$ species. The graph on the left shows monosaccharide fragmentation at *m/z* 529.10, and the one on the right disaccharide fragmentation at *m/z* 691.132. Fragment ion yield= Total fragment ion intensity/ (Total fragment ion intensity+ Precursor ion intensity).

## 2.5. Conclusion

Tandem mass spectrometry has been used to analyze glucose oligomerization reactions in order to further characterize the products. High resolution mass spectrometry confirmed the presence of oligomers from dimers up to octamers. Alongside $^{1}H$ and $^{13}C$ NMR data, MS/MS confirmed the presence of 1,6-, 1,4-, 1,3-, and 1,2- linkages with the primary linkage present being 1,6-. Given the wide functional roles exhibited by polysaccharides,[108-112] we hypothesize that oligosaccharides that are accessible via such wet-dry cycles could have been readily available to facilitate prebiotically-relevant chemical transformations or impact the properties of other classes of molecules. This could involve (a) direct participation in chemical conversions and becoming part of structural scaffolds and/or (b) altering the physical properties of the environment (e.g. lowering water activity) by acting as gelling agents or viscogens. In order to further investigate the regio- and stereochemical diversity of these oligomers, a new boronic acid shift reagent, 3C5NBA was investigated as a shift reagent for ion mobility separation prior to MS/MS analysis. This reagent provides fast and simple derivatization of sugars under mild conditions, while preserving their original configuration, resulting in separations of eight disaccharides and four monosaccharides that compared favorably with those reported in the literature to date. Covalently modified sugars generate specific and robust fragments in MS/MS experiments, and significant differences in energy-resolved fragment ion yield curves, which can be used as an additional method for confirming sugar identity. Future applications involve coupling this method to LC separations with the aim of further improving resolution and peak capacity for the complete characterization of complex mixtures of mono and disaccharide isomers. We expect the development of such analytical tools to aid in the analysis of the complex mixtures of di- and oligo-saccharides that would be generated in an abiotic context, an endeavor that is currently underway in our laboratories.

# CHAPTER 3. Carbohydrate isomer resolution *via* multi-site derivatization cyclic ion mobility-mass spectrometry

*Adapted from*

McKenna, K. R.; Li, L.; Baker, A. G.; Ujma, J.; Krishnamurthy, R.; Liotta, C. L.; Fernández, F. M. *Analyst*, **2019**, *144*, 7220-7226. K.R. McKenna designed experiments and analyzed cIM data and cIM-MS/MS data. A. G. Baker and J. Ujma were involved in the development of the cIM instrument, performed experiments, and assisted with the design of tandem ion mobility experiments. R. Krishnamurthy, C. L. Liotta, and F. M. Fernández assisted with the design of experiments and provided advisory roles.

## 3.1. Abstract

Oligosaccharides serve many roles in extant life and may have had a significant role in prebiotic chemistry in early Earth. In both these contexts, the structural and isomeric diversity among carbohydrates presents analytical challenges necessitating improved separations. Here, we showcase a chemical derivatization approach, where 3-carboxy-5-nitrophenylboronic acid (3C5NBA) is used to label vicinal hydroxyl groups, amplifying the structural difference between isomers. We explore the applicability of state-of-the-art ion mobility – mass spectrometry (IM-MS) instrumentation in the analysis of derivatized carbohydrates. In particular we focus on the resolving power required for IM separation of derivatized isomers. A recently developed cyclic ion mobility (cIM) mass spectrometer (MS) was chosen for this study as it allows for multi-pass IM separations, with variable resolving power ($R_p$). Three passes around the cIM ($R_p$~120) enabled separation of all possible pairs of four monosaccharide standards, and all but two pairs of eight disaccharide standards. Combining cIM methodology with tandem mass spectrometry (MS/MS) experiments allowed for the major products of each of the 3C5NBA carbohydrate derivatization reactions to be resolved and unequivocally identified.

## 3.2. Introduction

Understanding the chemical processes leading to the origins of life on Earth is one of the greatest scientific questions of our time.[113] With the Miller-Urey experiment[58] leading to decades of scientific research in prebiotic chemistry, the non-enzymatic origin of biopolymers such as nucleic acids and peptides has been studied at length.[114-116] Carbohydrates are also critical components of life, and are responsible for maintaining cell structure, intercellular communication, and various other central biological processes.[1, 3, 5, 7-8] As carbohydrates aid in the co-solubility of biopolymers, can serve as cross-linkers, and provide rudimentary catalytic activity, it is highly likely they were also important for the development of early life on the prebiotic Earth.[117]

The structures of mono- and oligosaccharides determine their properties and function, so it is critical that their characterization is performed beyond their molecular weight. For example, certain sugars are non-reducing and can protect other molecules from stress caused by pH or temperature changes, whereas reducing sugars can react with amino acids and other biologically-relevant molecules.[2, 118-119] Carbohydrates are structurally diverse and complex, and have received less attention in prebiotic chemistry when compared to peptides and nucleic acids.[120-121] Polysaccharides contain a great diversity of monomeric units, each with several possible linkages, as well as the potential for branching. Additionally, each anomeric carbon can have either an α or β configuration, doubling the possible number of structures to be detected and resolved. Because of their identical elemental formulas, these isobars cannot be distinguished even with the use of ultrahigh resolution-mass spectrometry (MS).

Several analytical methods have been utilized to characterize oligosaccharides. Tandem mass spectrometry (MS/MS), for example, can efficiently distinguish relatively pure disaccharide samples. It cannot, however, effectively characterize lower abundance components in complex mixtures of isobaric carbohydrates.[16-17] Nuclear magnetic resonance (NMR) spectroscopy can also be very useful, but requires higher concentrations, and can therefore be more time consuming.[122-124] Liquid chromatography (LC) has been extensively used for disaccharide identification, but it is relatively slow and may require

derivatization for higher resolution separations.[13-14] Capillary electrophoresis (CE) is also an effective method for carbohydrate separations, but some degree of *a priori* knowledge about the oligosaccharides being separated is typically required.[125-127]

Ion mobility (IM) separations coupled to mass spectrometric detection (IM-MS) have been shown to be a viable complement to other established, yet limited, techniques. This method requires lower sample concentrations than NMR, shorter analysis times than either NMR or LC and, with sufficient resolving power $\left(\boldsymbol{R_p} = \frac{\boldsymbol{t_d}}{\Delta \boldsymbol{t_d}}\right)$,[128] can distinguish isomeric species in complex mixtures. IM separations depend on the mobility coefficient (*K*), which determines the velocity of the gas phase ions in the electric field. *K* depends on a variety of instrumental parameters, masses of ion and gas molecules, and their rotationally-averaged collision cross section (CCS). The latter parameter can be correlated to the 3D structure of ions.[129]

Traveling wave IM spectrometry (TWIMS) is an IM technique wherein the mobility separator is comprised of a series of electrodes enclosed in a gas filled cell (~2 mbar $N_2$). A series of voltage pulses is applied sequentially to each electrode, propelling ions through the device.[41] Ions can "surf" or "roll over" the wave falling back into the preceding wave. Ions of lower mobility undergo more roll over events than higher mobility ions, effectively leading to mobility separation. Drift times ($t_d$) measured in TWIMS can be converted to CCS using calibration procedures.[42-44] A number of calibrant compounds have been proposed.[45] Resolving power ($R_p$) of an IM separator can be improved by increasing its length.[46] Recently, Giles *et al.* developed a travelling wave-enabled, cyclic IM (cIM) instrument with multi-pass capabilities.[47] In this instrument, IM resolving power increases as a function of the square root of the number of passes, *n* ($\boldsymbol{R_p \sim 70\sqrt{nz}}$);[47] here 70 is the approximate, single pass resolving power and z is the ion's charge state. Normally, the maximum number of passes is limited by the so called "wrap-around" effect that occurs when the spatial width of the separated ion packets exceeds the length of the cIM device.[48] The cIM control enables selective ejection of ions in a specified range of arrival times from the

cIM device that can be followed by activation and/or further separation of product ions ($IMS^n$).[48-49] These functionalities have been used previously for structural studies of carbohydrate[49-50] and protein ions.[51]

Isomeric pentasaccharides, including anomers, have been shown to be able to be separated by the cIM system.[49] Typically, isobaric mono- and disaccharides do not have sufficiently-different CCS values to be separated by commercially-available IM systems. To mitigate this issue, shift reagents — ligands that can bind either covalently or non-covalently to amplify CCS differences between isobaric carbohydrates — have been utilized. Previous examples of shift reagents include alkali and alkaline earth metal cations, and 1-phenyl-3-methyl-5-pyrazolone.[11-12, 52] In recent work, we reported a new shift reagent for carbohydrates, 3-carboxy-5-nitrophenyl boronic acid (3C5NBA) that rapidly reacts with mono- and disaccharides, enhancing their IM separation.[53] Due to the initial promise shown by 3C5NBA, we here evaluate its applicability in combination with high-resolution cIM-MS instrumentation. In addition, we utilized the tandem IMS ($IMS^2$) capability to probe the possibility of interconversion between mobility separated mannose derivatives.

## 3.3. Experimental

### *3.3.1. Reagents and Chemicals*

Isomaltose, trehalose, cellobiose, D-fructose, and 3-carboxy-5-nitrophenylboronic acid (3C5NBA) were obtained from TCI (Philadelphia, PA). As stated by the manufacturer, the purchased 3C5NBA contained both the monomer and the anhydride dimer. This was verified by detection of the $[M-H]^-$ ions for these species at *m/z* 210.0 and 403.0, respectively, as shown in Figure S-1. Maltose, lactose, lactulose, sucrose, D-(+)-glucose, and D-(+) galactose were purchased from Sigma Aldrich (St. Louis, MO). Melibiose was obtained from Fluka. D-mannose was purchased from VWR.

### *3.3.2. Multi-Site Derivatization of Carbohydrates*

Stock solutions of carbohydrate standards (1 mM) were prepared in water. A 1 mM 3C5NBA stock solution was prepared in acetonitrile and kept refrigerated at 5 °C until used. Previously reported

reaction methods were utilized.[53] In short, a solution of 5 µL of the 1 mM carbohydrate solution and 10 µL of the 1 mM 3C5NBA solution were incubated at room temperature for 5 minutes for disaccharides and 30 minutes for monosaccharides. The reaction mixture was then diluted to 1 mL with deionized water prior to IM-MS analysis.[130]

### *3.3.3. Ion Mobility-Mass Spectrometry Experiment Parameters*

Ion mobility experiments were performed using either a standard SYNAPT G2-S*i* (Q-IM-ToF) or a prototype, quadrupole cyclic ion mobility orthogonal time-of-flight mass spectrometer (Q-cIM-ToF) (Waters, Wilmslow, UK).[101] All experiments used direct infusion electrospray ionization in negative ion mode. Instrument ion source settings were as follows: capillary voltage, 2.2 kV; cone voltage, 100 V; source offset, 60 V; source temperature, 100 °C; desolvation temperature, 250 °C; desolvation gas flow, 600 L $h^{-1}$; and cone gas flow, 50 L $h^{-1}$. For the SYNAPT G2-S*i*, the travelling wave height was 40 V, the travelling wave velocity was 500 m $sec^{-1}$, the helium cell was operated at 180 mL $min^{-1}$, and nitrogen was used as the IM gas (90 mL $min^{-1}$). For the cIM system, source parameters were the same as above; the helium cell was operated at 80 mL $min^{-1}$ and nitrogen IM gas at 70 mL $min^{-1}$. The travelling wave height was 35 V and the travelling wave velocity was 375 m $sec^{-1}$. Mannose derivatives were investigated by $IMS^2$. Following three passes around the cIM, the separated ions were selectively ejected from the cIM device and re-injected using a higher voltage offset (115 V), resulting in activation. Activated ions were then subjected to additional three passes around the cIM device. This method was meant to probe whether certain features in the ATD could interconvert.

Arrival time distributions were extracted from MassLynx 4.2 into OriginPro 8.5 and fitted with Gaussian functions to more precisely determine peak maxima. Reported arrival times include the "dead time" (the time spent between the exit of the cIM and detector), which ranged from 6.29-6.78 ms for monosaccharide derivatives and 2.77-3.75 ms for disaccharide derivatives.

### *3.3.4. Tandem Mass Spectrometry Experiments*

For MS/MS experiments, the ions of interest were quadrupole-selected and subjected to collision induced dissociation (CID) in the transfer region of the Q-cIM-ToF instrument following IM separation. The doubly derivatized monosaccharide precursor ions were selected at *m/*z 529.10, and the doubly derivatized disaccharide precursors were selected at *m/*z 691.13. The transfer collision energy was 18 eV for disaccharide derivatives, and 12 eV for monosaccharide derivatives.

## 3.4. Results and Discussion

### *3.4.1. Derivatization Reactions*

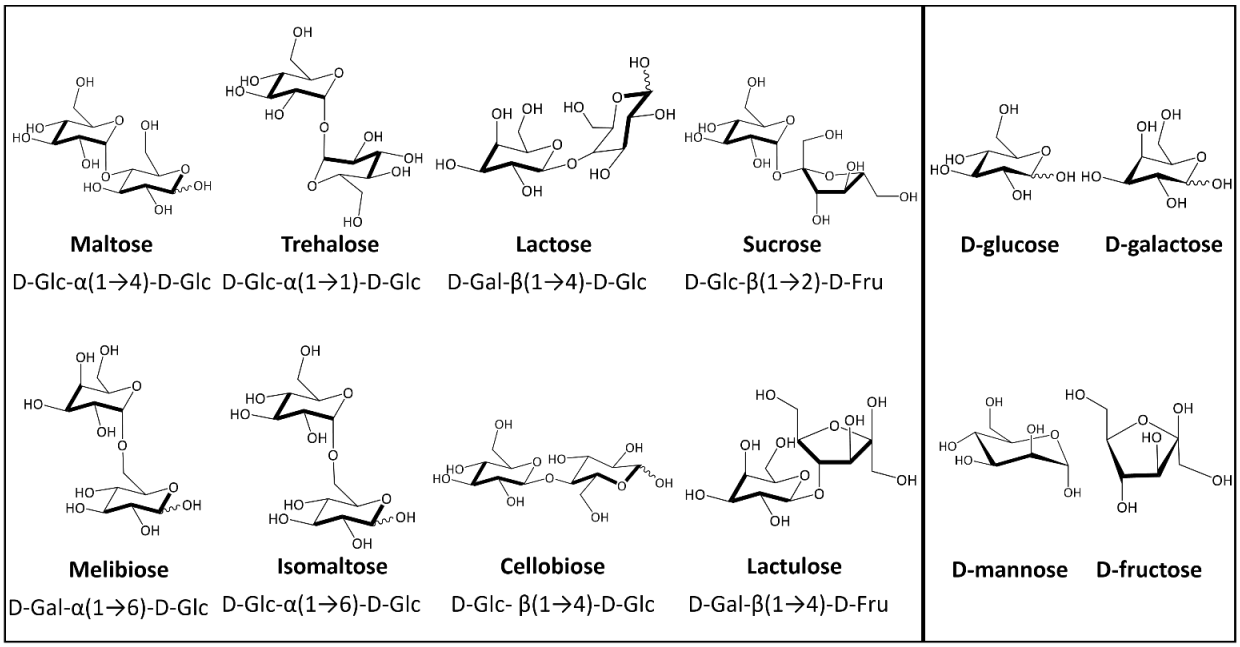


**Figure 3.1.** Structures of isobaric disaccharide and monosaccharide standards utilized in this study.

The four monosaccharide and eight disaccharide standards that were tested in this study are shown in Figure 3.1. Notably, maltose, trehalose, isomaltose, and cellobiose are all glucose dimers (*i.e.* glucopyranosyl-glucose isomers). Maltose and cellobiose are anomers, isomers that only differ in the stereochemistry of the anomeric carbon. The remaining disaccharides included in the study contained at least one of the monosaccharide units above. Glucose, galactose, and mannose are aldose epimers that differ only in their stereochemistry, while fructose is a ketose.

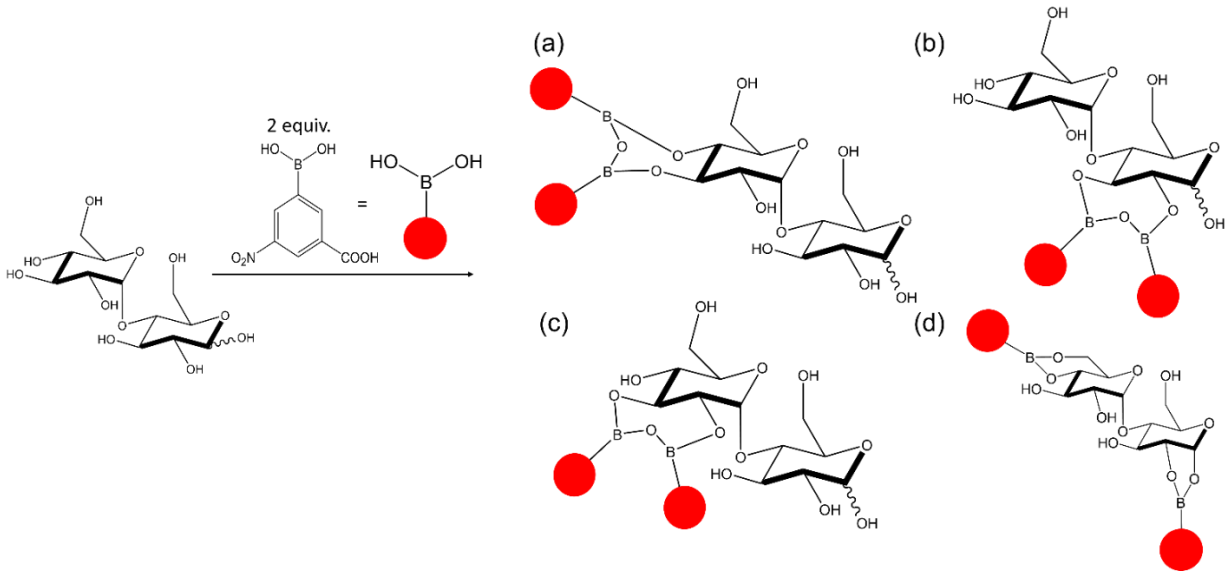


**Figure 3.2.** Example reaction scheme for maltose with 3C5NBA. The red circle indicates the 3-carboxy-5-nitrophenyl group in 3C5NBA. Anhydride derivatives were mainly observed as their water loss deprotonated ions $[M\text{-}H_2O\text{-}H]^-$.

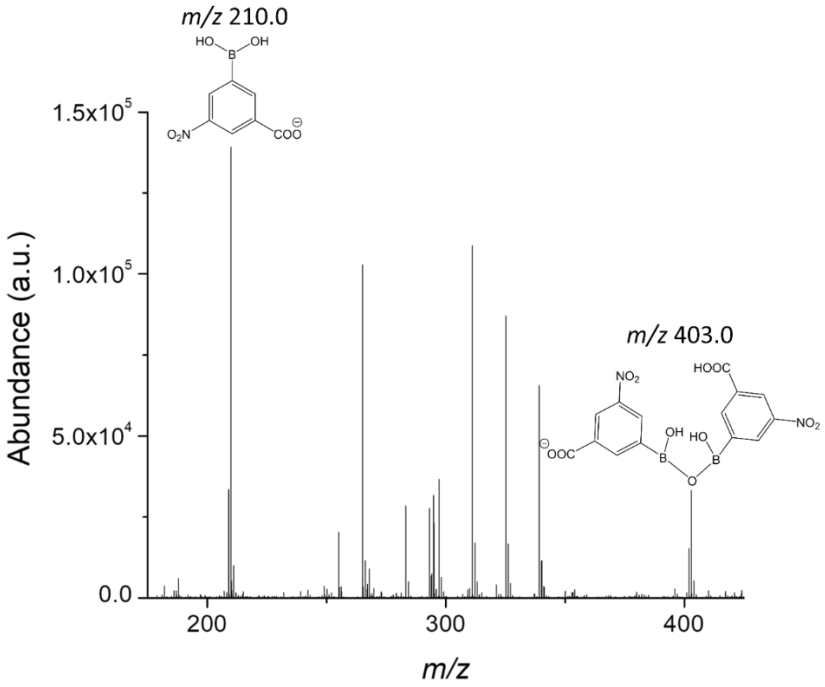


**Figure 3.3.** Full scan MS data showing evidence for the presence of the anhydride dimer in the 3C5NBA reagent.

3C5NBA was selected as a shift reagent to amplify CCS differences between isomeric carbohydrates.[53] As an example, the 3C5NBA derivatization reaction for maltose is presented in Figure 3.2. Here, 3C5NBA can react with two different *cis* diols to form two rings with either five

or six members as well as two *trans* diols on $C_4$ and $C_6$ to form a six-membered ring (Figure 3.2d).[131] Additionally, the 3C5NBA reagent also contains the anhydride dimer, as shown in Figure 3.3. This anhydride, B-(3-carboxy-5-nitrophenylboronic acid)-3- carboxy-5-nitrophenylboronic acid, can react with two *trans* diols to form a seven-membered ring product (Figure 3.2a-c).[132] The number of expected products for each carbohydrate investigated as well as a breakdown of the products for each reagent (3C5NBA or its anhydride dimer) are shown in Table 3.1. Although the fact that multiple products were formed by most of these reactions may somewhat limit the applicability of this derivatization reagent for quantitative experiments, the availability of multiple CCS values could also help confirm the analyte's identity when identifying unknowns. These doubly-derivatized products were chosen for further characterization by IM-MS.

**Table 3.1.** The number of possible regio- and functional isomers possible for each carbohydrate when reacting with two separate 3C5NBA molecules (left), the anhydride dimer of 3C5NBA (middle), and the total expected number of structures from the derivatization reaction for each carbohydrate (right). * indicates that the sugar can undergo mutarotation, so more derivatives would be expected than for one stereoisomer.

| Carbohydrate | # of Possible Boronic Acid Derivatives | # of Possible Dehydrated Anhydride Derivatives | Total Possible Derivatives |
|---|---|---|---|
| Fructose | 1 | 1 | 2 |
| Galactose | 2 | 1 | 3 |
| Glucose | 1 | 2 | 3 |
| Mannose | 2 | 1 | 3 |
| Cellobiose* | 1 | 3 | 4 |
| Isomaltose | 1 | 4 | 5 |
| Lactose* | 2 | 2 | 4 |
| Lactulose | 4 | 1 | 5 |
| Maltose | 1 | 3 | 4 |
| Melibiose | 2 | 3 | 5 |
| Sucrose | 3 | 3 | 6 |
| Trehalose | 1 | 2 | 3 |

### *3.4.2. Cyclic Ion Mobility Separations*

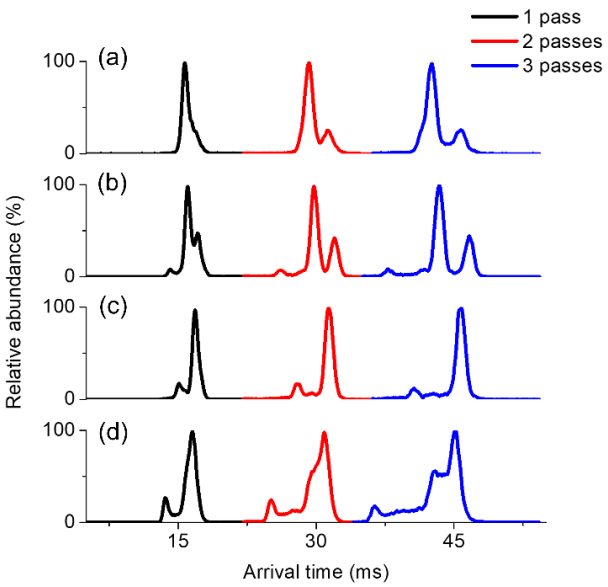


**Figure 3.4.** Arrival time distributions (ATDs) of doubly-derivatized monosaccharides (*m/z* 529.04) including (a) fructose, (b) galactose, (c) glucose, and (d) mannose with a varying number of passes using the cIM instrument. Sections of the ATDs without features were truncated for clarity.

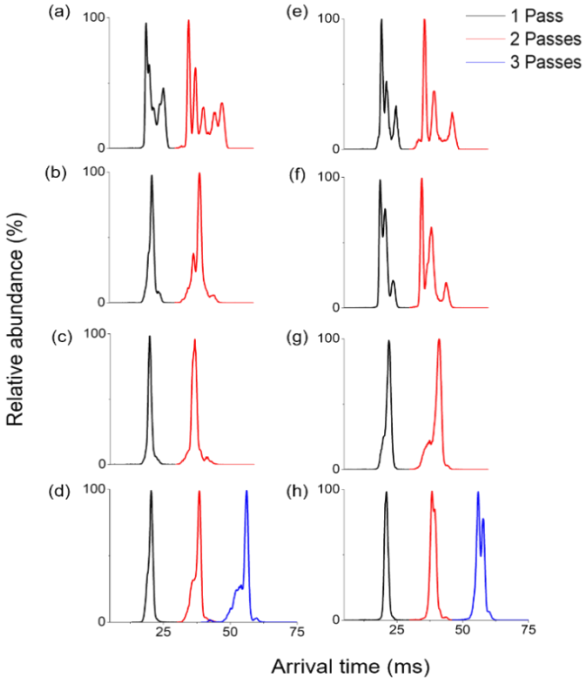


**Figure 3.5.** Doubly-derivatized disaccharides analyzed on the cyclic IM instrument. The studied disaccharides were (a) cellobiose, (b) isomaltose, (c) lactose, (d) lactulose, (e) maltose, (f) melibiose, (g) sucrose, and (h) trehalose. Only two passes are shown in cases where the wraparound effect was observed after three passes.

Arrival time distributions (ATDs) of doubly-derivatized monosaccharides and disaccharides obtained after various passes around the cIM are shown in Figures 3.4 and 3.5, respectively. Each panel in the figure represents a single carbohydrate subjected to $n$=1, 2 and 3 passes around the cIM device. The corresponding, estimated $R_p$ values were ~70, ~100 and ~120, respectively. As expected, the number of resolved features increased with $n$; these were attributed to positional and functional isomers with different 3C5NBA derivatization sites (Table 3.1). For fructose, for example, two derivatives are expected, and two features appeared resolved in the ATD (Figure 3.4a). Similarly, three derivatives are expected for both galactose and glucose, and three features were seen in their ATDs (Figure 3.4b-c). In contrast, six derivatives are possible for sucrose, while only three features were resolved in the ATD (Figure 3.5g), likely due to spectral overlap or insufficient yield of some of the derivatives. Figure 3.6 shows the peak areas for the glucose derivative observed after one, two and three passes around the cIM. In line with the previous observations by Giles *et al.*,[48] the transmission losses were minimal.

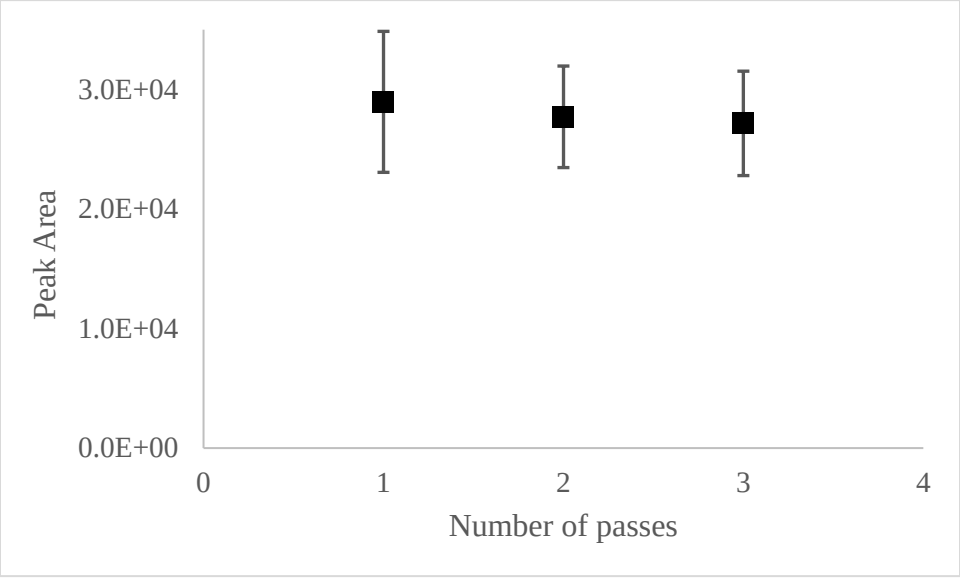


**Figure 3.6.** Peak areas of the doubly derivatized glucose (*m/z* 529) ion *vs*. the number of passes in the cyclic ion mobility device. Data points and error bars correspond to average and standard deviations from eight measurements, respectively.

Although in most cases regio- and functional isomers of derivatized monosaccharides were resolved after one pass (Figure 3.4), this was not the case for derivatized disaccharides (Figure 3.5). For

these analytes, the CCS shift introduced by 3C5NBA derivatization was proportionally smaller, and thus a higher number of passes around the cIM was required to resolve them. For example, only two isomers of doubly-derivatized cellobiose were resolved after one pass; however, after three passes five features were seen in the ATD (Figure 3.5a). Several other disaccharides were also observed to behave in a similar manner. For isomaltose, melibiose, sucrose, and trehalose, between two and three passes were sufficient to resolve two to three otherwise overlapping peaks. While further increasing the number of passes can be a powerful tool to improve $R_p$, there was a limit to the number of passes that could be performed without observing wraparound effects, as discussed by Giles *et al.*[48]

Some ATD features, such as those observed for mannose derivatives (Figure 3.4d), showed significant fronting and/or tailing, which would normally indicate species interconversion. In order to investigate this further, $IMS^2$ experiments were performed in which each of the features observed were isolated and activated. The presence of the same ATD with only a single peak for each of the non-activated and activated features indicated this was not the case (Figure 3.7), with the additional species observed at higher number of cycles likely being due to components that were unresolved at a lower number of cycles.

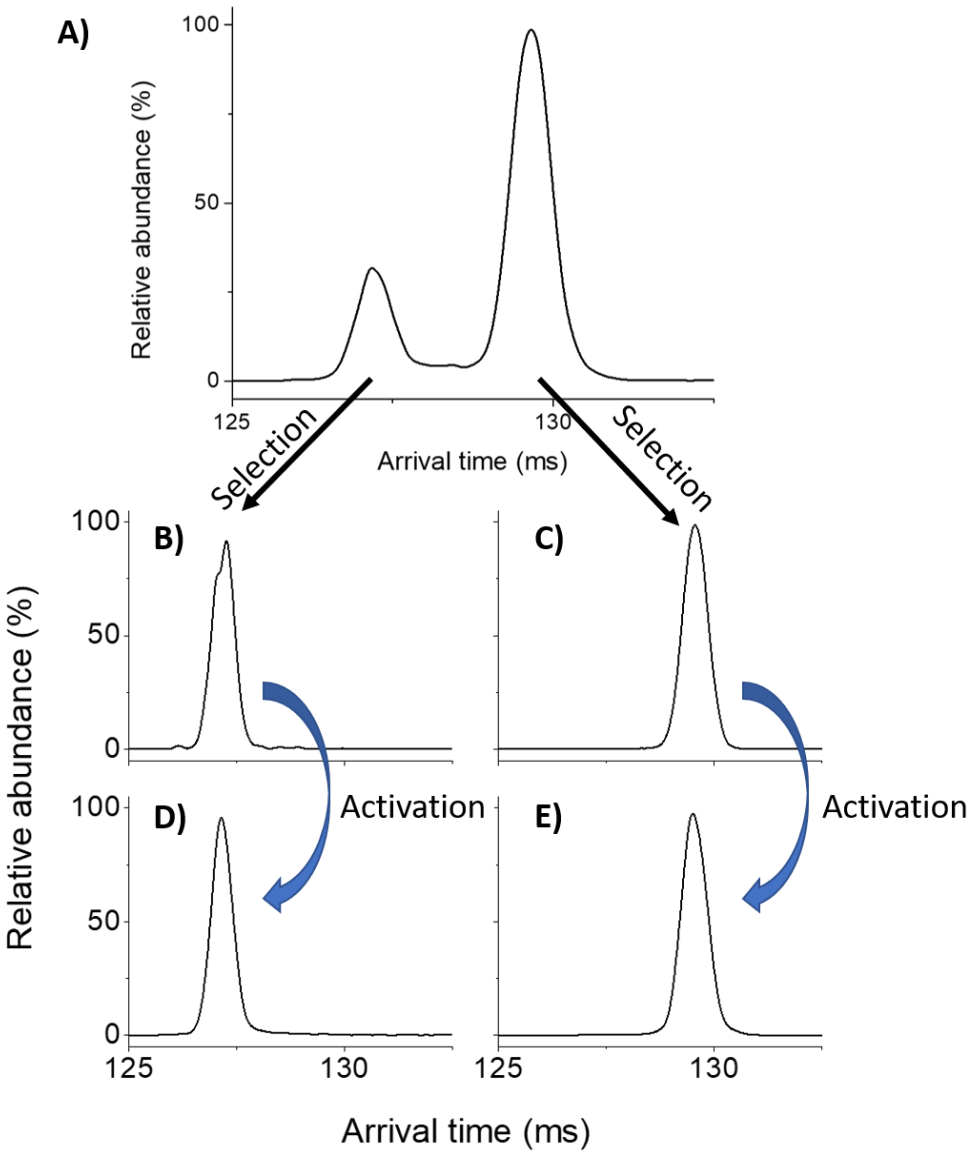


**Figure 3.7.** (A) Arrival time distribution of doubly 3C5NBA-derivatized mannose after three cIM passes, followed by a frontflush of the mobility peaks with arrival times lower than 30 ms and an additional four passes. The selection of the mobility region containing each peak (injection into a pre-cIM store) after three cIM passes followed by an additional four passes after reinjection is shown in B) and C), with the results of the same method with the addition of activation during reinjection with a voltage offset (115 V) shown in D) and E). If there had been interconversion between these species, two peaks would have been observed in the ATD after activation.

It is of interest to compare the separation of the most abundant species of each of the pairs of mono- and disaccharides after three passes around cIM with that obtained using the SYNAPT instrument incorporating the linear TWIMS device. Figures 3.8 and 3.9 show ATDs of doubly derivatized monosaccharides and disaccharides obtained on the two platforms. The two-peak resolution ($R_{pp} =$

$1.18\frac{t_{dB}-t_{dA}}{\Delta t_{dB}+\Delta t_{dA}}$)[46] was calculated for all possible pairs of monosaccharides and disaccharides to enable quantitative comparisons (Tables 3.2 and 3.3). The $R_{pp}$ values calculated from cIM data were (expectedly) higher than the corresponding SYNAPT values, with one notable exception. For isomaltose *vs.* melibiose, the $R_{pp}$ was the same for both platforms. We attributed this observation to the presence of several closely related structures. This phenomenon has been well documented for protein ions, with examples including Koeniger *et al.,*[133] Allen *et al.,* [134] and Eldrid *et al.*[51] For both melibiose and isomaltose, we predicted 5 possible derivatives, but only three asymmetric features were observed in the ATDs, suggesting the presence of more, unresolved components.

**Table 3.2.** Two-peak resolution ($R_{pp}$) of the most abundant monosaccharide 3C5NBA derivatives on the Synapt and the cIM systems after three passes.

| **Monosaccharide Pair** | $R_{pp}$ **(Synapt)** | $R_{pp}$ **(3 passes)** |
|---|---|---|
| Fructose *vs.* Galactose | 0.14 | 0.53 |
| Fructose *vs*. Glucose | 0.58 | 1.92 |
| Fructose *vs.* Mannose | 0.32 | 1.36 |
| Galactose *vs.* Glucose | 0.49 | 1.58 |
| Galactose *vs.* Mannose | 0.23 | 1.00 |
| Glucose *vs.* Mannose | 0.20 | 0.38 |

**Table 3.3.** Two-peak resolution ($R_{pp}$) of the most abundant disaccharide 3C5NBA derivatives on the Synapt and cIM systems after three passes.

| **Disaccharide Pair** | $R_{pp}$ **(Synapt)** | $R_{pp}$ **(3 passes)** |
|---|---|---|
| Cellobiose *vs.* Isomaltose | 1.57 | 3.37 |
| Cellobiose *vs.* Lactose | 0.87 | 1.44 |
| Cellobiose *vs.* Lactulose | 1.01 | 3.14 |
| Cellobiose *vs*. Maltose | 0.16 | 0.38 |
| Cellobiose *vs*. Melibiose | 1.09 | 1.55 |
| Cellobiose *vs*. Sucrose | 0.53 | 0.94 |
| Cellobiose *vs*. Trehalose | 1.12 | 2.89 |
| Isomaltose *vs.* Lactose | 0.63 | 0.99 |
| Isomaltose *vs.* Lactulose | 0.32 | 0.50 |

| | | |
|---|---|---|
| Isomaltose *vs*. Maltose | 1.26 | 2.94 |
| Isomaltose *vs*. Melibiose | 0.07 | 0.07 |
| Isomaltose *vs*. Sucrose | 1.97 | 4.69 |
| Isomaltose *vs*. Trehalose | 0.13 | 0.88 |
| Lactose *vs*. Lactulose | 0.24 | 0.67 |
| Lactose *vs*. Maltose | 0.64 | 1.17 |
| Lactose *vs*. Melibiose | 0.50 | 0.60 |
| Lactose *vs*. Sucrose | 1.30 | 2.16 |
| Lactose *vs*. Trehalose | 0.39 | 0.42 |
| Lactulose *vs*. Maltose | 0.79 | 2.67 |
| Lactulose *vs*. Melibiose | 0.29 | 0.31 |
| Lactulose *vs*. Sucrose | 1.38 | 4.60 |
| Lactulose *vs*. Trehalose | 0.16 | 0.39 |
| Maltose *vs*. Melibiose | 0.92 | 1.38 |
| Maltose *vs*. Sucrose | 0.62 | 1.36 |
| Maltose *vs*. Trehalose | 0.91 | 2.41 |
| Melibiose *vs*. Sucrose | 1.36 | 1.93 |
| Melibiose *vs*. Trehalose | 0.15 | 0.47 |
| Sucrose *vs*. Trehalose | 1.45 | 4.40 |

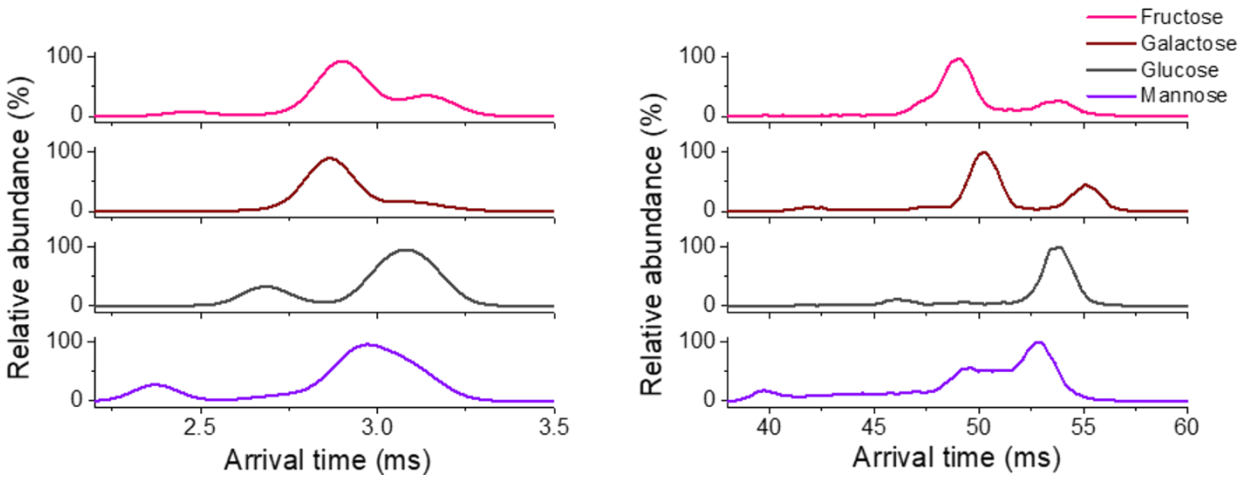

**Figure 3.8.** Doubly 3C5NBA-derivatized monosaccharides analyzed on the Synapt G2-Si (left) and after three passes on the cIM instrument (right).

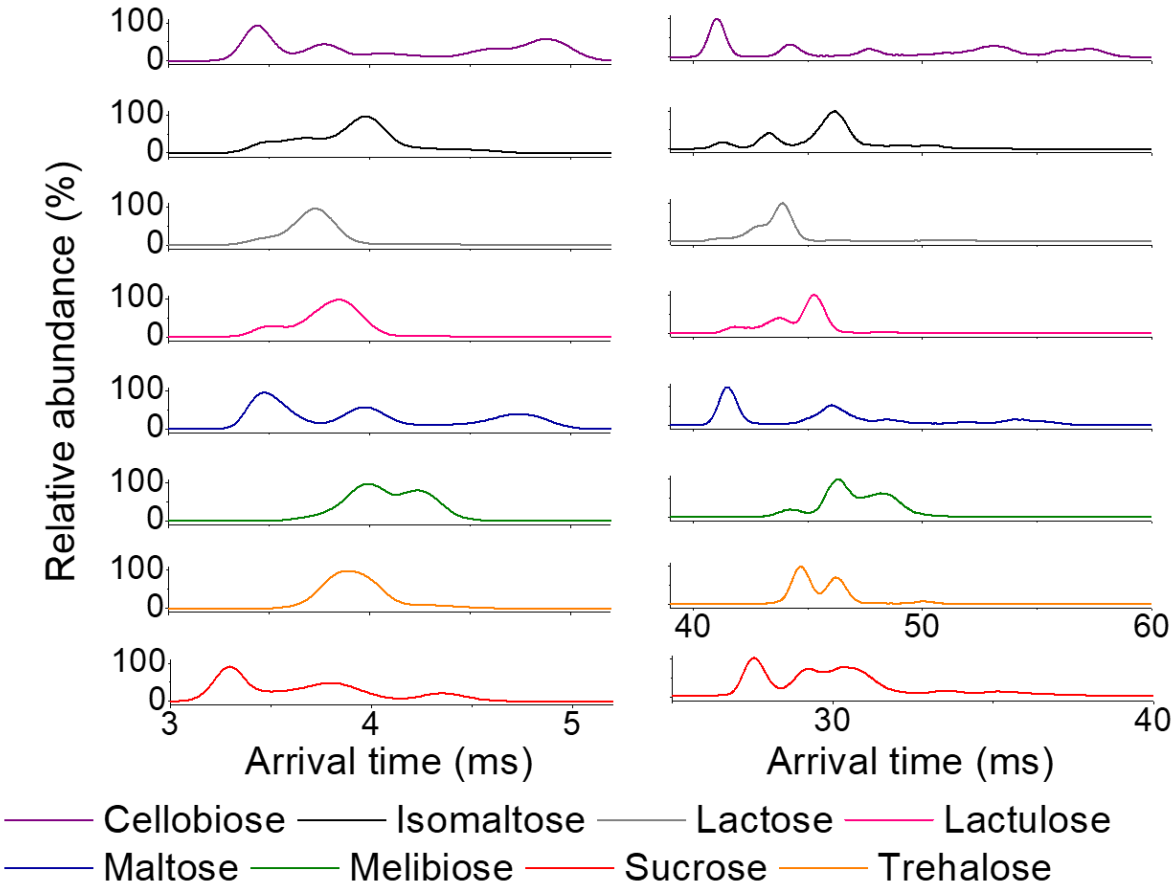


**Figure 3.9.** Doubly 3C5NBA-derivatized disaccharides analyzed on a SYNAPT instrument (left) and the same analytes after three passes in the cyclic IM instrument (right). The right ATD for sucrose is shown after only two passes due to the observation of wraparound effects after three passes.

### *3.4.3. Structural Analysis by Tandem Mass Spectrometry*

The ATD features that are resolved after 3 passes were investigated in more detail using post-IM collision induced dissociation (CID). Because no further IM separation takes place, ATDs of product ions are time-aligned with precursor ATD features. Thus, diagnostic product ions can be used to deduce 3C5NBA derivatization sites in precursor isomers as well as to identify isomers not fully resolved in ATD space.

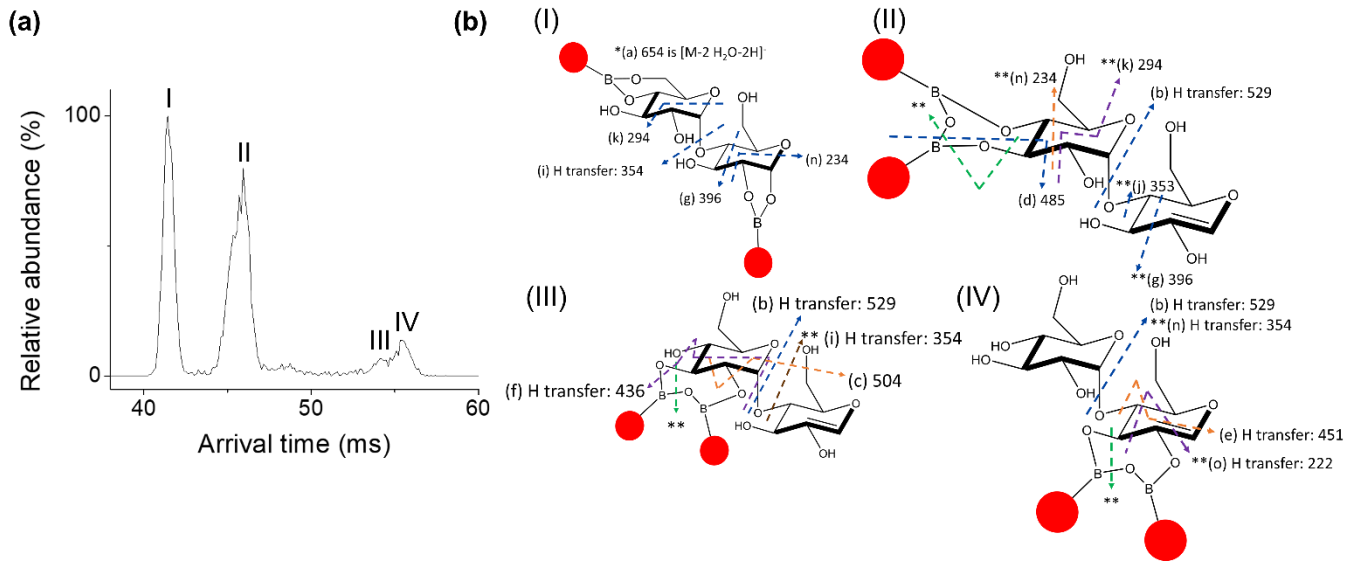


**Figure 3.10**. Post-IM CID experiment on doubly-derivatized maltose. (a) ATD of precursor ions after 3 passes around the cIM device; three features are resolved (I at 41.5 ms, II at 45.7 ms, and another feature formed from two partially unresolved peaks III at 52.8 ms and IV at 55.4 ms). (b) The proposed structural assignments for features I-IV in Figure 5 are based upon the fragmentation patterns shown. Fragment *m/z* correspond with Figure S-6: (a) 654 ($C_{26}H_{22}B_2N_2O_{17}$), (b) 529 ($C_{20}H_{17}B_2N_2O_{14}$), (c) 504 ($C_{18}H_{16}B_2N_2O_{14}$), (d) 485 ($C_{18}H_{19}BNO_{14}$), (e) 451 ($C_{18}H_{11}B_2N_2O_{11}$), (f) 436 ($C_{17}H_8B_2N_2O_{11}$), (g) 396 ($C_{15}H_{16}BNO_{11}$), (h) 392 ($C_{16}H_{16}BNO_{10}$), (i) 354($C_{13}H_{14}BNO_{10}$), (j) 353 ($C_{13}H_{13}BNO_{10}$), (k) 294 ($C_{11}H_{10}BNO_8$), (l) 281 ($C_{14}H_9BNO_5$), (m) 255 ($C_{12}H_7BNO_5$), (n) 234 ($C_9H_6BNO_6$), and (o) 222 ($C_8H_6BNO_6$). Fragments h, l, and m require rearrangements and are therefore not included in this figure. ** represents a loss of one 3-carboxy-5-nitrophenyl-borane group.

The proposed structural assignments of features resolved in the ATD of doubly-derivatized maltose provide an interesting example of the post-IM CID capabilities of the cIM system (Figure 3.10). Four main mobility features were identified (I-IV), with corresponding CID product ion spectra presented in Figure 3.11 a-d, respectively. The ATD for each of these fragments is shown in Figure 3.12. Certain fragments aligned almost entirely with a single ATD peak, such as *m/z* 654, 485, and 451 aligned with feature I, II, and IV, respectively (Figure 3.12a,d,e). Most fragments aligned with at least two of the peaks, such as *m/z* 529 and 354 (Figure 3.12b,i). A summary of the correlation of each fragment's *m/z* and arrival time distribution is shown in Figure 3.13. The dominant *m/z* peaks produced from feature I were *m/z* 396 ($C_{15}H_{15}BNO_{11}$), 294 ($C_{11}H_9BNO_8$), and 354 ($C_{13}H_{13}BNO_{10}$), which corresponded to a 3,4 cross-ring cleavage on the former reducing end of the sugar, a 1,2 cross-ring cleavage on the non-reducing end, and a cleavage of the glycosidic bond followed by a proton transfer, respectively (Figure 3.10). These

fragments are only plausible for a derivative with each 3C5NBA molecule on a separate glucose residue, such as the product shown in Figure 3.2d. The most abundant product ions that originated from feature II are *m/z* 485 ($C_{19}H_{15}B_2N_2O_{12}$), which was produced by a 2,6 ring cleavage followed by a proton transfer, 353 ($C_{13}H_{12}BNO_{10}$) from a loss of one 3-carboxy-5-nitrophenyl-borane (** in Figure 3.10) and a cleavage of the glycosidic bond, 396 ($C_{15}H_{15}BNO_{11}$), from the same ** loss followed by a 3,4 ring cleavage on the former reducing end of the sugar, and 294 ($C_{11}H_9BNO_8$), from the loss of ** followed by a 3,6 ring cleavage on the non-reducing end (Figure 3.10). For feature III, the major fragments were *m/z* 504 ($C_{18}H_{16}B_2N_2O_{14}$), which originated from a loss of ** followed by the cleavage of the glycosidic bond and 436 ($C_{18}H_{11}B_2N_2O_{10}$), originating from the cleavage of the glycosidic bond, a 1,4 ring cleavage, a loss of an oxygen atom, and a water loss (Figure 3.10). The most abundant fragments for feature IV are *m/z* 354 and 529, which have been described for other features as well as *m/z* 255 ($C_{12}H_7BNO_5$), which requires rearrangement to be produced. Interestingly, the diagnostic product ion at m/z 529 can only be produced by the 3C5NBA anhydride dimer reacting with two trans diols on the maltose unit (Figure 3.2a-c) and not with two 3C5NBA molecules reacting with two cis diols each on maltose. Certain fragments only appeared in significant yields for one feature, leading to the possibility for tentative structural identification, as shown in Figures 3.9 and 3.10. For example, *m/z* 654 ($C_{26}H_{22}B_2N_2O_{17}$) was unique for feature I, m/z 485 ($C_{18}H_{19}BNO_{14}$) was unique for feature II, *m/z* 436 ($C_{17}H_8B_2N_2O_{11}$) was unique for feature III, and *m/z* 451 ($C_{18}H_{11}B_2N_2O_{11}$) was unique for feature IV.

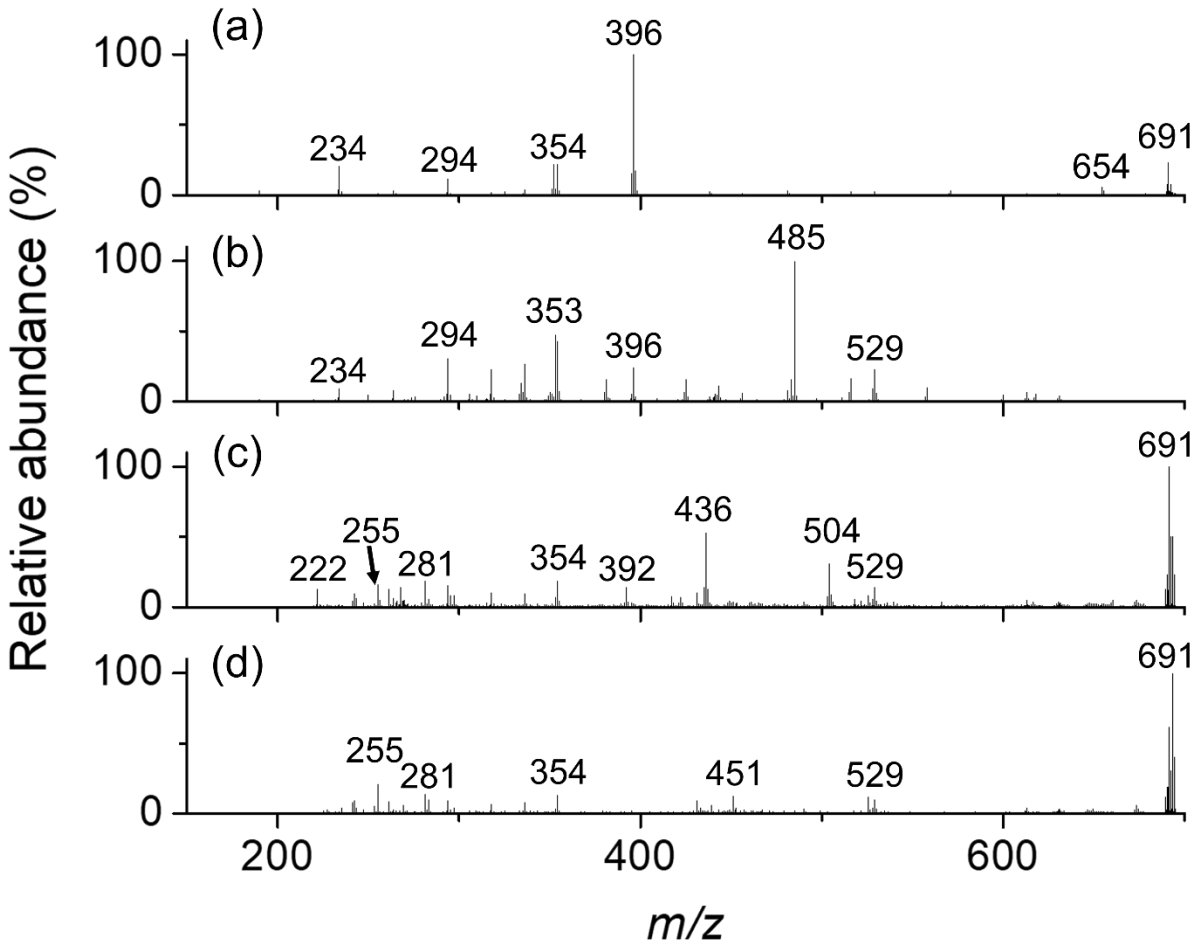


**Figure 3.11.** Tandem MS spectra shown in a-d correspond to CID product ions generated from features I-IV in the maltose derivative ATDs in Figure 3.10.

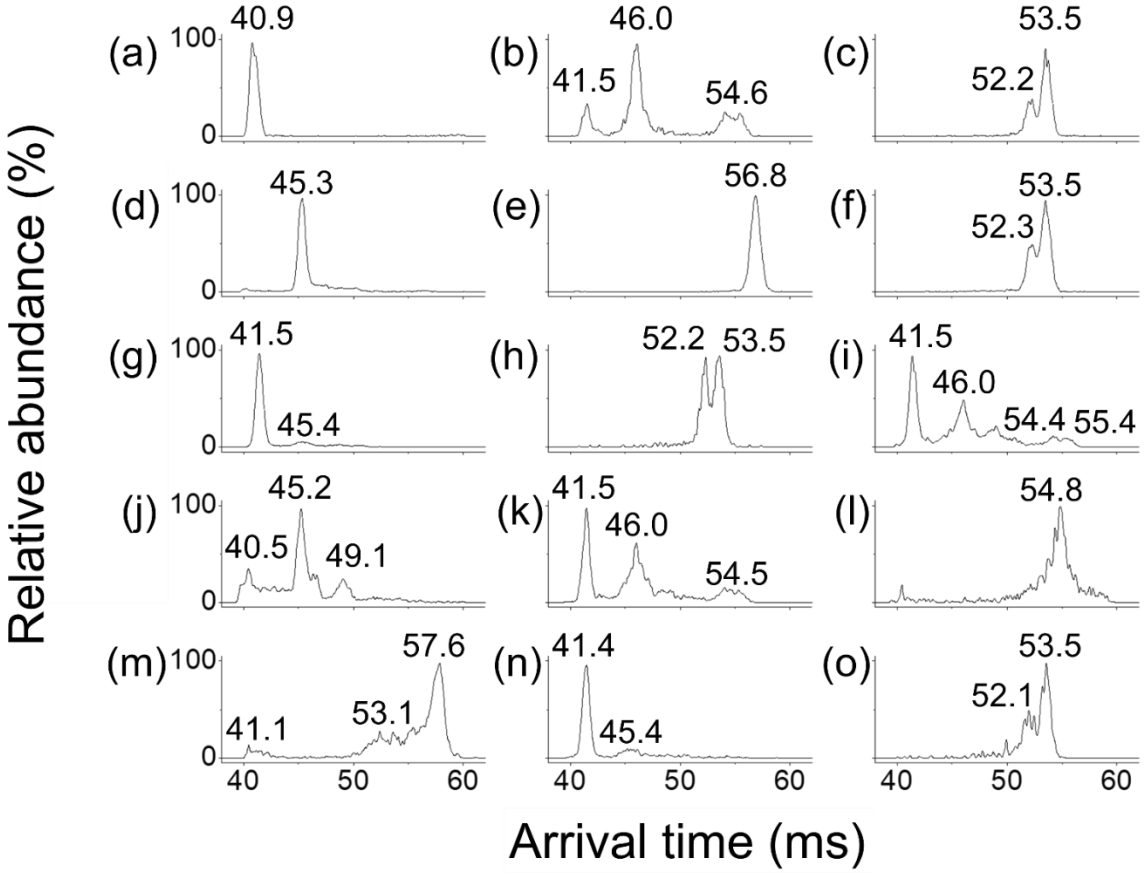


**Figure 3.12.** ATDs for the doubly 3C5NBA-derivatized maltose precursor and MS/MS product ions at *m/z* (a) 654 ($C_{26}H_{22}B_2N_2O_{17}$), (b) 529 ($C_{20}H_{17}B_2N_2O_{14}$), (c) 504 ($C_{18}H_{16}B_2N_2O_{14}$), (d) 485 ($C_{18}H_{19}BNO_{14}$), (e) 451 ($C_{18}H_{11}B_2N_2O_{11}$), (f) 436 ($C_{17}H_8B_2N_2O_{11}$), (g) 396 ($C_{15}H_{16}BNO_{11}$), (h) 392 ($C_{16}H_{16}BNO_{10}$), (i) 354($C_{13}H_{14}BNO_{10}$), (j) 353 ($C_{13}H_{13}BNO_{10}$), (k) 294 ($C_{11}H_{10}BNO_8$), (l) 281 ($C_{14}H_9BNO_5$), (m) 255 ($C_{12}H_7BNO_5$), (n) 234 ($C_9H_6BNO_6$), and (o) 222 ($C_8H_6BNO_6$). Certain fragments that correspond to the lowest abundance isomer III show some deviation in drift time, most likely due to low abundance and the overlap between III and IV convoluting the drift times.

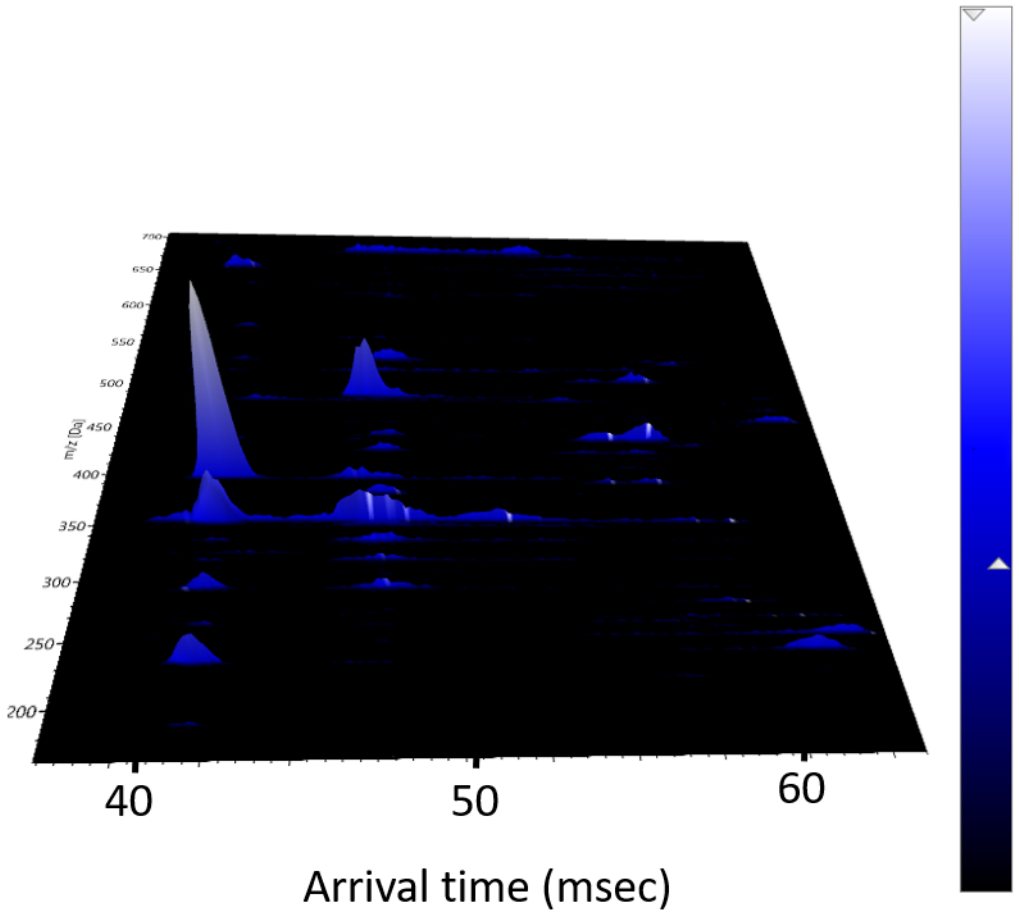


**Figure 3.13.** A 2-dimensional plot showing the correlation between *m/z* and drift time of each of the doubly 3C5NBA-derivatized maltose MS/MS fragments.

IM-CID-MS experiments can also aid with identification of the carbohydrates investigated, which would be particularly beneficial for analysis of a mixture containing various saccharides. For example, based on 3-pass ATD information alone, mannose could not be mobility separated from glucose ($R_{pp}$ = 0.38); and fructose could not be separated from galactose ($R_{pp}$ = 0.53). However, the combined technique of IM-CID-MS distinguished mannose and glucose by their unique diagnostic product ions at *m/z* 438.97 for mannose and 402.96, 353.97, and 441.02 for glucose (Table 3.4). Fructose and galactose also had unique product ions that distinguished them, as the fructose derivative produced the product ions at *m/z* 438.97 and 441.02, which galactose did not. Galactose produced product ions at *m/z* 353.97, 384.94, and 402.96, which fructose did not. Only galactose displayed a unique product ion at *m/z* 468.99.

**Table 3.4.** MS/MS fragments observed for each monosaccharide derivative. Unique fragments are highlighted in yellow. Highlighted in blue are fragments that can distinguish isomers that have less than 1.00 resolution at three cIM passes without including isomers that are separated in the mobility dimension.

| Fructose | Galactose | Glucose | Mannose |
|---|---|---|---|
| 165.90 | 165.90 | 165.90 | 165.90 |
| 191.89 | 191.89 | 191.89 | 191.89 |
| 209.90 | 209.90 | 209.90 | 209.90 |
| 219.92 | 219.92 | 219.92 | 219.92 |
| 263.92 | 263.92 | 263.92 | 263.92 |
| 293.93 | 293.93 | 293.93 | 293.93 |
| 317.94 | 317.94 | 317.94 | 317.94 |
| 335.95 | 335.95 | 335.95 | 335.95 |
| | 353.97 | 353.97 | |
| | 384.94 | 384.94 | 384.94 |
| | 402.96 | 402.96 | |
| 438.97 | | | 438.97 |
| 441.02 | | 441.02 | |
| | 468.99 | | |
| | | 511.01 | 511.01 |

For the eight disaccharide derivatives, unique product ions were seen for lactulose (*m/z* 493.08, 469.07), maltose (*m/z* 678.19, 558.10), melibiose (*m/z* 480.04), sucrose (*m/z* 194.89), and trehalose (*m/z* 675.15, 424.95), as described in Table 3.5. Doubly-derivatized disaccharides that could not be differentiated based on IM separation alone were cellobiose/sucrose and isomaltose/lactulose/trehalose. Cellobiose generated diagnostic product ions at *m/z* 631.1, 485.023, and 456.03 that were not observed for sucrose (Table 3.5). Isomaltose produced ions at *m/z* 631.10, 441.02, 409.03, 395.99, 349.00, and 275.92 that did not appear for either lactulose or trehalose (Table 3.5). In summary, combining high-

resolution IM separations with post IM CID is clearly useful for identifying these sugar derivatives and pursuing in depth analysis of their structural characteristics.

**Table 3.5.** MS/MS fragments listed for each disaccharide derivative. Unique fragments are highlighted in yellow.

| Cellobiose | Isomaltose | Lactose | Lactulose | Maltose | Melibiose | Sucrose | Trehalose |
|---|---|---|---|---|---|---|---|
| | | | | 683.15 | | 683.15 | 683.15 |
| | | | | 678.19 | | | |
| | | | | | | | 675.15 |
| | 673.13 | 673.13 | 673.13 | | | | |
| | | | | 668.16 | | 668.16 | |
| | 655.11 | | | | 655.19 | | |
| | | | | | | 647.14 | 647.14 |
| 631.11 | 631.10 | 631.19 | | | 631.19 | | |
| 613.09 | | 613.08 | | | 613.98 | 613.97 | |
| | | | | | | 603.13 | 603.13 |
| | | 571.15 | | 571.06 | 571.15 | | |
| | | | | 558.10 | | | |
| 529.03 | 529.03 | 529.03 | 529.03 | 529.03 | 529.03 | 529.03 | 529.03 |
| | | | | 516.07 | | | 516.08 |
| 511.02 | 511.01 | 511.02 | 511.02 | | | 511.10 | 511.11 |
| | | | 493.08 | | | | |
| 485.02 | 485.02 | | | | | | 485.02 |
| | | | | | 480.04 | | |
| | | | 469.07 | | | | |
| 456.03 | 456.03 | 456.03 | | | 456.03 | | |
| | 441.02 | | | | | 441.02 | 441.03 |
| | | | | | | | 424.95 |
| | 409.03 | 409.04 | | 409.04 | | | |
| 395.99 | 395.99 | 395.99 | | 395.99 | 395.99 | | |
| | | | 367.02 | | | 367.02 | |
| 353.97 | 353.97 | 353.97 | 353.97 | 354.00 | 353.97 | 353.97 | 353.97 |
| | 349.00 | | | | 349.00 | 349.00 | |

| | | | | | | | |
|---|---|---|---|---|---|---|---|
| 335.95 | 335.95 | 335.95 | 335.95 | 335.95 | 335.95 | 335.95 | 335.96 |
| 317.94 | 317.94 | 317.94 | 317.94 | 317.94 | 317.94 | 317.94 | |
| | | 309.97 | 309.97 | 309.97 | | | 309.97 |
| 293.93 | 293.93 | 293.93 | 293.93 | 293.93 | 293.93 | 293.93 | 293.94 |
| | 275.92 | | | | 275.92 | | |
| 263.92 | 263.92 | 263.92 | 263.92 | 263.92 | 263.92 | 263.92 | 263.92 |
| 249.94 | 249.93 | 249.93 | 249.93 | | 249.94 | 249.93 | 249.94 |
| 233.90 | 233.90 | 233.90 | 233.90 | 233.90 | 233.90 | 233.90 | 233.94 |
| 219.92 | 219.92 | 219.92 | 219.92 | 219.92 | 219.92 | 219.92 | 219.92 |
| 209.90 | 209.90 | 209.90 | 209.90 | 209.90 | 209.90 | 209.90 | 209.90 |
| | | | | | | 194.89 | |
| | | | 191.8863 | | 191.88 | | |
| 189.91 | 189.90 | 189.91 | | 189.91 | 189.91 | 189.90 | 189.90 |
| 165.89 | 165.91 | 165.91 | 165.91 | 165.88 | 165.90 | 165.89 | 165.90 |

### 3.5. Conclusion

Separations with cIM allowed for the identification and structural characterisation of 3C5NBA derivatives of mono- and disaccharides. After 3 passes around the cIM device ($R_p$~120), 3C5NBA carbohydrate derivatives were resolved in all cases for four monosaccharide standards, and all but two cases for eight disaccharide standards. Additional passes could improve separations of isomers with overlapping ATDs; however, there is a limit to the number of additional passes that maybe performed. In the future, novel cIM methods using a selection based upon ion mobility in an analogous way to heartcuts in chromatography will help to overcome these issues.[48-49] This methodology involves the selection of a window of arrival times similar to *m/z* selection in MS/MS. This would allow for a greater number of passes to be performed for these analytes, which would further enhance separations. With the improved resolving power made accessible by these techniques, cIM-MS/MS may be a viable method to characterize

complex mixtures of carbohydrates. These methods could then be utilized to study mixtures of carbohydrates formed under abiotic conditions, which are currently under investigation in our laboratory.

# CHAPTER 4. Organic Acid Shift Reagents for the Discrimination of Carbohydrate Isobars by Ion Mobility-Mass Spectrometry

*Adapted from*

McKenna, K. R.; Li, L.; Krishnamurthy, R.; Liotta, C. L.; Fernández, F. M. *Analyst*, **2020**, *145*, 8008-8015. K. R. McKenna designed and performed the experiments within this chapter. L. Li developed the idea for using amino and α-hydroxy acids as IM shift reagents for disaccharides. R. Krishnamurthy, C. L. Liotta, and F. M. Fernández assisted with the design of experiments and provided advisory roles.

## 4.1. Abstract

Carbohydrates are the most abundant class of biomolecules on Earth with a diverse array of biological functions. It is hypothesized that they likely had an important role in the development of life on the primoridal Earth as well. Since sugars have a variety of possible isobaric structures, it is necessary to characterize oligosaccharides beyond their molecular weight. Ion mobility-mass spectrometry (IM-MS) is a promising characterization technique for this purpose, as it is based on differences in charge and collision cross section (CCS). This study reports on the use of new noncovalent ligands as shift reagents to aid in the IM separations of disaccharides. A variety of organic acids were tested as shift reagents with traveling wave IM with the most promising ones being further investigated by drift tube IM. Drift tube IM provided higher resolution separations for the large majority of disaccharide complexes studied. Combining CCS results of the two most promising shift reagents allowed for the complete differentiation of all eight disaccharide standards examined in this study.

## 4.2. Introduction

Understanding the chemical processes leading to the origins of life on Earth is one of the greatest scientific questions of our time.[113] With the Miller-Urey experiment[58] leading to decades of scientific research in prebiotic chemistry, the non-enzymatic origin of biopolymers such as nucleic acids and peptides has been studied at length.[114-116] Carbohydrates are also critical

components of life, and are responsible for maintaining cell structure, intercellular communication, and various other central biological processes.[1, 3, 5, 7-8] As carbohydrates aid in the co-solubility of biopolymers, can serve as cross-linkers, and provide rudimentary catalytic activity, it is highly likely they were also important for the development of early life on the prebiotic Earth.[117]

The structures of mono- and oligosaccharides determine their properties and function, so it is critical that their characterization is performed beyond their molecular weight. For example, certain sugars are non-reducing and can protect other molecules from stress caused by pH or temperature changes, whereas reducing sugars can react with amino acids and other biologically-relevant molecules.[2, 118-119] Carbohydrates are structurally diverse and complex, and have received less attention in prebiotic chemistry when compared to peptides and nucleic acids.[120-121] Polysaccharides contain a great diversity of monomeric units, each with several possible linkages, as well as the potential for branching. Additionally, each anomeric carbon can have either an α or β configuration, doubling the possible number of structures to be detected and resolved. Because of their identical elemental formulas, these isobars cannot be distinguished even with the use of ultrahigh resolution-mass spectrometry (MS).

Several analytical methods have been utilized to characterize oligosaccharides. Tandem mass spectrometry (MS/MS), for example, can efficiently distinguish relatively pure disaccharide samples. It cannot, however, effectively characterize lower abundance components in complex mixtures of isobaric carbohydrates.[16-17] Nuclear magnetic resonance (NMR) spectroscopy can also be very useful, but requires higher concentrations, and can therefore be more time consuming.[122-124] Liquid chromatography (LC) has been extensively used for disaccharide identification, but it is relatively slow and may require derivatization for higher resolution separations.[13-14] Capillary

electrophoresis (CE) is also an effective method for carbohydrate separations, but some degree of *a priori* knowledge about the oligosaccharides being separated is typically required.[125-127]

Ion mobility (IM) separations coupled to mass spectrometric detection (IM-MS) have been shown to be a viable complement to other established, yet limited, techniques. This method requires lower sample concentrations than NMR, shorter analysis times than either NMR or LC and, with sufficient resolving power $\left(\boldsymbol{R_p = \frac{t_d}{\Delta t_d}}\right)$,[128] can distinguish isomeric species in complex mixtures. IM separations depend on the mobility coefficient (*K*), which determines the velocity of the gas phase ions in the electric field. *K* depends on a variety of instrumental parameters, masses of ion and gas molecules, and their rotationally-averaged collision cross section (CCS). The latter parameter can be correlated to the 3D structure of ions.[129]

Traveling wave IM spectrometry (TWIMS) is an IM technique wherein the mobility separator is comprised of a series of electrodes enclosed in a gas filled cell (~2 mbar $N_2$). A series of voltage pulses is applied sequentially to each electrode, propelling ions through the device.[41] Ions can "surf" or "roll over" the wave falling back into the preceding wave. Ions of lower mobility undergo more roll over events than higher mobility ions, effectively leading to mobility separation. Drift times ($t_d$) measured in TWIMS can be converted to CCS using calibration procedures.[42-44] A number of calibrant compounds have been proposed.[45] Resolving power ($R_p$) of an IM separator can be improved by increasing its length.[46] Recently, Giles *et al.* developed a traveling wave-enabled, cyclic IM (cIM) instrument with multi-pass capabilities.[47] In this instrument, IM resolving power increases as a function of the square root of the number of passes, *n* ($\boldsymbol{R_p \sim 70\sqrt{nz}}$);[47] here 70 is the approximate, single pass resolving power and z is the ion's charge state. Normally, the maximum number of passes is limited by the so called "wrap-around" effect that occurs when the spatial width of the separated ion packets exceeds the length of the cIM device.[48] The cIM control enables selective ejection of ions in a specified range of arrival times

from the cIM device that can be followed by activation and/or further separation of product ions ($IMS^n$).[48-49] These functionalities have been used previously for structural studies of carbohydrate[49-50] and protein ions.[51]

Isomeric pentasaccharides, including anomers, have been shown to be able to be separated by the cIM system.[49] Typically, isobaric mono- and disaccharides do not have sufficiently-different CCS values to be separated by commercially-available IM systems. To mitigate this issue, shift reagents — ligands that can bind either covalently or non-covalently to amplify CCS differences between isobaric carbohydrates — have been utilized. Previous examples of shift reagents include alkali and alkaline earth metal cations, and 1-phenyl-3-methyl-5-pyrazolone.[11-12, 52] In recent work, we reported a new shift reagent for carbohydrates, 3-carboxy-5-nitrophenyl boronic acid (3C5NBA) that rapidly reacts with mono- and disaccharides, enhancing their IM separation.[53] Due to the initial promise shown by 3C5NBA, we here evaluate its applicability in combination with high-resolution cIM-MS instrumentation. In addition, we utilized the tandem IMS ($IMS^2$) capability to probe the possibility of interconversion between mobility separated mannose derivatives.

## 4.3. Experimental

### *4.3.1. Reagents and Chemicals*

Isomaltose, trehalose, and cellobiose were obtained from TCI (Philadelphia, PA). Maltose, lactose, lactulose, sucrose, NMDA, arginine, tyrosine, lactic acid, 2-hydroxyhexanoic acid, N-methyl-L-glutamic acid, citric acid, and N-methyl-DL-aspartic acid were purchased from Sigma Aldrich (St. Louis, MO). Melibiose was obtained from Fluka. L-malic acid and L-tartaric acid were purchased from VWR (Radnor, PA).

### *4.3.2. Noncovalent Modification of Carbohydrates*

Stock solutions (1 mM) of carbohydrate standards (cellobiose, isomaltose, lactose, lactulose, maltose, melibiose, sucrose, and trehalose) and shift reagents (L-malic acid, NMDA, tyrosine, lactic acid, 2-hydroxyhexanoic acid, tartaric acid, arginine, N-methyl-L-glutamic acid, N-methyl-DL-aspartic acid, and citric acid) were prepared in water. Five µL of the 1 mM carbohydrate solution and 5 µL of the 1 mM shift reagent solution were added to 990 µL of unbuffered deionized water prior to analysis.

### *4.3.3. Traveling Wave Ion Mobility-Mass Spectrometry Analysis*

Traveling wave arrival time distribution (ATD) measurements were performed using SYNAPT G2 and G2-S HDMS ion mobility-mass spectrometers (Waters Corp., Wilmslow, UK). All experiments used direct infusion electrospray ionization. Ion source settings for positive and negative ion mode were as follows, respectively: capillary voltage, 3.0/-2.5 kV; cone voltage, 40 V; source temperature, 80 °C; desolvation temperature, 100/150 °C; desolvation gas flow 500 L $h^{-1}$; cone gas flow, 0 L $h^{-1}$. The travelling wave velocity was 500 m $sec^{-1}$ with a wave height of 40 V. Nitrogen was used as the drift gas in all cases. $^{TWIM}CCS_{N2}$ calibration in negative ion mode was performed with both polyalanine and polymalic acid according to the methods reported by Forsythe *et al.*[130] In positive ion mode, $^{TWIM}CCS_{N2}$ calibration was performed using polyalanine as the sole calibrant, following CCS values reported by Bush *et al.*[130, 135] Tandem MS experiments were performed without IM on the Synapt G2-S instrument with collision energies of 1 and 2 eV and LM resolution values of 15 and 9 for positive and negative ion modes, respectively. For negative ion mode MS/MS experiments, the concentration for both lactose and L-malic acid were 10 µM. For positive ion mode MS/MS experiments, the concentration for lactose and NMDA acid were 5 and 50 µM, respectively. These concentrations were determined empirically to produce signals for MS/MS with good signal-to-noise ratios. For breakdown curve MS/MS experiments,

an equal concentration of 35 μM of lactose and each respective shift reagent was used. The resulting sigmoidal curves were fit in Origin 8.5 to determine their inflection points.

### *4.3.4. Molecular Dynamics Calculations*

The L-malic acid and NMDA complexes for each of the eight disaccharide standards were investigated by density functional theory calculations based on those reported by Zheng *et al.*[136] Two-dimensional structures for each of the eight standards and the two shift reagents were obtained from Chemspider as .mol files.[137] The Chemaxon Marvin Suite was used to calculate the $pK_a$ of each hydrogen on each molecule to determine the most likely shift reagent binding sites. Avogadro was utilized to convert the two-dimensional structures into three-dimensional structures, as well as combining the disaccharide and shift reagent into the same file.[138] Preliminary geometry optimization was performed in Avogadro, followed by further optimization in NWChem[139] at the B3LYP theory level[140] using the 6-31G(d) basis set.[141]

### *4.3.5. Drift Tube Ion Mobility Experiments*

An EXCELLIMS MA3100 drift tube ion mobility spectrometer was coupled with an Orbitrap mass spectrometer for DTIM measurements at atmospheric pressure, as described previously by Keelor *et al.*[142] The drift gas temperature was 100 ºC for positive ion mode experiments and 90 ºC for negative ion mode experiments. The electrospray ion source was operated at 2.3 kV and -2.2 kV in positive and negative ion modes, respectively. The maximum injection time for the Orbitrap was set to 1000 ms. The length of the drift tube was 10.55 cm, and electric fields in the 758-853 V $cm^{-1}$ range were used. Gating voltages of 60 V for gate 1, and 81 V for gate 2 were empirically optimized to maximize ion transmission without excessive ion gate leakage. The drift gas was infused at 2.00 L $min^{-1}$. and removed at 0.50 L $min^{-1}$ to keep the system at atmospheric pressure (~740 Torr in Atlanta, GA, USA). The EXCELLIMS software program VisIon was used in "scan mode" to pulse the gates for 200 μs, with a delay of 20 ms between gates.

Results were manually extracted from the Orbitrap software Xcalibur to Excel, and then processed in Origin 8.5.

## 4.4. Results and Discussion

### *4.4.1. Noncovalent Modification*

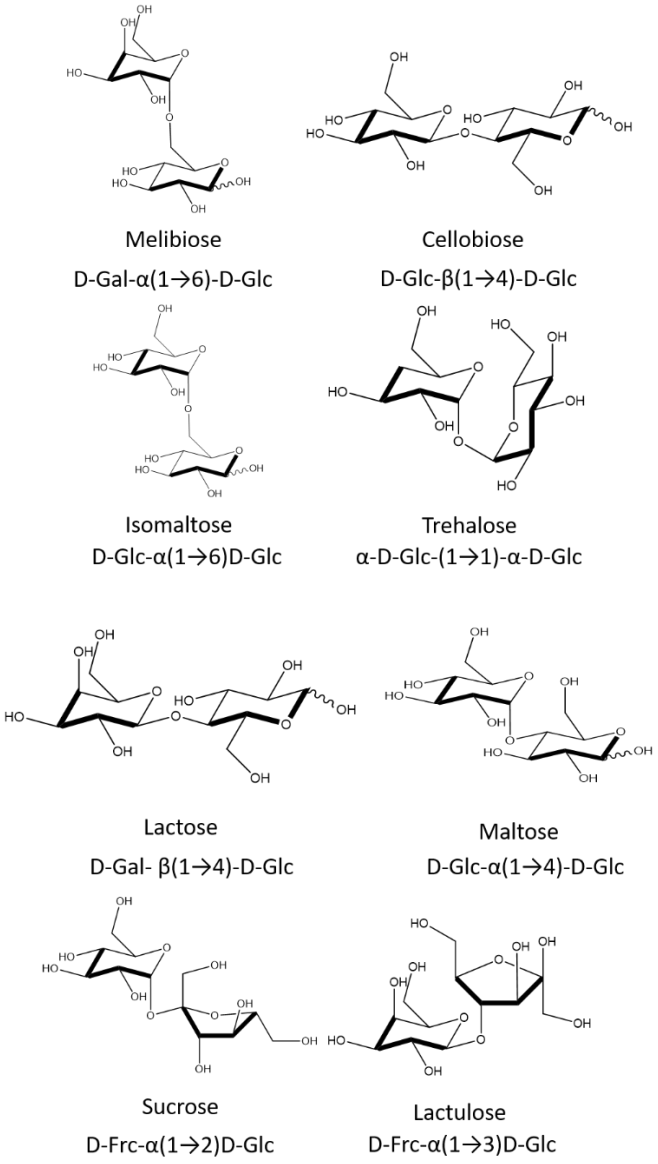


**Figure 4.1.** Structures of the isobaric disaccharides examined in this study.

The eight disaccharide analytes tested in this study are depicted in Figure 4.1. Maltose, trehalose, isomaltose, and cellobiose are all glucopyranosyl-glucose isomers. The remaining disaccharides included in the study contained glucose, galactose, and fructose as monomeric units.

One pair of anomers, maltose and cellobiose, was included with the purpose of evaluating the utility of the studied shift reagents for distinguishing closely related stereoisomers.

### *4.4.2. Traveling Wave Ion Mobility Separations*

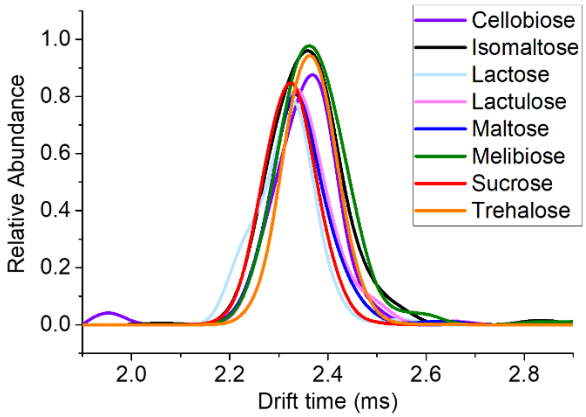


**Figure 4.2.** Overlaid arrival time distributions for the [M-H]- ion of each of the eight disaccharide analytes studied. No shift reagents were used in these experiments, which were conducted by direct infusion on a Synapt G2 TWIM-MS system in negative mode with nitrogen as the buffer gas. The wave height and wave velocity were 40 V and 500 m $s^{-1}$, respectively.

Initial TWIM experiments without the addition of shift reagents showed that none of these disaccharides could be separated as their $[M-H]^-$ ions, as seen in Figure 4.2. This was in agreement with previous studies, including one by Li *et al.*, which demonstrated that the use of ion adduction or clustering was required to separate disaccharide-derived monosaccharide-glycolaldehyde isomers using a TWIM-based approach.[143] As seen in Figure 4.2, all of the ATDs overlapped nearly completely, with none of them being baseline resolved. The $^{TWIM}CCS_{N2}$ values for the $[M-H]^-$ ions of the eight disaccharide standards are recorded in Table 4.1. These $^{TWIM}CCS_{N2}$ values varied from 159.6 for maltose to 163.9 for trehalose. This is a relative difference of 2.6% for the highest and lowest CCS analytes. When an established noncovalent shift reagent such as sodium, potassium, or chloride was added, a modest separation for certain pairs was observed, as shown in Figure 4.3.[11] For example, sucrose and maltose were partially resolved ($R_{pp}$ = $\mathbf{1.18}\left(\frac{t_{dB}-t_{dA}}{\Delta t_{dB}+\Delta t_{dA}}\right)=\mathbf{0.84}$) as their potassium adducts. It was noted, however, that improvements

in the separation were still needed to resolve other disaccharides, which is of particular importance in more complex mixtures where various species could co-exist.

**Table 4.1.** Ion-neutral CCS values for disaccharide $[M-H]^-$ ions calculated from negative ion mode TWIM-MS experiments performed on the Synapt G2 platform, using polyalanine as a calibrant. The error represents the 95% confidence interval from three trials.

| | $^{TWIM}CCS_{N2}$ (Å$^2$) polyalanine |
|---|---|
| **Cellobiose** | 163.2 ± 0.4 |
| **Isomaltose** | 161.1 ± 0.4 |
| **Lactose** | 163.2 ± 0.4 |
| **Lactulose** | 161.8 ± 0.4 |
| **Maltose** | 159.6 ± 0.4 |
| **Melibiose** | 160.4 ± 0.4 |
| **Sucrose** | 161.1 ± 0.4 |
| **Trehalose** | 163.9 ± 0.4 |

To this end, ten different α-amino or α-hydroxy acids (L-malic acid, NMDA, tyrosine, lactic acid, 2-hydroxyhexanoic acid, tartaric acid, arginine, N-methyl-L-glutamic acid, N-methyl-DL-aspartic acid, and citric acid) were evaluated for their potential as non-covalent IM shift reagents. These candidates were selected based on previous reports on some amino acids showing promise for monosaccharide separations.[57] Of the ten candidates tested, citrate was the only shift reagent considered that showed no detectable binding to any of the disaccharides investigated in this study under the studied conditions. This is likely due to citrate ionizing much more efficiently than the citrate-disaccharide noncovalent complexes.

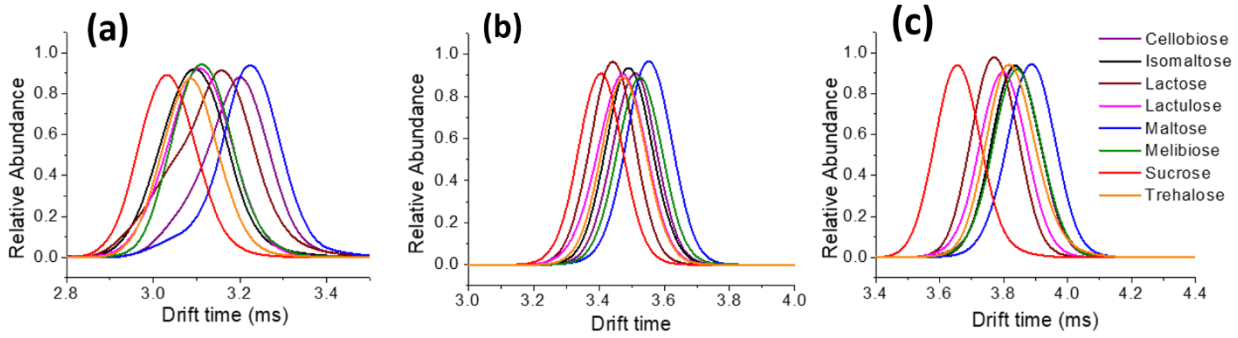


**Figure 4.3.** Overlaid arrival time distributions for (a) $[M+Cl]^-$ ions in negative mode, (b) $[M+Na]^+$ ions in positive mode, and (c) $[M+K]^+$ ions in positive mode, for each of the eight disaccharides tested, where M denotes the neutral disaccharide molecule. These experiments were performed on a Synapt G2 instrument with nitrogen as the buffer gas. The wave height and wave velocity were 40 V and 500 m $s^{-1}$, respectively.

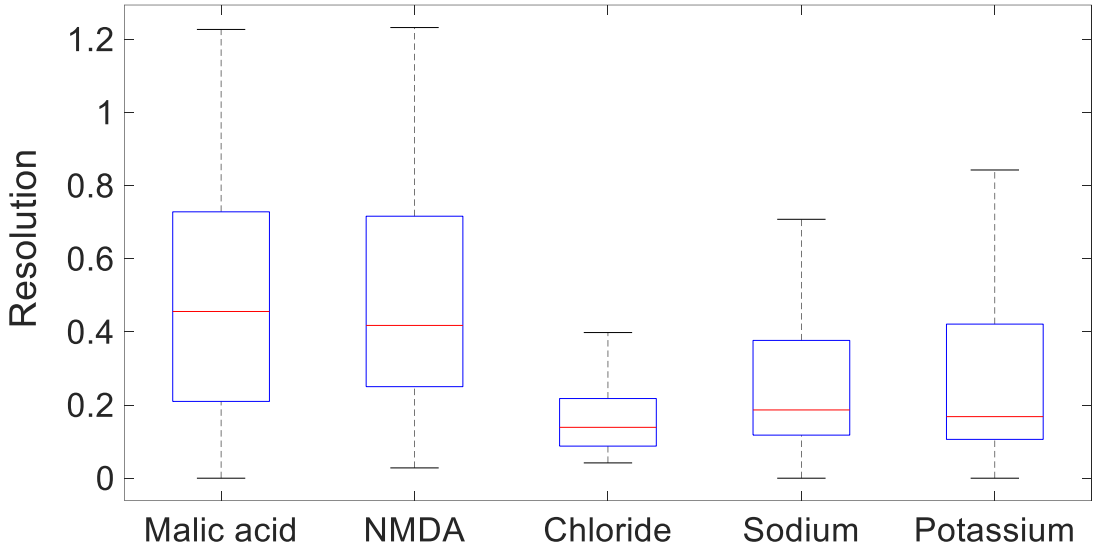


**Figure 4.4.** Boxplot showing the median and range for the ion mobility resolution of the malic acid and NMDA complexes and the chloride, sodium, and potassium adducts with the eight disaccharide standards investigated in this study.

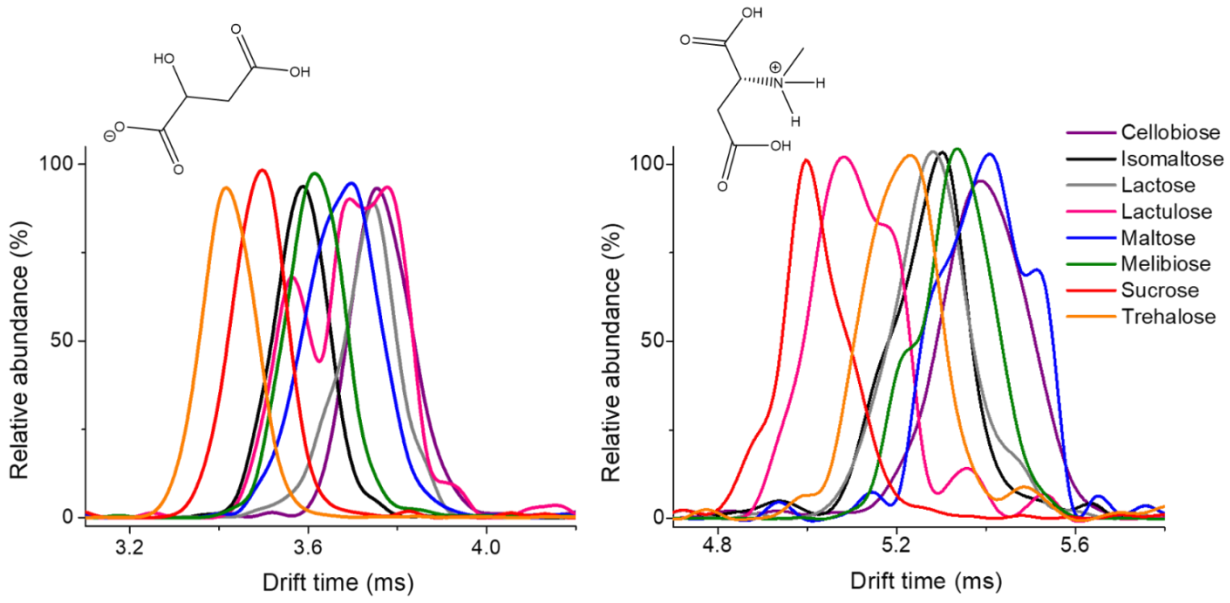


**Figure 4.5.** Overlaid arrival time distributions obtained with the Synapt G2 TWIM-MS platform for disaccharide noncovalent complexes with L-malic acid in negative ion mode (left) and N-methyl-D-aspartic acid in positive ion mode (right). The species observed are the $[M+L-H]^-$ ions (*m/z* 475.13) in negative ion mode and $[M+NMDA+H]^+$ ions (*m/z* 490.18) in positive ion mode, with M representing the neutral disaccharide and L representing neutral L-malic acid, and NMDA representing neutral N-methyl-D-aspartic acid. The wave height and wave velocity were 40 V and 500 m $s^{-1}$, respectively. B-spline connection was used to display these data, which smooths the peaks and may result in certain peaks appearing to be less than 100% in relative abundance.

From these screening experiments, L-malic acid in negative ion mode and NMDA in positive ion mode were identified as the most promising shift reagents, as they showed the highest average resolution values for each possible pair of the eight disaccharides. These reagents were compared to the more established shift reagents included in Figure 4.3 by assessing the resolution values as a boxplot, shown in Figure 4.4. The median resolution values for the L-malic acid and NMDA complexes significantly exceeded those of chloride. While they appeared to have a higher median resolution than the sodium and potassium complexes as well, this was not a significant difference due to the high variability in resolution values. The ATD for the complexes of L-malic acid and NMDA with each of the disaccharides are shown in Figure 4.5. Most of the complexes showed a single peak in the ATD, implying either a single major structure or multiple structures that are too close in CCS to be resolved. However, two major peaks were observed for the

lactulose/L-malic acid complex, most likely due to the shift reagent binding to different sites on lactulose. Both L-malic acid and NMDA allowed for the differentiation of most, but not all, of the disaccharide standard complexes. For example, L-malic acid showed good separation for sucrose and melibiose but less separation of cellobiose and lactulose, whereas NMDA showed good separation for cellobiose and lactulose with less separation for trehalose and cellobiose. Separations were evaluated based upon the 95% confidence interval for the CCS. Certain disaccharides were separated very well with both shift reagents, such as sucrose and cellobiose; others were more difficult to separate, such as melibiose and isomaltose. TWIM resolution for the separation of the disaccharide adducts ranged from 0.03-1.2 for NMDA and 0-1.2 for L-malic acid, as shown in Table 4.2.

### *4.4.3. Characterization of the Complexes Through Experimental and Molecular Dynamics Methods*

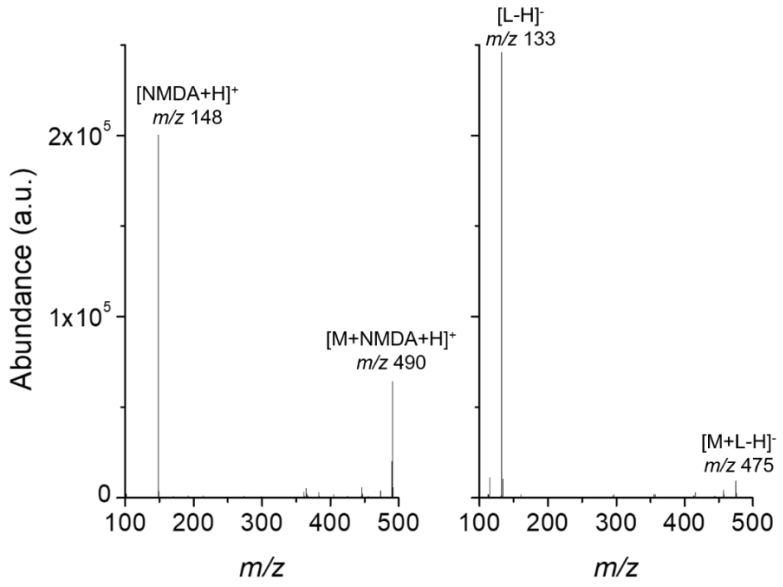


**Figure 4.6.** Tandem mass spectrometry of the $[M+NMDA+H]^+$ (left) and $[M+L-H]^-$ (right) complexes where M is lactose, a representative disaccharide, NMDA is N-methyl-D-aspartic acid, and L is L-malic acid. These experiments were performed on the Synapt G2-S HDMS platform without IM. These experiments were conducted with collision energies of 1 and 2 eV and LM resolution values of 15 and 9 for positive and negative ion modes, respectively.

L-malic acid and NMDA noncovalent complexes with all disaccharide standards were also characterized by MS/MS experiments at low collision energies. Example MS/MS results for the NMDA and L-malic acid complexes of lactose in positive and negative ion modes, respectively, are shown in Figure 4.6. Due to the lower polarity of the sugar analytes relative to the shift reagents, the major product ion for each of the complexes was the ionized shift reagent itself: $[NMDA+H]^+$ in positive ion mode, and $[malic\ acid-H]^-$ in negative mode. Tandem MS was further used to characterize the relative binding strength of the noncovalent complexes of lactose with each of the ten shift reagents used in this study that showed detectable levels of binding. Each of these lactose complexes was fragmented at various collision energies, and the area of the precursor ion relative to the total ion area was calculated, as shown in Figure 4.7. Based upon the inflection point of fitted sigmoidal curves, the strength of the binding was ranked. L-malic acid, NMDA, and tartaric acid were the weakest binding shift reagents, as ≥25% fragmentation occurred before any collision energy was applied. The remaining complexes could be ranked from weakest to strongest binding as follows: N-methyl-DL-aspartic acid< N-methyl-L-glutamic acid< L-glutamic acid< lactic acid< 2-hydroxyhexanoic acid< tyrosine< arginine.

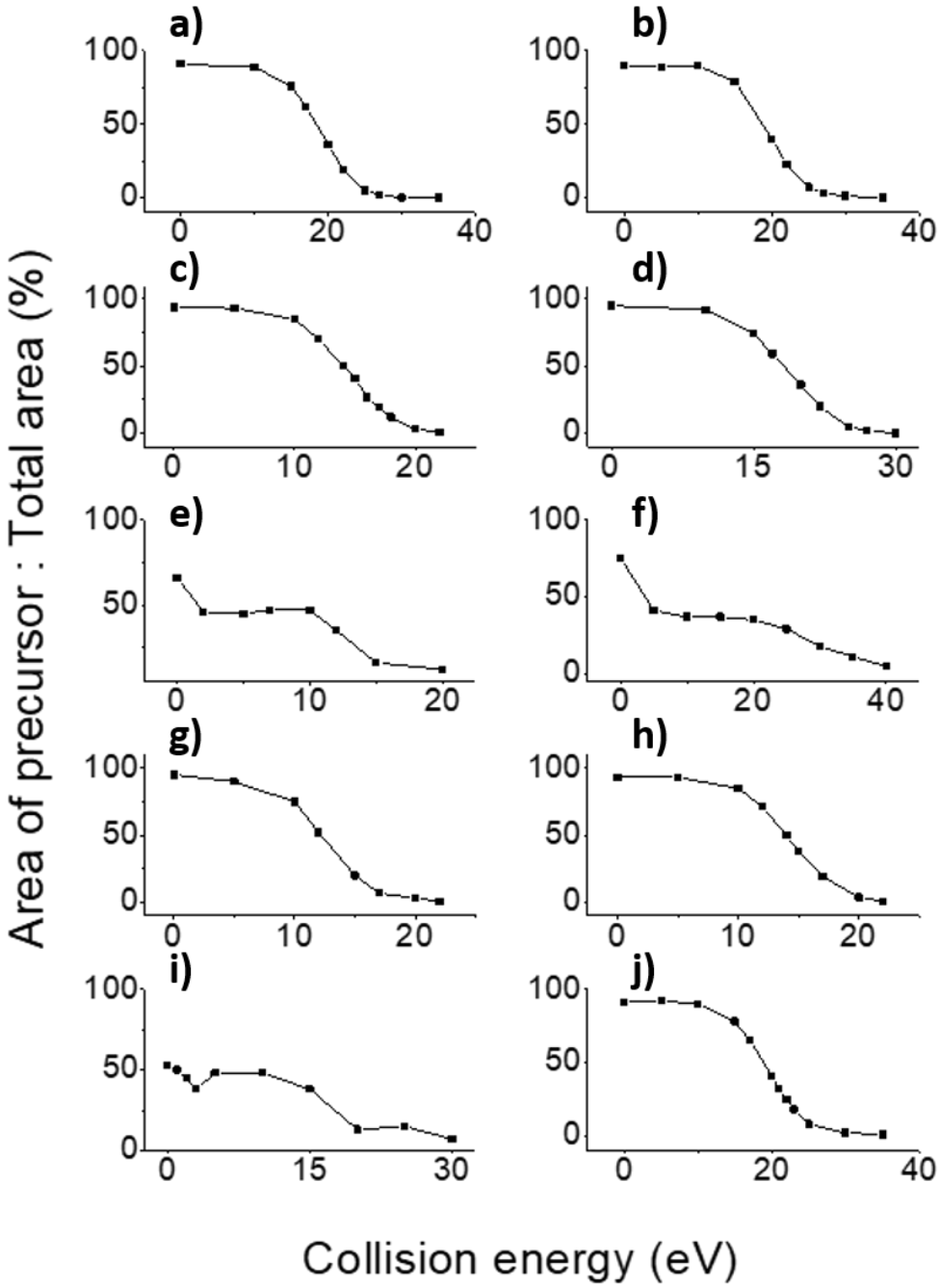


**Figure 4.7.** Breakdown curves for noncovalent lactose complexes with a) 2-hydroxyhexanoic acid, b) arginine, c) L-glutamic acid, d) lactic acid, e) L-malic acid, f) N-methyl-D-aspartic acid, g) N-methyl-DL-aspartic acid, h) N-methyl-L-glutamic acid, i) tartaric acid, and j) tyrosine. All experiments were performed in negative ion mode except for those involving the N-methyl-D-aspartic acid complex, which was performed in positive ion mode.

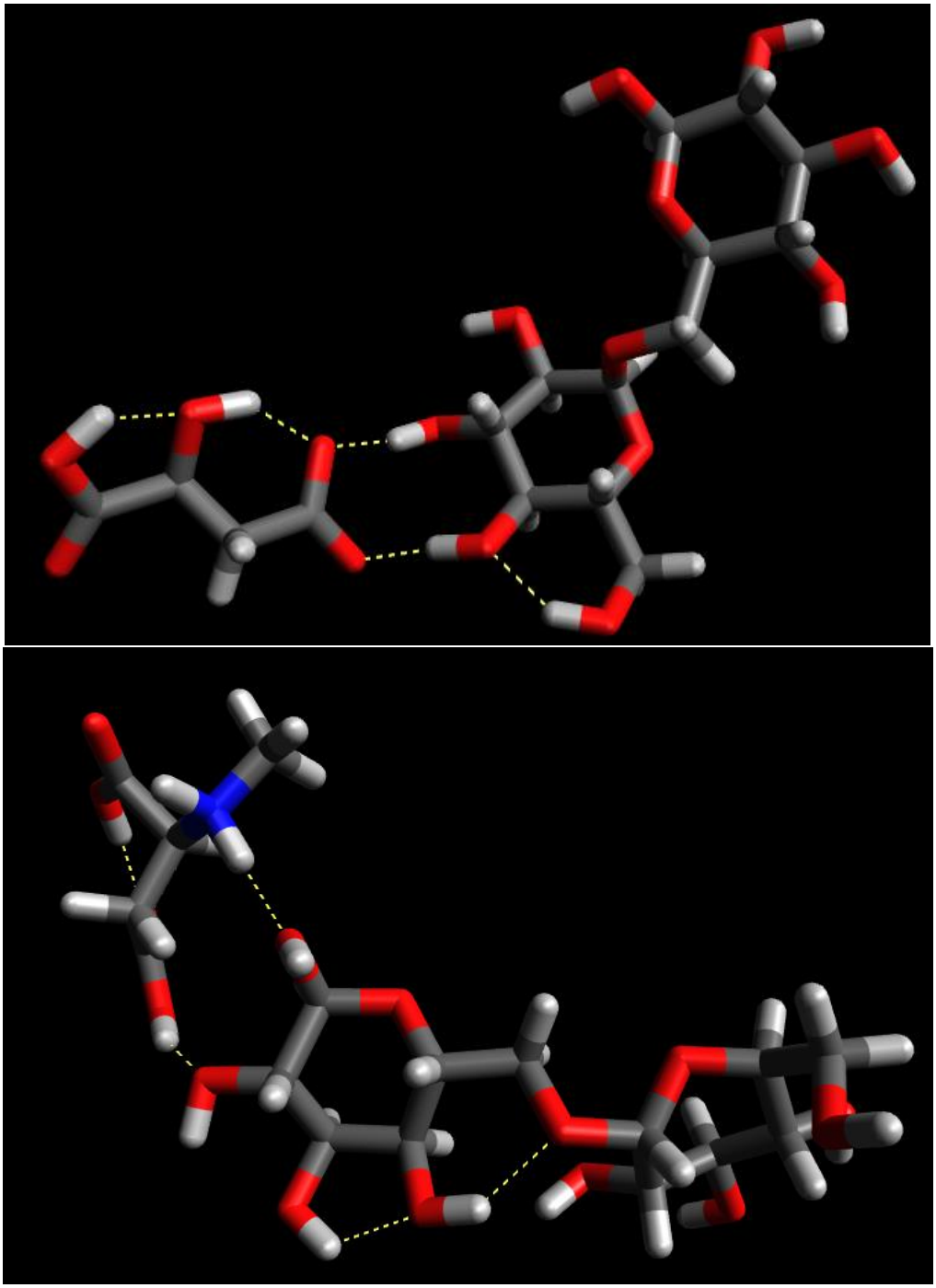

**Figure 4.8.** Molecular dynamics simulation of the lowest energy conformation of the complex of isomaltose with L-malic acid (top) and the complex of melibiose with N-methyl-D-aspartic acid (bottom). These geometries were optimized in NWChem at the B3LYP theory level using the 6-31G(d) basis set, and visualized in Avogadro.

The noncovalent interactions between these two model shift reagents and the analytes were further characterized using molecular simulations. As an example, the lactose/L-malic acid and melibiose/NMDA complexes are shown in Figure 4.8. Generally, hydrogen bonding between a

hydroxyl group on the disaccharide and the charged group of the shift reagent was suggested by these calculations. Additional hydrogen bonds between hydroxyl groups on the shift reagent and disaccharide were also implied for many of these complexes. In the examples shown, two hydrogen bonds between the L-malic acid carboxylic group with two separate hydroxyl groups on the lactose, as well as an intramolecular hydrogen bond on the lactose were suggested. For the melibiose/NMDA complex, hydrogen bonds between the charged amine group on NMDA as well as the uncharged carboxylic acid group and two separate hydroxyl groups on the melibiose were involved, as well as one intramolecular hydrogen bond on the NMDA ion, and two on the melibiose molecule.

ATDs for the remaining eight shift reagents that showed binding to disaccharides, albeit with lower IM resolution are given in Figure 4.9. Although there was certain degree of separation for a small number of the disaccharide pairs, there was also a significant degree of overlap for many of the complexes, so they were not pursued in further experiments.

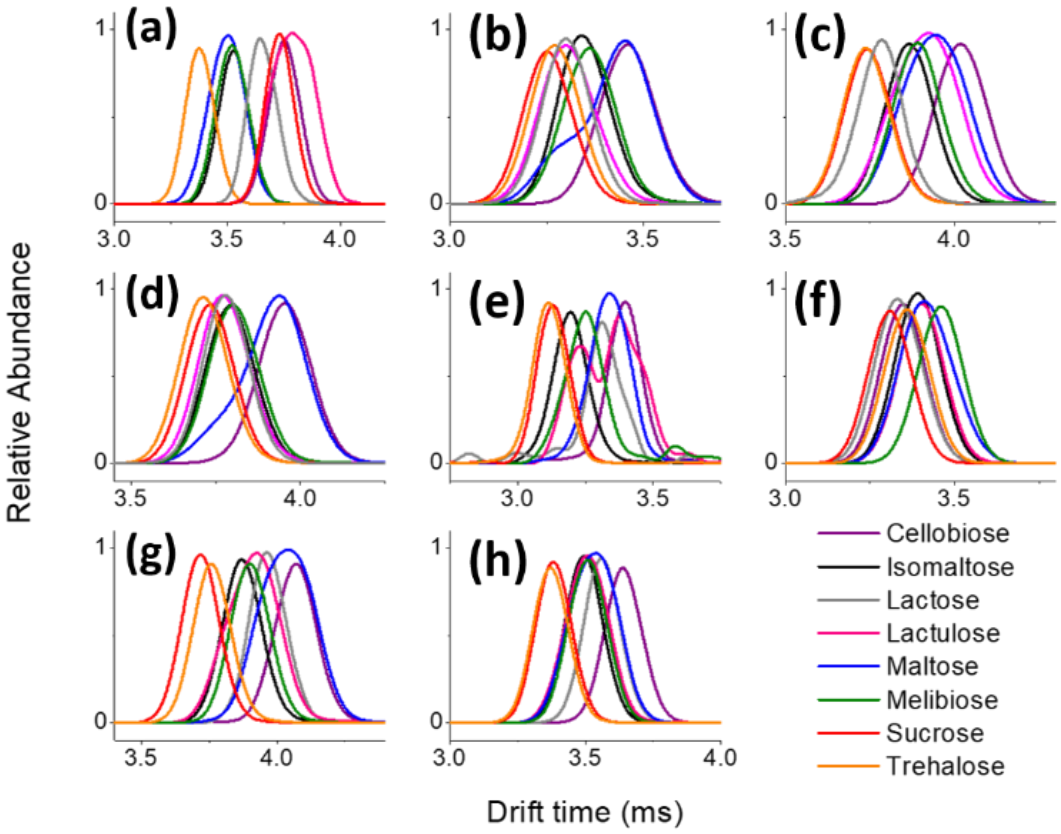


**Figure 4.9.** Overlaid arrival time distributions obtained in direct infusion experiments in the Synapt G2 TWIM-MS platform in negative ion mode for disaccharides with the least promising shift reagents including (a) tyrosine, (b) lactic acid, (c) glutamic acid, (d) 2-hydroxyhexanoic acid, (e) tartaric acid, (f) arginine, (g) N-methyl-L-glutamic acid, and (h) N-methyl-DL-aspartic acid. The species observed are the $[M+L-H]^-$ ions with M representing the neutral disaccharide and L representing the neutral shift reagent. The wave height and wave velocity were 40 V and 500 m $s^{-1}$, respectively. The non-reducing sugars, trehalose and sucrose, were often the highest mobility species observed. Sucrose and cellobiose were often distinguished with close to baseline separation when bound to most of the tested shift reagents, with the exception of tyrosine and arginine, suggesting that their different regiochemistry and monomeric composition leads to very different gas-phase structures when binding to amino and α-hydroxy acids.

### *4.4.4. Drift Tube Ion Mobility Separations*

DTIM-MS experiments were conducted to investigate whether alternative instrumentation could better resolve some of the complexes of the analyte pairs not resolved in TWIM-MS experiments. Experiments were carried out at higher overall concentrations to compensate for the lower duty cycle of the DTIM-MS instrument.[142] Overall, DTIM-MS yielded higher resolution than TWIMS (Table 4.2), as seen in the arrival time distributions for L-malic acid complexes shown in Figure 4.10. This effect is mainly due to the higher pressure in the DTIM cell, which results in a higher number of collisions with

the buffer gas. Instrumental IM resolving power $\left(\boldsymbol{R_p = \frac{t_d}{\Delta t_d}}\right)$ for the eight L-malic acid adducts studied improved from an average of 23 ± 5 for TWIM to 89 ± 23 for DTIM. This gain in resolving power, led to improvements in the resolution of the isobaric disaccharide analytes. While a mixture of cellobiose, melibiose, and trehalose complexes with L-malic acid appeared as two unresolved features in the ATD when using TWIM, the DTIM method was able to fully resolve one of these isomeric complexes and partially resolve the other two. This qualitatively demonstrates the advantage of using DTIM, which was quantitatively shown in Table 4.2.

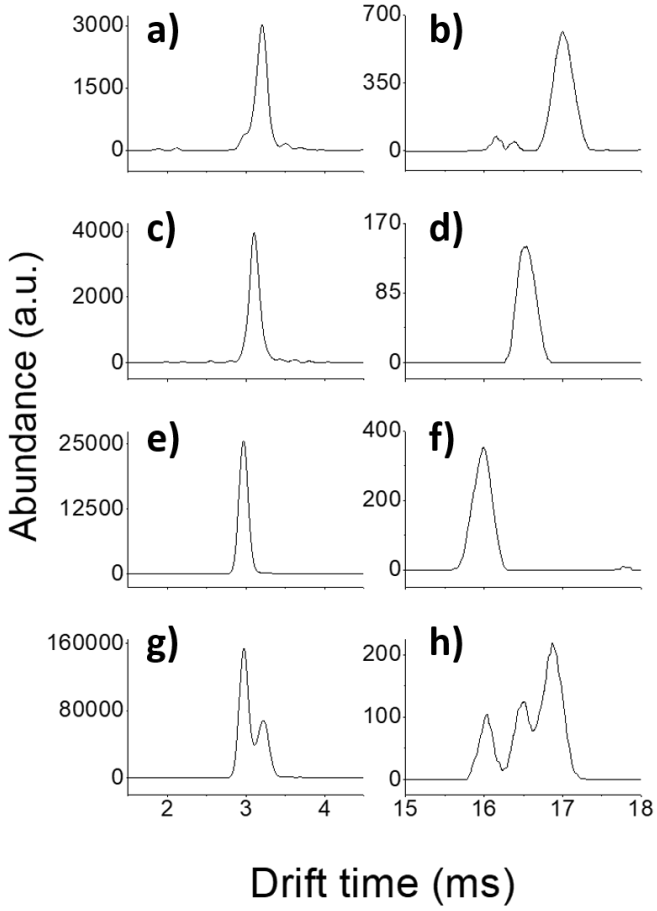


**Figure 4.10.** Comparison of arrival time distributions observed in negative ion mode Synapt G2 TWIM-MS (left column) and EXCELLIMS DTIM-Orbitrap MS (right column) experiments for selected disaccharide L-malic acid complexes. a) and b) represent the cellobiose complex, c) and d) represent that of melibiose, e) and f) represent the trehalose complex, and g) and h) represent a mixture of these three disaccharides as their L-malic acid complexes. Nitrogen was used as the buffer gas in all cases. For Synapt G2 experiments, the wave height and wave velocity were 40 V and 500 m $s^{-1}$, respectively. For the drift tube-Orbitrap experiment, the electric field was 765 V $cm^{-1}$. DTIM data was smoothed with a first order Savitzky-Golay polynomial function using a window width of 12.

**Table 4.2.** Quantitative comparison of resolution [$R_{pp} = 1.18\left(\frac{t_{dB}-t_{dA}}{(\Delta t_{dB}+\Delta t_{dA})/2}\right)$] values from traveling wave and drift tube ion mobility experiments for each pair of disaccharides as NMDA complexes in positive ion mode and L-malic acid complexes in negative ion mode. Italicized pairs are unusual in that they showed a lower resolution in DTIM than in TWIM.

| | (-) TWIM | (-) DTIM | (+) TWIM | (+) DTIM |
|---|---|---|---|---|
| Cellobiose *vs.* Isomaltose | 0.58 | 2.1 | 0.39 | 1.9 |
| Cellobiose *vs.* Lactose | 0.04 | 0.26 | 0.29 | 2 |
| Cellobiose *vs.* Lactulose | 0 | 1.4 | 0.8 | 2.2 |
| Cellobiose *vs.* Maltose | 0.19 | 1.96 | 0.03 | 1.3 |
| Cellobiose *vs.* Melibiose | 0.46 | 0.64 | 0.21 | 2 |
| Cellobiose *vs.* Sucrose | 0.93 | 1.9 | 1.1 | 9.5 |
| Cellobiose *vs.* Trehalose | 1.2 | 1.7 | 0.56 | 3.9 |
| Isomaltose *vs.* Lactose | 0.5 | 2.7 | 0.059 | 0.069 |
| Isomaltose *vs.* Lactulose | 0.46 | 4.3 | *0.49* | *0.33* |
| Isomaltose *vs.* Maltose | *0.35* | *0.047* | 0.45 | 0.83 |
| Isomaltose *vs.* Melibiose | 0.13 | 1.9 | 0.15 | 0.2 |
| Isomaltose *vs.* Sucrose | 0.32 | 0.6 | 0.85 | 4 |
| Isomaltose *vs.* Trehalose | 0.59 | 0.85 | 0.23 | 0.72 |
| Lactose *vs.* Lactulose | 0.03 | 1.3 | *0.49* | *0.27* |
| Lactose *vs.* Maltose | 0.14 | 2.6 | 0.34 | 0.81 |
| Lactose *vs.* Melibiose | 0.39 | 1.1 | 0.079 | 0.13 |
| Lactose *vs.* Sucrose | 0.83 | 2.6 | 0.79 | 4.4 |
| Lactose *vs.* Trehalose | 1.1 | 2.5 | 0.25 | 0.86 |
| Lactulose *vs.* Maltose | 0.15 | 4 | *0.9* | *0.68* |
| Lactulose *vs.* Melibiose | 0.36 | 2.7 | *0.58* | *0.13* |
| Lactulose *vs.* Sucrose | 0.72 | 4.4 | 0.35 | 5.8 |
| Lactulose *vs.* Trehalose | 0.94 | 4.4 | 0.25 | 1.4 |
| Maltose *vs.* Melibiose | 0.23 | 1.8 | 0.26 | 0.71 |
| Maltose *vs.* Sucrose | 0.66 | 0.52 | 1.2 | 6.3 |
| Maltose *vs.* Trehalose | 0.92 | 0.75 | 0.64 | 2 |
| Melibiose *vs.* Sucrose | 0.46 | 1.6 | 0.89 | 4.9 |
| Melibiose *vs.* Trehalose | 0.73 | 1.4 | 0.34 | 1.1 |
| Sucrose *vs.* Trehalose | 0.27 | 0.26 | 0.59 | 4.3 |

Analogous to the improvements in resolution seen for L-malic acid disaccharide complexes in Figure 4.10 and Table 4.2, DTIM also improved the resolution of NMDA complexes of cellobiose,

lactose, and lactulose, as shown in Figure 4.11 and in Table 4.2. On average, the resolving power for the eight NMDA complexes improved from 26 ± 2 for TWIM to 107 ± 43 for DTIM. The average resolution increased from 0.49 to 1.87 in negative ion mode and from 0.48 to 2.2 in positive ion mode when comparing TWIM to DTIM (Table 4.2). These results showcase the advantages of DTIM in terms of resolution, but have to be weighed against losses in sensitivity that accompany atmospheric pressure IM drift cells, mainly due to ion losses at the atmospheric pressure interface and low ion gating duty cycle.[142] The latter, however, can be offset by introducing multiplexing schemes based on Hadamard or Fourier approaches.[30, 33, 38] Cyclic TWIM-MS approaches could also be leveraged to enhance performance in combination with the new shift reagents presented here, with minimal impact on sensitivity.[49, 56]

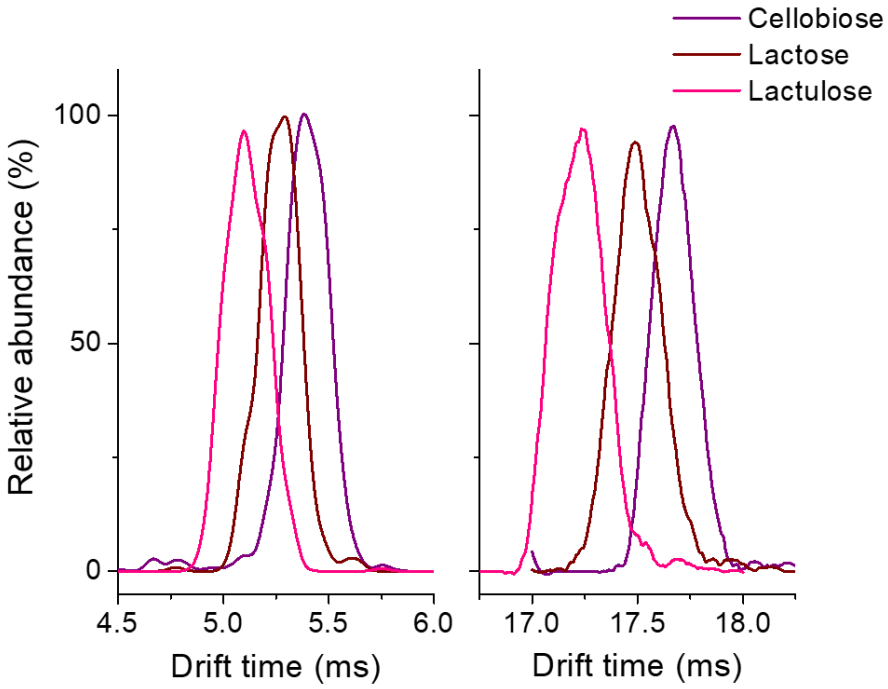


**Figure 4.11.** Comparison of arrival time distributions observed with a Synapt G2 TWIM-MS (left) and EXCELLIMS DTIM-Orbitrap MS (right) for selected pairs of disaccharide N-methyl-D-aspartic acid adducts in positive ion mode. Nitrogen was used as the buffer gas in all cases. For Synapt G2 experiments, the wave height and wave velocity were 40 V and 500 m $s^{-1}$, respectively. For EXCELLIMS-Orbitrap experiments, the electric field was 780 V $cm^{-1}$. DTIM data was smoothed with a third order Savitzky-Golay polynomial function, using a window width of 25.

While both L-malic acid and NMDA demonstrated an advantage over more traditional noncovalent shift reagents such as group I metal cations, neither achieved full IM separation of

all possible combinations of the eight analytes with either IM method tested in this study. For example, cellobiose/lactulose and cellobiose/lactose were separated as their NMDA complexes but not as their L-malic acid complexes. In contrast, lactose/isomaltose and maltose/cellobiose were differentiated as their L-malic acid complexes but not as their NMDA complexes.

**Table 4.3.** Ion-neutral CCS values for disaccharide/L-malic acid complexes calculated from negative ion mode TWIM-MS experiments performed on the Synapt G2 platform, using polymalic acid (left) and polyalanine (middle) as calibrants. The CCS from drift tube ion mobility experiments is shown in the last column to the right. The errors shown represent the 95% confidence intervals from four trials for TWIM experiments, and six trials with different electric fields from 791-890 V $cm^{-1}$ for DTIM.

| | $^{TWIM}CCS_{N2}$ (Å$^2$) polymalic acid | $^{TWIM}CCS_{N2}$ (Å$^2$) polyalanine | $^{DTIM}CCS_{N2}$ (Å2) |
|---|---|---|---|
| **Cellobiose** | 201.7 ± 1.0 | 202.1 ± 0.5 | 310.9 ± 0.3 |
| **Isomaltose** | 197.3 ± 0.8 | 196.4 ± 0.5 | 309.0 ± 0.2 |
| **Lactose** | 200.6 ± 0.9 | 201.1 ± 0.5 | 316.1 ± 0.4 |
| **Lactulose** | 201.8 ± 0.6 | 202.6 ± 0.7 | 320.7 ± 0.4 |
| **Maltose** | 199.8 ± 0.5 | 199.9 ± 0.5 | 314.0 ± 0.2 |
| **Melibiose** | 197.7 ± 0.5 | 197.4 ± 0.3 | 306.1 ± 0.2 |
| **Sucrose** | 194.2 ± 0.5 | 193.6 ± 0.5 | 306.2 ± 0.2 |
| **Trehalose** | 192.5 ± 0.3 | 191.6 ± 0.5 | 298.3 ± 0.2 |

**Table 4.4.** Ion-neutral CCS values for disaccharide/N-methyl-D-aspartic acid complexes calculated from positive ion mode TWIM-MS experiments performed on the Synapt G2 platform, using polyalanine as the calibrant, and CCS for the same complexes calculated directly from drift tube ion mobility experiments. The error represents the 95% confidence interval from four trials for the TWIM experiments and six trials with different electric fields from 791-890 V $cm^{-1}$ for DTIM.

| | $^{TWIM}CCS_{N2}$ (Å$^2$) | $^{DTIM}CCS_{N2}$ (Å2) |
|---|---|---|
| **Cellobiose** | 206.9 ± 0.4 | 319.8 ± 0.8 |
| **Isomaltose** | 204.0 ± 0.4 | 313.7 ± 0.7 |
| **Lactose** | 204.2 ± 0.3 | 326.8 ± 0.7 |
| **Lactulose** | 200.4 ± 0.4 | 308.7 ± 1.7 |
| **Maltose** | 206.8 ± 0.4 | 314.2 ± 1.8 |
| **Melibiose** | 205.3 ± 0.5 | 318.2 ± 1.5 |
| **Sucrose** | 198.3 ± 0.4 | 306.5 ± 0.7 |
| **Trehalose** | 202.6 ± 0.5 | 312.8 ± 0.5 |

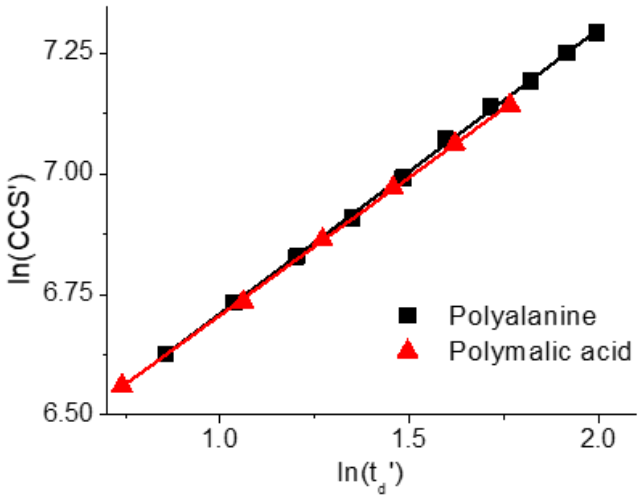


**Figure 4.12.** Collision cross section (CCS) calibration curves for polyalanine and polymalic acid obtained with the Synapt G2 by direct infusion in negative ion mode using CCS values reported by Forsythe *et al.* for calibration.[130]

To further examine alternative approaches for distinguishing between these analytes, collision cross section (CCS) values for each of the L-malic acid and NMDA complexes were calculated from their TWIM arrival times, following methods reported by Forsythe *et al.*[130] CCS values were also directly calculated from DTIM measurements (Tables 4.3 and 4.4). $^{\mathbf{TWIM}}\mathbf{CCS_{N2}}$ calibration curves for polymalic acid and polyalanine in negative ion mode are provided in Figure 4.12, showing excellent linearity. Overall, TWIM results showed that $^{TWIM}CCS_{N2}$ values for L-malic acid complexes ranged from 194.2 Å$^2$ for sucrose to 201.8 Å$^2$ for lactulose, while the NMDA complexes ranged from 198.3 Å$^2$ for sucrose to 206.9 Å$^2$ for cellobiose. Negative ion mode $^{TWIM}CCS_{N2}$ values calculated by calibration with polymalic acid and polyalanine were not significantly different at the 95% confidence level for any of the L-malic acid complexes (n=4). NMDA complexes were only calibrated with polyalanine, as polymalic acid does not ionize well in positive mode. Due to differences in the temperature and pressure operating ranges of the DTIM and TWIM IM-MS platforms utilized in this study, $^{TWIM}CCS_{N2}$ and $^{DTIM}CCS_{N2}$ values could not be directly compared and were not expected to match. $^{DTIM}CCS_{N2}$ values were significantly larger than $^{TWIM}CCS_{N2}$ values, with the L-malic

acid complexes ranging from 298.3 Å$^2$ for trehalose to 320.7 Å$^2$ for lactulose, and the NMDA complexes ranging from 312.8 Å$^2$ for sucrose to 326.8 Å$^2$ for lactose.

### *4.4.5. Combining Shift Reagents for Two-Dimensional Separations*

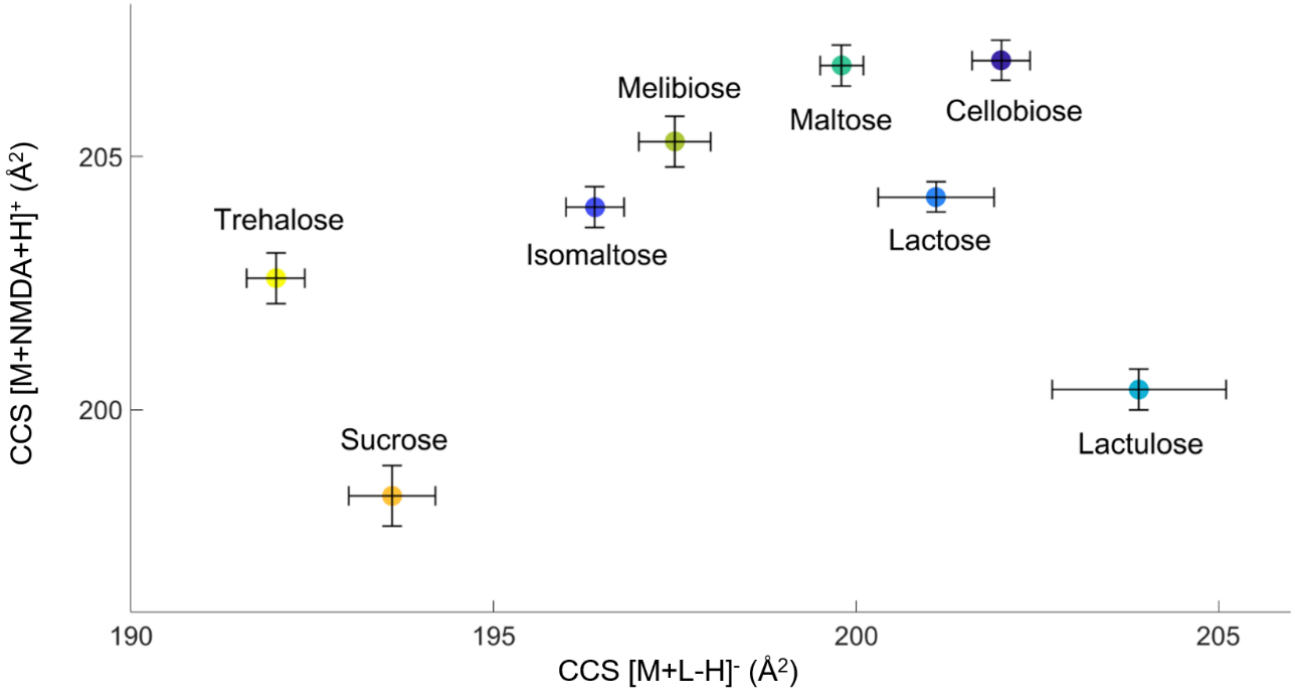


**Figure 4.13.** Ion-neutral $^{TWIM}CCS_{N2}$ values for the dominant feature in the arrival time distribution for each of the various tested disaccharides as their $[M+NMDA+H]^+$ N-methyl-D-aspartic complexes versus their corresponding $^{TWIM}CCS_{N2}$ for the $[M+L-H]^-$ L-malic acid complexes. Error bars represent the 95% confidence interval determined by four trials per complex. The colormap corresponds to the L-malic acid complex CCS. All CCS values are the average of four measurements with polyalanine used for calibration.

We hypothesized that L-malic acid and NMDA CCS values could be used in a complementary manner to distinguish every analyte within this study. The use of a combination of IM-derived CCS values for several shift reagent complexes has been reported in the past.[11, 57, 136] Gaye *et al.*, for example, showed that the combination of $[M+L\text{-serine}+H]^+$, $[M+L\text{-phenylalanine}-\text{glycine}+H]^+$, and $[Mn^{II} + (L\text{- phenylalanine}-\text{glycine}-H)+M]^+$ resulted in the "virtual separation" of 16 monosaccharide isobars when their CCS values were represented in 3D space.[57] Accordingly, $^{\mathbf{TWIM}}\mathbf{CCS_{N2}}$ values for NMDA and L-malic acid disaccharide complexes

were combined, which allowed for all of the eight analytes to be fully distinguished from one another at the 95% confidence level (Figure 4.13).

## 4.5. Conclusion

Noncovalent α-hydroxy and amino acid shift reagents, specifically L-malic acid and NMDA, showed promise in separating disaccharide isomers by IM-MS. By TWIM, eight disaccharides could be distinguished at 95% confidence by determining the CCS of their L-malic acid adducts in negative ion mode and their NMDA adducts in positive ion mode. Using DTIM, the resolution of these separations was further improved. Additional high-resolution techniques, such as cyclic IM could be used to apply this method to more complex mixtures of disaccharides. The proposed methodology could be combined with other shift reagents or additional separation techniques (*e.g.* LC) to characterize complex mixtures of carbohydrates, such as those generated by the model prebiotic reactions that mimic early Earth conditions or biological extracts. We expect that quantitation would be possible if adequate chemical standards are available for appropriate calibration without significant interferences or matrix effects.

# CHAPTER 5. Separations of Carbohydrates with Noncovalent Shift Reagents by Frequency-Modulated Ion Mobility-Orbitrap Mass Spectrometry

*Adapted from*

McKenna, K. R.; Clowers, B. H.; Krishnamurthy, R.; Liotta, C. L.; Fernández, F. M. Separations of Carbohydrates with Noncovalent Shift Reagents by Frequency-Modulated Ion Mobility-Orbitrap Mass Spectrometry. *J. Am. Soc. Mass Spectrom.,* Accepted. K. R. McKenna designed experiments for noncovalent carbohydrate complex analysis. B. H. Clowers developed frequency sweep sequence code that was adapted for Matlab and served in an advisory capacity. R. Krishnamurthy, C. L. Liotta, and F. M. Fernández assisted with the design of experiments and provided advisory roles.

## 5.1. Abstract

An increased focus on characterizing the structural heterogeneity of carbohydrates has been driven by their many significant roles in extant life and potential roles in chemical evolution and the origin of life. In this work, multiplexed drift tube ion mobility-Orbitrap mass spectrometry methods were developed to analyze mixtures of disaccharides modified with noncovalent shift reagents. Since traditional coupling of atmospheric pressure drift tube ion mobility cells with Orbitrap mass analyzers suffers from low duty cycles (<0.1%), a frequency modulation scheme was applied to improve the signal-to-noise ratios (SNR). Several parameters such as the resolution setting and maximum injection time of the Orbitrap analyzer and the magnitude and duration of the frequency sweep were investigated for their impact on the sensitivity gains and resolution of disaccharide-shift reagent adducts. The sweep time and disaccharide concentration had a positive correlation with SNR. The magnitude of the frequency sweep had a negative correlation with SNR. However, increasing the frequency sweep improved the resolution of mixtures of disaccharide analytes. Application of frequency-modulated ion mobility-Orbitrap mass spectrometry to four

noncovalently-modified glucose dimers allowed for the differentiation of three out of these four analytes.

## 5.2. Introduction

Carbohydrates are the most abundant class of biomolecules on Earth by mass and serve many functions in processes such as metabolism,[5] protein modification,[4, 7-8] and the formation of cell wall structures.[1] Due to their role in extant life, it has been hypothesized that carbohydrates may have also played an important role in the origin of life.[66, 117] Two major mechanisms have been proposed for the formation of monosaccharides in an origins-of-life scenario,[144-146] and a pathway for the potential prebiotic formation of oligosaccharides with glucose as the starting monomer has recently been reported.[66] Common to all these reactions is the production of complex mixtures that require more sensitive, rapid, and precise methods for their characterization. However, the potential for a variety of isomers, which can differ in their linkage position, monomeric composition, and stereochemistry, makes chemical characterization very challenging.[147]

The most common methods for analyzing carbohydrate mixtures involve liquid chromatography (LC) followed by nuclear magnetic resonance (NMR) spectroscopy and/or mass spectrometry (MS).[148-150] However, multiple LC columns are often required, and lengthy derivatization steps cause these analyses to be time-consuming. In the case of NMR, relatively large amounts of sample are typically needed, which leads to these methods often requiring isolation and purification of the species of interest. Tandem MS is a more sensitive method for carbohydrate isomer identification, but it may not yield definitive answers, as isomeric oligosaccharides often produce similar fragment ions, albeit at different ratios.[16-17]

Ion mobility-MS (IM-MS) has shown promise for resolving isomeric carbohydrates, with several types of IM available as potential solutions to this challenging problem. For example, travelling wave IM has been shown to have the capability to separate some disaccharides as their monosaccharide-

glycolaldehyde derivatives.[143] Also, a cyclic travelling wave IM-based system has been recently reported to separate anomeric pentasaccharide isomers as well as their open-ring conformations.[49]

Many IM methods to separate oligosaccharides have involved the use of shift reagents –covalent or noncovalent ligands that alter the drift time of the ion.[11-12, 52-53] These shift reagents often enhance the resolution of analyte pairs that are difficult to separate. They may also improve ionization efficiency, which is of particular importance for carbohydrates. For example, the study by Li *et al.* investigated sodium and chloride adducts of disaccharide derivatives as well as their $[M-H]^-$ ions in terms of the obtainable IM resolution.[143] In a study by Morrison *et al.,* tetrasaccharide regio- and stereoisomers were separated by atmospheric pressure drift tube IM-MS (DTIM-MS) as adducts with various metals.[9]

Atmospheric pressure DTIM-MS of oligosaccharides offers higher resolving power than lower pressure IM approaches,[29] but generally suffers from low duty cycle, defined as the ratio of ions detected to those produced in the source. This occurs because ions can only pass through when the gates are open, and to have reasonably useful resolution, the gates will each be open for approximately 1% of the duration of each scan. Therefore, ions that pass through both gates will only be approximately 0.01% of the ions produced. In order to reach the necessary sensitivity for the analysis of realistic mixtures, some type of IM multiplexing approach is often necessary to increase duty cycle.

Ion mobility multiplexing involves simultaneously collecting multiple signals that must be deconvoluted in order to obtain an arrival time distribution (ATD). One of the most popular forms of IM multiplexing is based on Hadamard schemes.[30-33] This approach involves pulsing the gate of the drift tube following a pseudorandom sequence and subsequently using the Hadamard transform to obtain the ATD from the raw data.[30, 34] A demonstrated drawback of Hadamard-based IM methods, however, is that they can produce echoes and artifacts that diminish signal-to-noise ratio (SNR) gains, even with the application of algorithms developed to ameliorate this issue.[33, 35]

An alternative approach to ion mobility multiplexing is frequency modulation-based Fourier transform IM (FTIM). This technique involves synchronously opening and closing two ion gates bracketing the IM drift region using a square wave with a linearly increasing frequency. FTIM was first implemented on a standalone IM instrument by Knorr *et al.*[36] and it has been coupled with time-of-flight (TOF) MS,[37] ion trap MS,[38] and Orbitrap MS.[39] FTIM-Orbitrap MS has been applied to native protein analysis,[39] but its performance for carbohydrate analysis has not yet been characterized in depth. In this study, we applied FTIMS to the analysis of disaccharides, using L-malic acid as a shift reagent. We previously reported this shift reagent as a higher resolution alternative to popular noncovalent shift reagents used in the field.[151] The combination of this new shift reagent to aid with resolution and frequency modulation multiplexing to gain duty cycle resulted in the successful DTIM-MS separations of several isomeric disaccharide pairs with very similar structures, including glucose dimers.

## 5.3. Experimental

### *5.3.1. Chemicals and Materials*

Isomaltose, trehalose, and cellobiose were obtained from TCI (Philadelphia, PA). Maltose and lactose were purchased from Sigma Aldrich (St. Louis, MO). Melibiose was obtained from Fluka. Stock solutions (1.0 mM) of each of the aforementioned chemicals were prepared in water. Noncovalent derivatization was performed by mixing solutions of 50 μL of the disaccharide stock solution (unless otherwise specified) and 2 μL of the L-malic acid stock solution in 80:20 methanol:water.

### *5.3.2. Instrumentation and System Parameters*

Experiments were performed on an atmospheric pressure, dual gate IM spectrometer (EXCELLIMS, Acton, MA) attached to the front end of a Q-Exactive Orbitrap mass spectrometer (Thermo Scientific, San Jose, CA), described in detail previously by Keelor *et al.*[142] The electrospray source of the drift tube was operated at 2.2 kV in negative ion mode, and the temperature inside of the

drift tube was 90 ºC. The drift tube was 10.55 cm. in length, with the voltage applied across the drift cell varying between 8000-9000 V, generating electric field strengths of 758-853 V $cm^{-1}$. Gating voltages of 60 V for gate 1 and 81 V for gate 2 were determined empirically to allow for maximum ion transmission with minimal ion leakage through closed gates. The drift gas was infused at 2.00 L $min^{-1}$ with an exhaust pump located at the front of the desolvation cell removing nitrogen at a rate of 0.50 L $min^{-1}$ to keep the system at atmospheric pressure (~740 Torr, Atlanta, GA, USA).

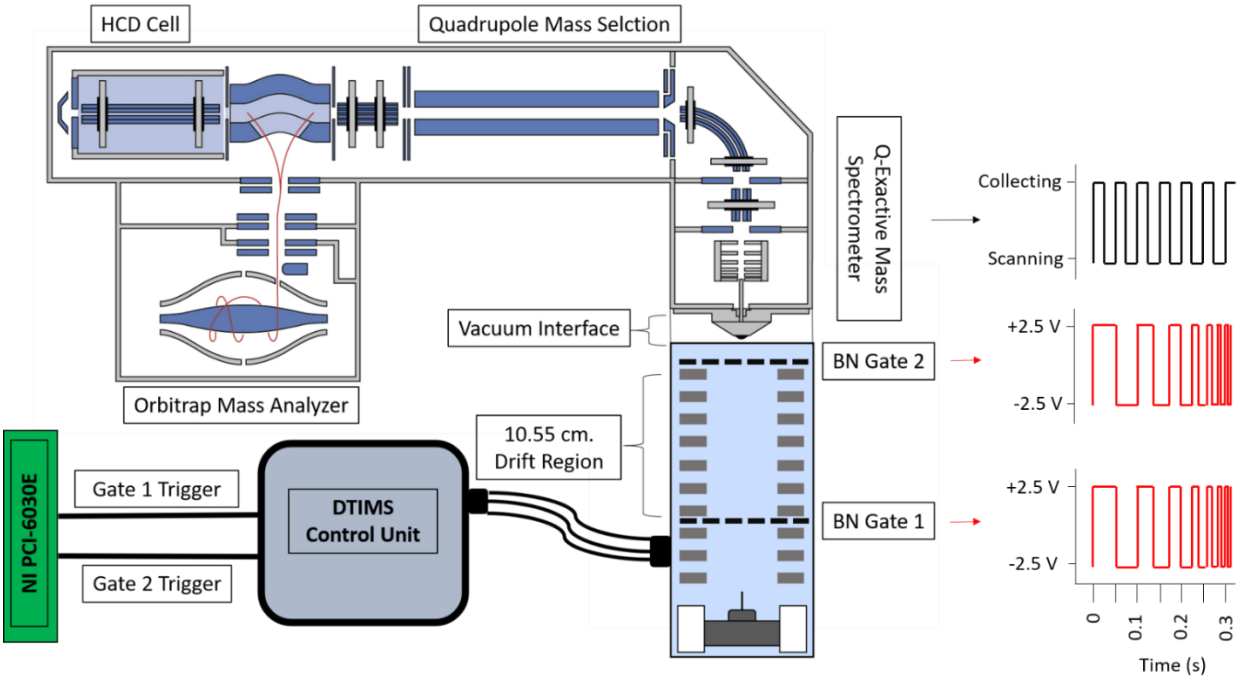


**Figure 5.1.** Schematic of the DTIMS-Orbitrap MS instrument, including the National Instruments PCI arbitrary waveform generator used for pulsing the IM gates. The IM spectrometer and Q-Exactive mass spectrometer were coupled without any major mechanical modification to either system, except for an override of the typical gate control electronics to allow for the frequency modulation pulsing scheme to be applied externally. The scanning cycle of the Orbitrap mass spectrometer and the linear frequency sweep applied to the gates of the IM spectrometer are also illustrated, which shows the opening and closing of the gates over time and the correlation to the Orbitrap ion collection cycle in the C-trap and mass analyzer scan.

Figure 5.1 shows a schematic for the instrumental setup, as well as an illustration of the square wave voltages applied to the drift tube Bradbury-Nielson gates by an arbitrary waveform generator (PCI-6030E, National Instruments, Austin, TX) and the scanning cycle of the Orbitrap mass analyzer. While the time scale is not necessarily exactly what was used in the experiments, it indicates the relative

differences in time scale between the Orbitrap scans and the gate pulses at the beginning of the experiment and then after several pulses. All frequency sweeps were performed as linearly increasing frequency chirps, with the two BN gates *synchronously* opening and closing starting at a low frequency and increasing in frequency throughout the FTIM experiment. Unless otherwise stated, the sweeps were performed from 5 to 7505 Hz, with a sweep time of 7 min., maximum Orbitrap injection time (MIT) of 100 ms, and Orbitrap resolution of 70,000. The automatic gain control of the Orbitrap was set to the maximum setting of $5x10^6$ counts, and manual checks were done to ensure the MIT was the actual injection time, and the automatic gain control was not shortening the MS scan time. The automatic gain control was deliberately set to the highest setting in order to make it unlikely that the target would be reached, so the full maximum injection time would be consistent across all scans for each experiment. The range of maximum drift times analyzed for FTIM experiments was 20-30 ms, since when the frequency sweep and sweep time were set to specific values, they translated into specific drift time ranges for a particular experiment. The average gate pulse was ~0.1 seconds for a 5-15005 Hz frequency sweep.

While a custom Matlab script was used to control the BN gates for FTIM experiments, the built-in software from EXCELLIMS (VisIon), was used in "scan mode" for signal averaging experiments. In scan mode, the maximum period for IM scans was 20 ms. To start each scan, the first Bradbury-Nielson gate is opened for 200 μs. Then, the second gate is opened for 200 μs at a variable delay (0-20 ms) from the first gate. The drift time of the ions that are transmitted through both gates matches the delay between the gate pulses. Identical drift tube and Orbitrap parameters were used in signal averaging experiments and FTIM experiments, with the exception that the Orbitrap MIT was increased to 1000 ms. This increased value was needed because there was little to no ion detection at lower MIT settings, which led to poor peak shape. Results were extracted manually from the Orbitrap software, Xcalibur. For FTIM experiments, these results were processed with a fast Fourier transform (FFT) followed by division by the frequency sweep rate using a custom script in Matlab (Mathworks, Natick, MA). In all cases, the signal-

to-noise ratio (SNR) was calculated by dividing the maximum signal detected by the noise. Noise was defined as the average abundance across eleven points in an arrival time range with no observed peak plus three times the standard deviation of that range.

## 5.4. Results and Discussion

The major expected benefit of frequency modulation over traditional scan-mode ion gating approaches to DTIM is an increase in SNR. Figure 5.2 shows the results of IM-MS experiments involving a seven-minute frequency modulation run for the lactose (M)/L-malic acid (L) species $[M+L-H]^-$, detected at *m/z* 475.13 (50 μM). Experimental transient data (Figure 5.2a) was processed with a fast Fourier transform followed by division by the frequency sweep rate (Figure 5.2b). A corresponding signal averaging experiment for the same species collected for the same amount of time is also shown for comparison purposes (Figure 5.2c). Note that in these signal averaging experiments a small, additional peak was observed at longer drift times, which was caused by ion "leakage" and imperfect gating through the ion gates while they are being closed.[152] A small difference between the drift times in Figure 5.2b and 5.2c of 400 μs was observed. This discrepancy is most likely due to precision limitations caused by the average gating time of each experiment, approximately 200 μs.

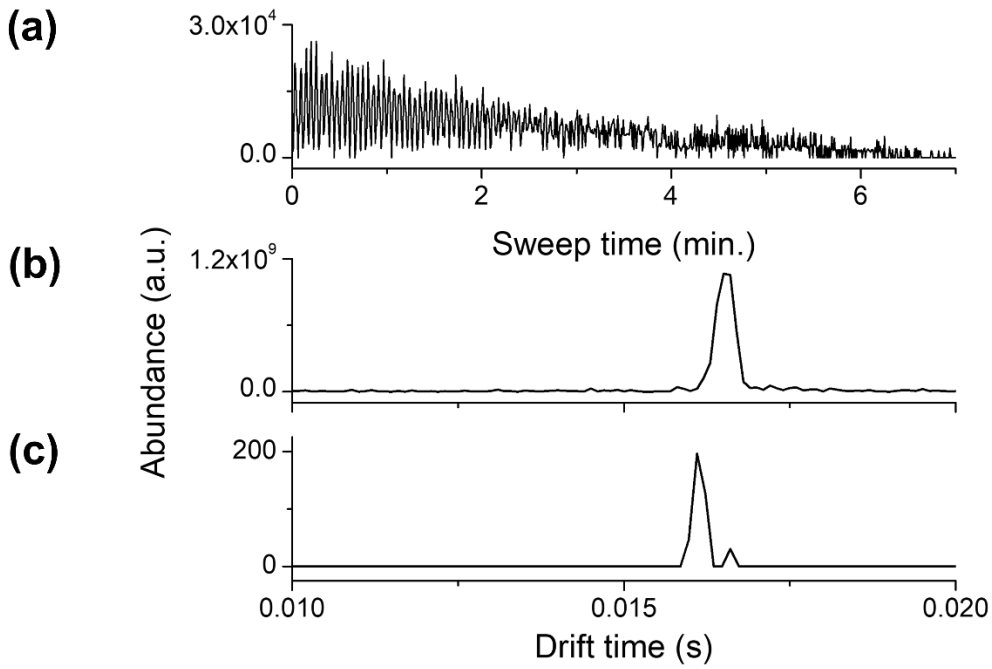


**Figure 5.2.** (a) Raw FTIM results for a 5-10005 Hz frequency sweep experiment, (b) the data shown in (a) processed by a fast Fourier transform followed by division by the sweep rate (23.8 Hz/s), (c) the arrival time distribution (ATD) from a scan-mode (averaging) experiment. Each of these experiments employed a 50 μM lactose and 2 μM L-malic acid mixture. The experiment duration was 7 min in all cases.

Overall, the frequency modulation experiment had a SNR of 118 ± 39 (95% confidence interval, *n*=3), while the corresponding SNR for three trials of the signal averaging experiment was 7 ± 1, for a 17x gain in SNR. These experiments were conducted for a total of eight disaccharide complexes with L-malic acid, with the structures of all disaccharides utilized in this study depicted in Figure 5.3. An improvement in SNR by approximately an order of magnitude was consistent for most disaccharide L-malic acid complexes analyzed by frequency modulation, as shown in Table 5.1. Overall, the improvement in SNR was 3-17 times the signal averaging value.

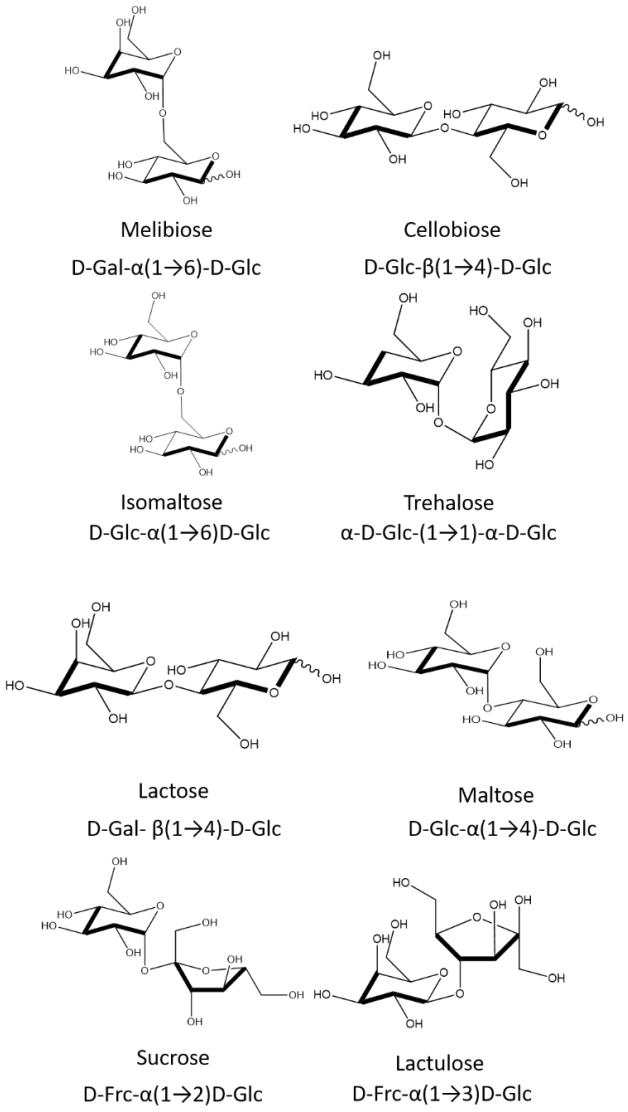


**Figure 5.3.** Structures of the isobaric disaccharides examined in this study.

**Table 5.1.** Signal to noise ratios for signal averaging and frequency modulated experiments. The disaccharide concentrations were 50 μM with L-malic acid at 2 μM. These experiments were each seven minutes in duration and measured arrival times from 0-20 ms.

| Disaccharide Malic Acid Complex | Signal Averaged SNR | FTIM SNR |
|---|---|---|
| Cellobiose | 6 ± 2 | 61 ± 15 |
| Isomaltose | 17 ± 5 | 166 ± 39 |
| Lactose | 7 ± 1 | 118 ± 39 |
| Lactulose | 45 ± 23 | 140 ± 72 |
| Maltose | 11 ± 5 | 39 ± 14 |
| Melibiose | 31 ± 5 | 107 ± 29 |
| Sucrose | 41 ± 20 | 149 ± 90 |

| | | |
|---|---|---|
| Trehalose | 5 ± 1 | 78 ± 26 |

Several experimental parameters were systematically varied to establish their effect on SNR, including the MIT and resolution setting of the Orbitrap mass spectrometer, sweep time, disaccharide concentration, and the magnitude of the frequency sweep. The frequency sweep was varied by keeping a fixed starting frequency and changing the terminal frequency to alter the net frequency sweep of the experiment.

### *5.4.1. Mass Spectrometry Parameters*

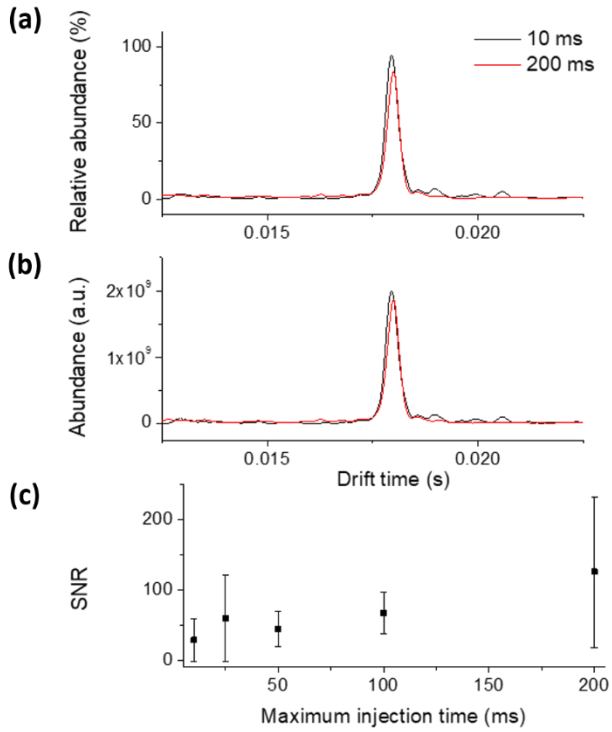


**Figure 5.4.** ATDs for the lactose L-malic acid $[M+L-H]^-$ complex at *m/z*=475.13, using 10 and 200 ms maximum injection time (MIT) Orbitrap settings showing their (a) relative and (b) absolute abundances. (c) Average signal-to-noise ratio (SNR) for three trials at each MIT tested. Error bars represent one standard deviation.

The first parameter investigated was the MIT of the Orbitrap mass spectrometer (Figure 5.4). The relative and absolute abundances observed in the ATDs of 10 and 200 ms experiments appeared to be similar (Figure 5.4a-b), with no significant SNR changes associated with changes in maximum injection

time (Figure 5.4c). At approximately 200 ms, the SNR became less precise, showing a nearly three times increase in the standard deviation compared to the average of the measurements at lower MITs. This higher level of uncertainty is largely attributed to the uneven spacing of the Orbitrap data acquisition rate and the number of frequency cycles sampled per MIT scan. Interestingly, the cycle time between subsequent scans in an Orbitrap is not static, rather a small, yet variable reset overhead is observed between successive scans. This establishes a scenario where the number of ion gating cycles sampled per Orbitrap scan can vary slightly during the FTIM experiment. It is important to note, however, that this slightly varying Orbitrap sampling frequency does not hinder the FTIM experiment.[38] The data were interpolated in Matlab using a spline function to provide evenly spaced points prior to processing with the FT. In this particular case, synchronization of the start and end times of the FTIM are essential, as these help define the sweep rate of the experiment. The sweep rate remains crucial to the FTIM experiment as this parameter is used to covert the frequencies observed from the Fourier transform of the raw data (*e.g.* Figure 5.2a) into drift time. By dividing the observed frequency in Hz by the sweep rate, expressed in Hz/s, the standard drift time in a drift tube experiment is obtained. However, to help explain the intensity variations observed for larger MIT, the sweep rate also defines how many different frequencies in the mobility domain are sampled in a single Orbitrap scan. Not surprisingly, a larger MIT will sample a wider range of modulated mobility frequencies and effectively average away subtle changes in ion current for different mobilities. For example, at the lowest MIT tested, 10 ms, there would be a mobility frequency range of ~0.2 Hz sampled per Orbitrap scan, whereas at the highest MIT, 200 ms, ~3.6 Hz is sampled per Orbitrap scan. In essence, by increasing the MIT the sampling statistics of the modulated ion beam are degraded, which increases the probability of introducing aliasing effects and the potential for phasing errors. While important to recognizing the key role of these experimental variables, the SNR did not change significantly within the 95% confidence intervals for the range of MITs probed. As a consequence,

a 50 ms setting was chosen for the rest of the frequency-modulated experiments based on the optimal SNR reproducibility.

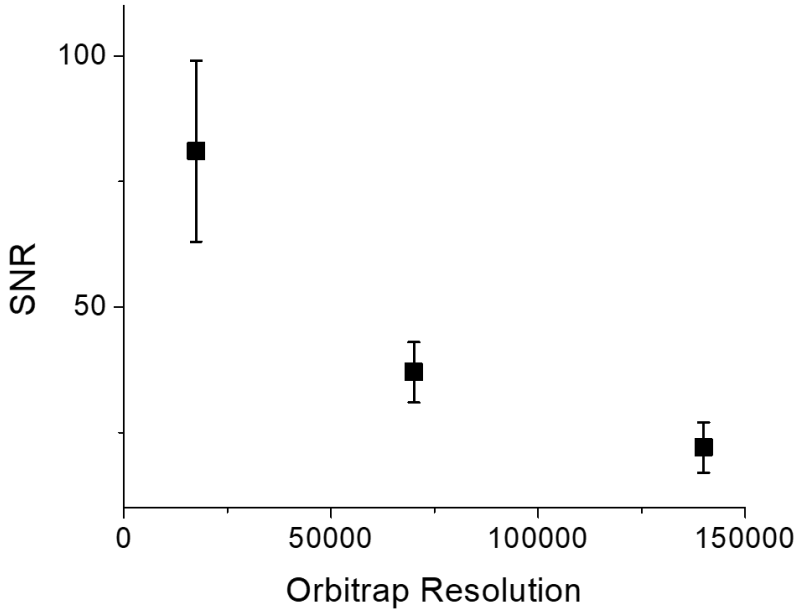


**Figure 5.5.** The effect of Orbitrap resolution setting on SNR for a solution of 50 μM lactose and 2 μM L-malic acid in 80% methanol, 20% water. The frequency sweep was 7.5 kHz, the sweep time was 5 min., and the MIT was 50 ms in all cases. The error bars represent one standard deviation of *n*=4 repeat experiments.

A second Orbitrap parameter investigated was the mass resolution setting. The SNR values for each Orbitrap resolution tested from the minimum of 17,500 (highest scan speed) to the maximum of 140,000 are shown in Figure 5.5. While these experiments involved isobaric analytes that would not be separated regardless of the mass resolution setting employed, applications in complex mixture analysis, such as treated wastewater analysis, where heteroatoms are commonly present in the saccharides[153] would benefit from high resolving power. Experiments showed a decrease in SNR as the Orbitrap resolution increased for all settings tested, with SNR 95% confidence intervals of 81 ± 18 and 22 ± 5 for the mass resolution of 17,500 and 140,000, respectively. While there is a significant decrease in SNR between the resolution settings of 17,500 and 140,000, the magnitude of the decrease was only ~3-4 fold. This lower SNR was due to the relationship between Orbitrap resolution and scan speed. Higher resolution necessitates slower scan speed, which leads to fewer scans and thus, a lower SNR. Due to mass resolution

having a greater impact on SNR than the MIT, it is likely that the MIT settings used were significantly lower than the effective Orbitrap transient time. A resolution of 70,000 was selected for subsequent experiments as it was adequate for these studies.

### *5.4.2. Concentration Effects*

In a subsequent set of experiments, the concentration of lactose was varied while keeping a constant L-malic acid concentration of 2 μM. Increasing the analyte concentration led to an increase in SNR that reached a maximum at approximately 7.5 μM lactose (Figure 5.6.). The SNR for the 2 μM lactose experiment was 19 ± 8, increasing to 142 ± 37 for the 100 μM lactose experiment. Although not significant, Figure 5.6a shows that there was a measurable decrease in the average SNR between 7.5 and 10 μM and between 25 and 50 μM, suggesting that the variation in SNR between replicates was larger than the variation caused by the change in lactose concentration. The effect of lactose concentration on the relative peak area of the main ATD peak was also investigated (Figure 5.6b). Linear behavior was observed between 2 and 10 μM, indicating that the signal increase at higher concentrations was accompanied with an increase in noise, as the SNR was relatively constant, while the relative peak area increased. The increase in lactose concentration from 2-7.5 μM is analogous to a 1:1-3.75:1 ratio of lactose to L-malic acid. The increase in SNR for this range indicates that the abundance for the complex increased without additional L-malic acid, implying that more complex was formed with this higher lactose:L-malic acid ratio until it reached a maximum around 3.75:1.

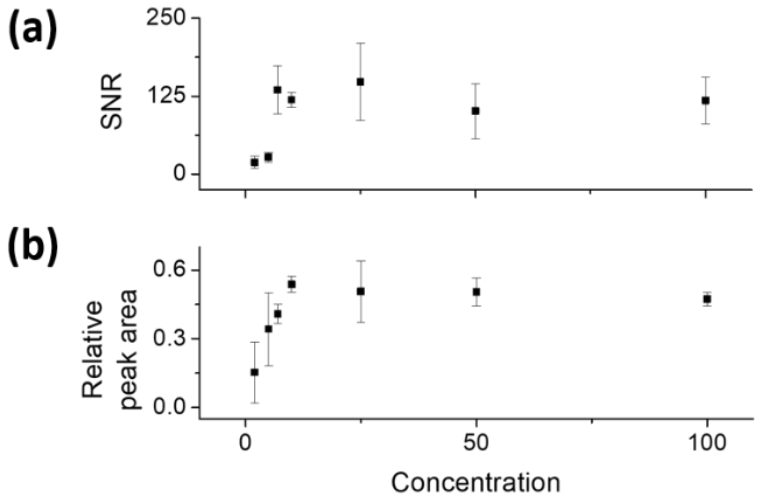


**Figure 5.6.** The (a) SNR and (b) relative peak area for the $[M+L-H]^-$ complex of lactose and L-malic acid *vs*. the total extracted area at *m/z* 475.13 for frequency modulated ion mobility experiments with varying lactose concentrations and a constant L-malic acid concentration of 2 μM.

In order to determine the impact of an excess of lactose, it was investigated whether dimer complexes *i.e.* $[2M+2L-2H]^-$ ions were forming at higher lactose concentrations, as these had previously been seen in studies of oligosaccharide complexes by Morrison *et al*.[9] However, there was no evidence of these complexes as no minor peaks in the ATDs were detected. Also, other complexes such as $[2M+L-H]^-$ or $[M+2L-H]^-$ were not detected in the mass spectrum, leading to the conclusion that the dimer complexes were most likely not formed at detectable quantities in the source.

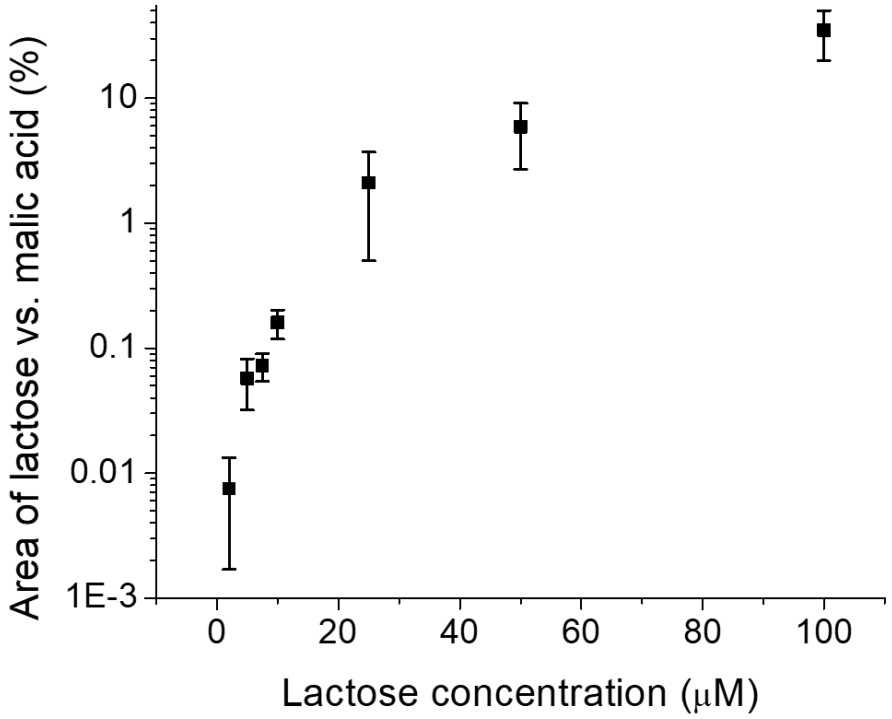


**Figure 5.7.** The ratio of the area of the main ATD peak for the $[M-H]^-$ ion for lactose (*m/z* 341.11) to that of malic acid (*m/z* 133.01) with a variable lactose concentration and a constant L-malic acid concentration of 2 μM. The frequency sweep was 7.5 kHz, the sweep time was 5 min., and the MIT was 50 ms in all cases. The error bars represent one standard deviation of *n*=4 repeat experiments.

To further investigate the impact of increasing the lactose concentration on the formed ions, the relative ratio of lactose to L-malic acid detected as their $[M-H]^-$ peaks was also investigated, as shown in Figure 5.7. Despite lactose having a higher concentration than L-malic acid at all concentrations used except for 2 μM, L-malic acid was detected with a higher signal and area of the main ATD peak at all lactose concentrations tested, up to 100 μM or a 50:1 ratio of lactose to L-malic acid, where the area of the main ATD peak for lactose was 35% of that of L-malic acid. Therefore, with an L-malic acid concentration of 2 μM, the complex forms the most around 7.5 μM lactose and above, as seen in Figure 5.6. The ratio of lactose ions to L-malic acid ions continues to increase with increasing lactose concentration at all concentrations tested. The propensity of L-malic acid to ionize better than either lactose or the L-malic acid/lactose complex leads to the $[M-H]^-$ ion of L-malic acid having the potential to overload the Orbitrap and prevent the detection of lactose and the complex. Therefore, the approximate concentration of disaccharides should be determined in order to determine an appropriate amount of L-

malic acid that will form a detectable amount of the complex without overwhelming the MS with L-malic acid ions.

### *5.4.3. Frequency Sweep Parameters*

After determining the optimum MS settings and analyte concentrations for these experiments, the effect of sweep time on SNR was investigated. As seen in Figure 5.8, SNR generally increased with increasing sweep time, leveling off at around 6 min. Since there are more scans averaged at longer experiment times, it was expected that higher sweep times would improve the SNR. The 95% confidence intervals for the two- and ten-min. experiments were 90 ± 41 and 356 ± 46, respectively, approximately a four-fold gain. Despite these gains, even at the lowest sweep time tested, the ATD peak shape was unaffected. Therefore, and despite a significant sacrifice in the SNR, a two-minute experiment yielded a Gaussian ATD suitable for qualitative and semi-quantitative analysis. These results also suggested that short experiments could be used in high throughput applications with good SNR and that longer experiments could be reserved for applications where low detection limits are required. Increasing the sweep time from eight to ten minutes did not yield a significant gain in the SNR at 95% confidence level, so a seven-minute experiment time was chosen to optimize SNR while allowing for sufficient points to be sampled across the experiment.

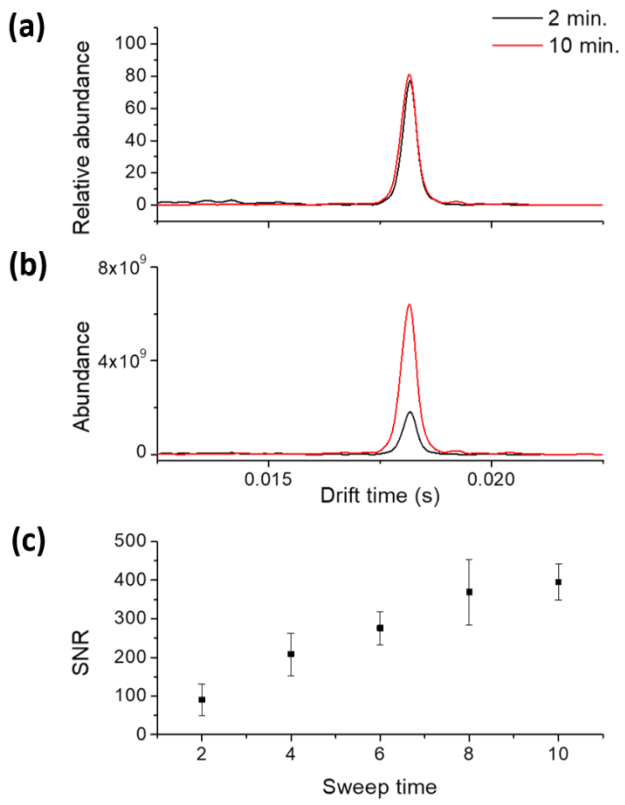


**Figure 5.8.** ATDs for the lactose L-malic acid $[M+L-H]^-$ complex at *m/z*=475.13 at 2 and 10 min. sweep times (88 and 17 Hz $s^{-1}$ sweep rates, respectively) showing (a) relative and (b) absolute abundances. (c) Average signal-to-noise ratio (SNR) for three trials at each sweep time tested. Error bars represent one standard deviation.

The effect of the magnitude of the frequency sweep on SNR can be seen in Figure 5.9. Generally, increasing the frequency sweep led to a decrease in SNR. The lowest and highest frequency sweep magnitudes tested, 5.5 and 15 kHz, had SNR of 218 ± 18 and 21 ± 10, respectively, within 95% confidence. There was not a significant improvement in SNR between the 15 and 10 kHz sweeps at the 95% confidence level. The decrease in SNR at increased frequency sweeps is caused by fewer ions passing through both gates at higher frequencies. Therefore, there is a larger portion of the experiment in which fewer ions are detected, leading to a decrease in SNR. While an increased frequency sweep generally led to a decrease in SNR, it also led to more points being sampled across the experiment, resulting in an improvement in peak shape. This can be observed in Figure 5.9a-b, with the 15 kHz experiment having a lower abundance and SNR, but a more Gaussian-like peak shape.

### *5.4.4. Analysis of Isomeric Carbohydrate Mixtures*

Following the analysis of the impact of the frequency sweep on a single complex, the relationship between frequency sweep and the resolution of pairs of complexes was investigated for mixtures of lactose, melibiose, and L-malic acid as the shift reagent. The ATDs for these disaccharide adducts at different frequency sweeps are shown in Figure 5.10, with the corresponding resolution values provided in Table 5.2. The measured lactose/melibiose resolution varied from 1.2 ± 0.3 at 5.5 kHz to 5.1 ± 0.2 at 20 kHz. Interestingly, a second peak appeared in the ATD at 20 kHz for the melibiose L-malic adduct. This is most likely due to the several different L-malic acid binding positions to melibiose that can engage via hydrogen bonding. Therefore, an experiment at 15 kHz with a resolution of 2.8 would be preferable in this case, as the major peaks for the two complexes could be resolved without losing signal to minor peaks. A frequency sweep of 15 kHz was used for subsequent experiments involving more complex mixtures. Since the frequency sweep impacts both SNR and resolution, it will need to be optimized for each mixture analyzed to balance these two important aspects of separations.

**Table 5.2.** Resolution values for the L-malic acid adducts of lactose and melibiose (*m/z*=475.13) at various frequency sweep magnitudes at the constant sweep time of seven minutes, MIT of 50 ms, and lactose and melibiose concentrations of 25 μM each.

| Frequency sweep | Resolution |
|---|---|
| 5.5 kHz | 1.2 ± 0.3 |
| 7.5 kHz | 1.7 ± 0.1 |
| 10 kHz | 1.8 ± 0.1 |
| 15 kHz | 2.8 ± 0.5 |
| 20 kHz | 5.1 ± 0.2 |

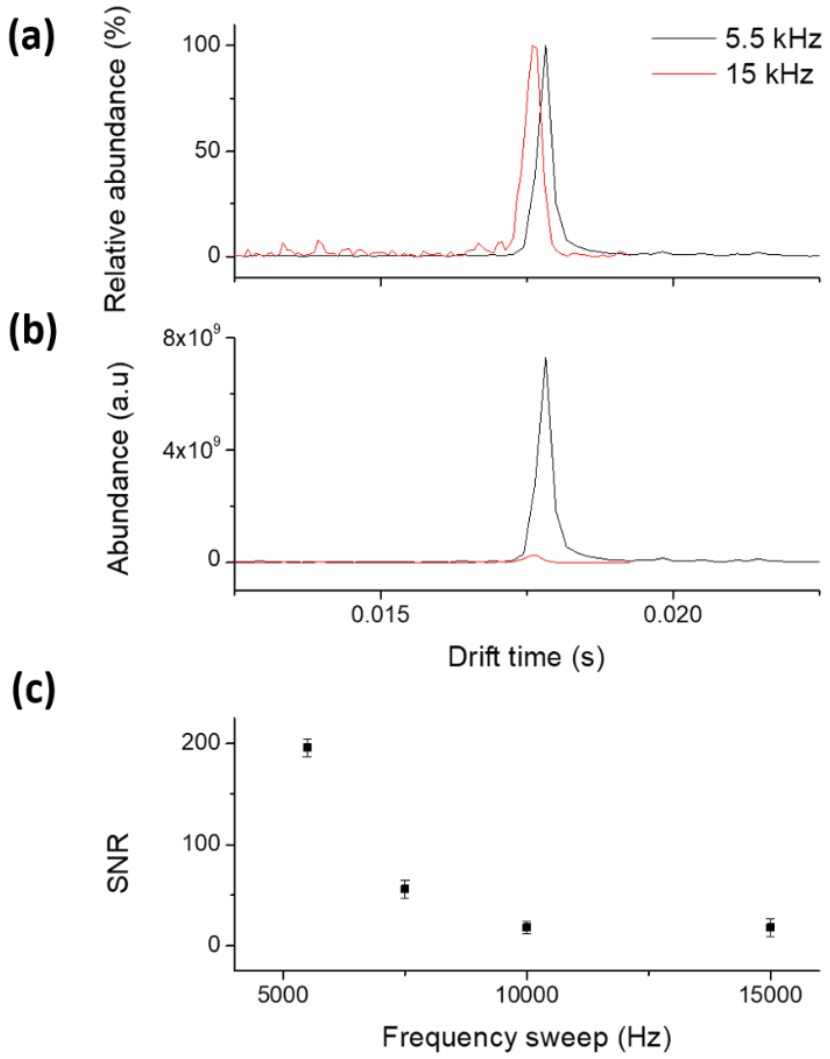


**Figure 5.9.** ATDs for the lactose L-malic acid $[M+L-H]^-$ complex at *m/z*=475.13 at 5.5 and 15 kHz frequency sweep magnitudes showing (a) relative and (b) absolute abundances. (c) Average signal-to-noise ratio (SNR) for *n*=3 trials at each frequency sweep magnitude tested. Error bars represent 95% confidence intervals.

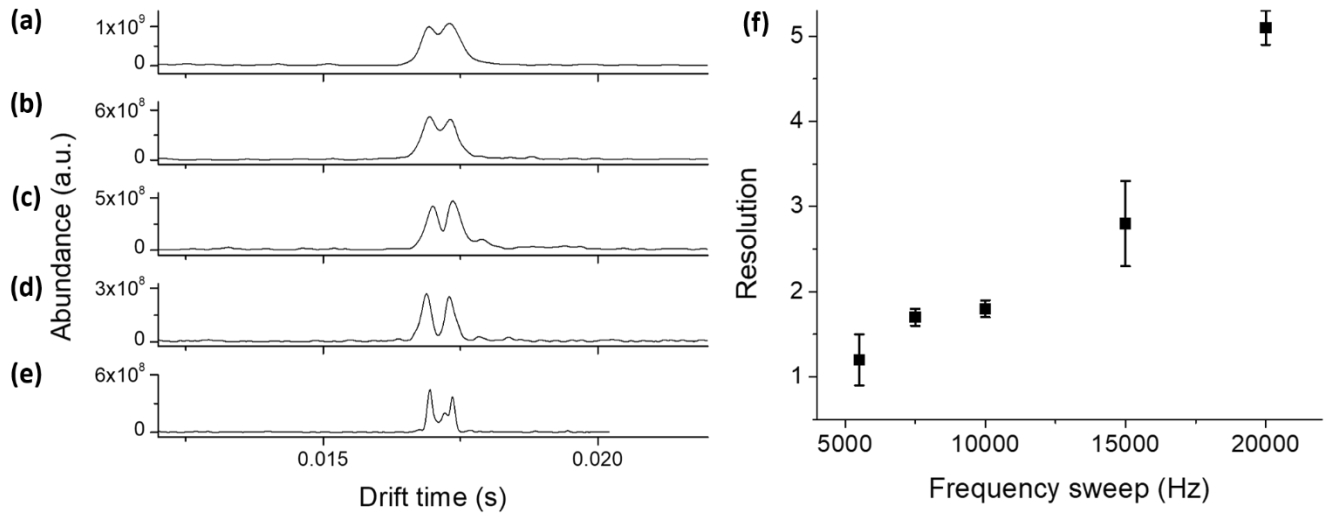


**Figure 5.10.** ATDs for a mixture of melibiose and lactose with L-malic acid as the shift reagent, using frequency sweeps of (a) 5.5 kHz, (b)7.5 kHz, (c) 10 kHz, (d) 15 kHz, (e) 20 kHz. The sweep time was kept consistent at 5 min. The tested solution was 50 μM lactose and 2 μM L-malic acid in 80% methanol, 20% water. (f) Resolution *vs*. frequency sweep magnitude for the ATDs displayed in (a)-(e).

Once it was established that this method could resolve specific pairs of disaccharide L-malic acid complexes, a more complex mixture was studied. In this case, four glucose dimer standards (cellobiose, isomaltose, maltose, and trehalose) were tested. The structures of these disaccharides can be seen in Figure 5.3. These rationale behind the choice of analytes was geared towards the use of this method to analyze the products of prebiotic carbohydrate-forming reactions. In previous work we have shown that it is possible to polymerize glucose monomers into complex oligomeric mixtures under plausible prebiotic conditions, yielding abundant dimers.[7] Figure 5.11a depicts the ATD for a mixture of these four glucose dimers with L-malic acid with Figure 5.11b-d showing the ATDs for single component mixtures of each disaccharide with malic acid. The ATD for the mixture contains three distinct peaks for the L-malic acid complexes of cellobiose, isomaltose, and trehalose. A minor shift in drift times (0.04-0.3 ms) from the single disaccharide solutions to the mixture was observed, likely due to imprecisions caused by the gate pulse timing in the FTIM experiment.

The trehalose complex appeared at the lowest drift time as a single peak, indicating that either malic acid binds at a single site or multiple sites that are too close in CCS to be resolved by this method. The trehalose complex is followed by the isomaltose complex which also produced a single peak in the ATD at a somewhat higher abundance. Maltose appeared to have three different binding sites for L-malic acid, indicated by the appearance of three unresolved peaks in Figure 5.11c. The lowest drift time peak appears to overlap with the isomaltose complex in the mixture in Figure 5.11a. The higher drift time peaks appear as a shoulder for the cellobiose complex, which has the highest drift time. Therefore, all four disaccharides were detected and three out of these four were baseline resolved in this seven-minute experiment. The results of Figure 5.11b-e demonstrate that the disaccharide L-malic acid complex have somewhat different ionization efficiencies, which is also apparent in the mixture shown in Figure 5.11a. This can lead to poor detection of less efficiently ionizing complexes, so frequency modulation may be necessary to detect all disaccharides present in complex mixtures especially if some components are more dilute than others.

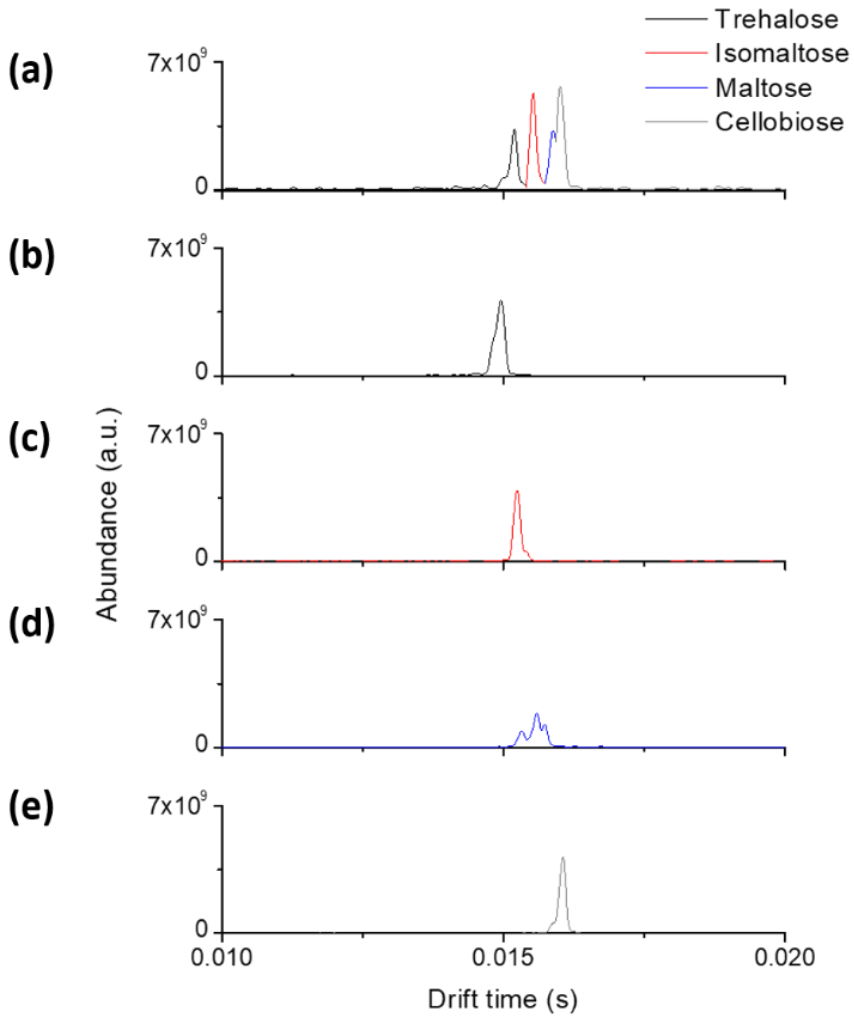


**Figure 5.11.** ATDs for the L-malic acid adducts (*m/z*=475.13) of (a) a mixture of cellobiose, isomaltose, maltose, and trehalose, (b) trehalose, (c) isomaltose (d) maltose, and (e) cellobiose. The concentration of each disaccharide was 50 μM with 8 μM L-malic acid. The solvent was 80% methanol, 20% water. The frequency sweep was 15 kHz, with a 7 min. sweep time. The MIT was 50 ms in all cases.

Overall, the majority of the results presented here agreed with previous studies conducted by Morrison *et al.*[38] with a similar ion mobility spectrometer connected to an ion trap system. In these, the MIT of the ion trap was also found to not have a significant effect on SNR. However, the decrease in precision at a higher MIT was not observed. Increasing the sweep time was found to improve SNR. Concentration also had a positive correlation with SNR, with this improvement leveling off at around 100 nM for $[\text{neurotensin+H}]^{3+}$. Increasing the frequency sweep had a

negative impact on SNR, whereas the resolving power increased. In their study, resolution at different frequency sweeps was not evaluated for isobaric species, but the improvement in resolving power would most likely improve IM resolution. Other FTIM studies have not looked at the systematic impact of these experimental parameters but rather focused on the impact of apo *vs.* holo enzymes[39] or the separation of carbohydrate-metal cation complexes.[9]

## 5.5. Conclusion

Carbohydrate isomer analysis requires the development of better separation strategies with enhanced SNR. This type of separations is important in a number of fields, including glycobiology, glycoproteomics, environmental chemistry, and prebiotic chemistry. Our group has previously shown the utility of L-malic acid as an effective shift reagent for disaccharides using both traveling wave and drift tube ion mobility spectrometry. Despite the advantages of high-resolution atmospheric pressure drift tube ion mobility over travelling wave ion mobility systems in terms of resolving power, its lower duty cycle is a major drawback. Here, we have shown that frequency modulation improves the SNR of DTIM coupled to MS, effectively removing the duty cycle limitation. Overall, a lower Orbitrap resolution setting, longer experiment time, and lower frequency sweep were found to improve the obtained SNR over a scan-mode experiment. The MIT of the Orbitrap mass spectrometer was shown to not have a significant effect on SNR. The concentration of lactose had a less straightforward effect on the SNR for the detected complex with the shift reagent, with the relative peak area responding more directly to the lactose concentration. Despite lowering the SNR, a higher frequency sweep was found to improve the peak shape and resolution of disaccharide isomers. Three out of four glucose dimer standards tested were readily distinguished by this frequency modulated DTIM-MS

method. This indicates that FTIM would be a suitable method for the analysis of isobaric oligosaccharide mixtures with shift reagents where the isobaric complexes have different ionization efficiencies, such as those produced by model prebiotic reactions. While the scan times of the experiment in its present form would not be amenable to coupling with LC, fractionated mixtures of carbohydrates could still be analyzed by this direct infusion FTIM-MS method.

# CHAPTER 6. Conclusions and Outlook

## 6.1. Abstract

This chapter presents a summary of the results of tandem mass spectrometry and ion mobility analyses of carbohydrate mixtures both as $[M-H]^-$ ions and with covalent derivatives or noncovalent modifiers. Ion mobility-tandem mass spectrometry is a powerful tool for the study of complex oligosaccharide mixtures. Covalent derivatization and noncovalent modification can improve the utility of ion mobility for distinguishing isomeric mono- and oligosaccharides. Future directions for this work are also proposed.

## 6.2. Progress with Carbohydrate Mixture Analysis

Carbohydrate analysis has been historically challenging due to the diversity of this class of biomolecules including various stereo- and regioisomers with the potential for branching and bonding at multiple sites. Due to these similarities, there is often a need for analysis beyond single stage mass spectrometry, which can determine the length of oligo- and polysaccharides in solution but does not give sufficient information to determine the different isobars composition. Tandem mass spectrometry can give some additional information, as certain regioisomers can generate characteristic fragments, depending on the fragmentation method used.[10] However, many stereo- and regioisomers produce identical fragment ions by MS/MS and vary only in the abundances of these fragment ions.[16-17] Therefore, using a combination of $^{1}H$ and $^{13}C$ NMR with MS/MS was necessary to confirm the presence of certain regio- and stereoisomers in model glucose polymerization reaction products, as shown in Chapter 2 of this dissertation.

As opposed to using NMR as a complementary technique, IM can be combined with MS/MS within the same experiment. Therefore, several shift reagents were analyzed for their potential to distinguish oligosaccharide mixtures by IM-MS/MS. 3C5NBA could be used as a

covalent derivatization agent with a reaction time of approximately 5 minutes for disaccharides and 30 minutes for monosaccharides at room temperature. This is significantly less than most previously reported covalent shift reagents such as 1-phenyl-3-methyl-5-pyrazolone, which takes 2 hours to react at 70 ºC, and requires a post-reaction workup procedure.[52] Experiments showed that 3C5NBA could distinguish six of the eight disaccharide standards and one of the four monosaccharides studied using IM-MS/MS.

### *6.2.1. Cyclic Ion Mobility Advancements*

Due to the promise of the 3C5NBA shift reagent, it was used with a higher resolution ion mobility spectrometer, the cyclic ion mobility-mass spectrometer that was a prototype at Waters Corporation at the time. Cyclic ion mobility was used to determine empirically how many passes could be used to maximize the IM resolution of these isobaric carbohydrate derivatives. This increase in IM resolution with a combination with MS/MS led to the ability to distinguish all eight disaccharide isomers and all four monosaccharide isomers, which was a great improvement over the Synapt HDMS which did not have cyclic ion mobility capabilities.

Cyclic ion mobility has been under development at Waters Corporation since 2017[47] with publications determining its utility emerging in 2019.[49-51, 56] This includes a study by Ujma *et al.* in which pentasaccharide anomers as well as their open ring conformer were separated by cIM.[49] Additionally, the utility for the technique for protein analysis was investigated through determining the stability of proteins after multiple passes.[51] Crude oil was also studied by cIM to determine its utility at distinguishing the isobars present.[154] Through these studies, it was determined that tandem ion mobility could be an additional feature to add to further investigate the structures of ions by cIM as well as increase the potential resolution of the instrument by allowing sections of the arrival

time distribution to be isolated and subjected to further passes without interference from other isobaric ions in the original solution. Through subjecting the ions to a lower energy version of collision induced dissociation that would not induce fragmentation, the conformation could be altered to determine whether interconversion is possible.

### *6.2.2. Noncovalent Shift Reagents for Carbohydrates*

Alongside studies of 3C5NBA as a covalent shift reagent, L-malic acid and NMDA were determined to improve IM resolution of disaccharides as noncovalent shift reagents. They were compared to previously used shift reagents such as alkali metals,[11] alkaline earth metals,[12] and chloride.[106] Amino acids had previously been investigated as IM shift reagents for monosaccharides[57] and tripeptides were investigated as disaccharide shift reagents;[155] however, amino acids and α-hydroxy have not been previously reported as IM shift reagents for disaccharides. The optimal shift reagents were determined empirically from a pool of ten amino and α-hydroxy shift reagents. L-malic acid and NMDA were found to improve the IM resolution for disaccharide separations over previously reported noncovalent shift reagents. As these are noncovalent interactions, the solutions can be analyzed immediately after mixing, which reduces sample preparation time. One drawback for these shift reagents was that they were not strongly binding. While this did not pose an issue for analysis by low pressure traveling wave IM analysis, it was an issue for atmospheric pressure drift tube IM experiments. Since the drift tube IM method improved the resolution of the separations, these shift reagents established in Chapter 4 were studied by a higher sensitivity IM method for Chapter 5.

### *6.2.3. Frequency Modulated Ion Mobility Progress*

There have been many multiplexing methods developed to improve the sensitivity of atmospheric pressure drift tube ion mobility experiments. For example, Hadamard transform-based multiplexing has been utilized for drift tube IM experiments with a Faraday plate detector[35] and time-of-flight[156] and Orbitrap mass analyzers.[31] Hadamard sequences involve pseudorandom gating sequences, and the sequence can be buffered with extended gate closures to assist with the typical issues that it encounters with artifacts.[31, 35] The other popular multiplexing technique for atmospheric pressure DTIM has been based on the Fourier transform. This was proposed in 1985 by Knorr *et al.*[36] and has been applied with time-of-flight,[37] ion trap,[38] and most recently, Orbitrap mass spectrometry detection.[39] The work presented in Chapter 5 indicates the first application of frequency modulated IM-Orbitrap MS to carbohydrates as well as its first application with a commercially available ion mobility spectrometer coupled to an Orbitrap mass analyzer.

## 6.3. Proposed Future Directions

### *6.3.1. Analysis of Prebiotic Carbohydrate Mixtures*

Since model prebiotic reactions that form monosaccharides such as the formose[82] and glyoxylose[146] reactions are generally not selective and have many different products, increasing the complexity of the initial monomer solution has been pursued and warrants further exploration. The products of different monomers in wet-cold/dry-hot cycling conditions as well as the products of mixtures of monomers will give insight into the mechanisms of these reactions and a more realistic scenario in which glucose was not the only monosaccharide present. cIM along with the previously used NMR and MS/MS techniques could provide an additional means of confirming which isomeric oligosaccharides are present. LC could also be used to support the quantitative NMR results.

### *6.3.2. Combining IM-MS/MS with Other Separation Techniques*

While IM-MS/MS has proven to be a useful technique for the rapid and sensitive analysis of oligosaccharide mixtures, as the complexity of solutions increases, it may be necessary to either add liquid chromatography separations or pre-analytical fractionation or enrichment of carbohydrates. Since carbohydrates generally have poor ionization efficiency,[105] mixtures involving multiple classes of biomolecules will likely require one of these techniques to be employed. cIM has recently been combined with LC in a study of 1-β-*O*-Acyl-glucuronides by Higton *et al.*[157] While cIM-MS/MS could distinguish the twelve carbohydrates studied, LC may be helpful for more complex mixtures involving various oligomer lengths and regio- and stereoisomers. LC would not be feasible to couple with the FTIM-Orbitrap MS method reported in Chapter 5 because the IM experiment sweep times were at least 2 minutes in all cases. For IM to be continuously analyzed after LC, the experiments would need to last at most around 1 second for good LC peak shape. However, pre-analytical methods such as fractionation or carbohydrate enrichment could be used with more complex samples to improve carbohydrate ionization for IM-MS analysis.

Tandem IM in which ions are activated but not fragmented between IM analyses also warrants further exploration. Olivier *et al.* recently reported an $IM^n$ method for mannoside analysis.[158] α1,2- and β1,2- mannooligosaccharide anomers, namely tri- and tetrasaccharides, were able to be separated by $IM^3$ with the Select Series Cyclic IMS from Waters Corp. This could be applied to further study the oligosaccharides formed by model prebiotic reactions. $IM^2$ was previously applied to the 3C5NBA derivatives of disaccharides, and it could also be applied to the 3C5NBA monosaccharide derivatives as well as other oligomers as $[M-H]^-$ ions and with various shift reagents.

### *6.3.3. TENG MS Analysis of Carbohydrate Mixtures*

A major drawback to carbohydrate MS analysis is the low ionization efficiency of this class of biomolecules. Certain covalent and noncovalent ligands can assist with this issue. Another approach is altering the ionization technique. TENG ionization was investigated for its impact on carbohydrate ionization when compared to standard electrospray with a DC power supply (Appendix A). TENG has shown promise for improving carbohydrate sensitivity with a limited sample of carbohydrates. 3C5NBA derivatives and L-malic acid and NMDA adducts could be investigated using TENG ionization to determine if the impact on sensitivity is consistent for modified carbohydrates. Due to the length of FTIM experiments, combining TENG ionization would be more complicated. ESI with a DC power supply is continuous, whereas TENG is pulsed; therefore, the TENG pulses and gate pulses for FTIM could cause interferences. However, TENG ionization could be coupled to cIM-MS in a relatively straightforward manner, due to the millisecond timescale for each experiment.

# APPENDIX A. Mechanisms of Triboelectric Ionization MS of Carbohydrates and Other Analytes: Charge competition effects

## A.1. Abstract

Electrospray ionization (ESI) mass spectrometry of neutral carbohydrates has historically suffered from sensitivity issues due to poor ionization efficiency for this class of biomolecules. Triboelectric nanogenerators (TENG) have recently been applied to mass spectrometry ionization sources as an alternative to ESI. While it has been established that TENG ionization improves the sensitivity of MS over ESI for several classes of biological molecules, there has yet to be a systematic study of the effects of the matrix on ionization efficiencies and charge competition between the two methods. This investigated was undertaken, but due to inconsistencies in the emitters used for electrospray and TENG caused by supply chain issues tied to the COVID-19 pandemic, the results were inconclusive and warrant further research.

## A.2. Introduction

As the most abundant class of biopolymers by mass, carbohydrates serve many functions in biology, including providing structure for cell walls,[1] modifying proteins,[4, 7-8] and serving integral roles in metabolism.[5] Mass spectrometry has been used extensively for carbohydrate analysis including studies on biological oligosaccharides[148, 150] and carbohydrates isolated from glycoproteins.[149] However, neutral carbohydrates often have a low ionization efficiency by ESI due to poor desolvation.[159] Additionally, ESI tends to ionize smaller carbohydrates more efficiently than larger ones, leading to decreased sensitivity for larger oligosaccharides. These issues can be less severe with the addition of a pre-ionization separation method such as LC. While LC improves sensitivity, it leads to much higher analysis times than direct infusion.

TENG ionization is an alternative to ESI that has shown promise in increasing MS sensitivity.[25] TENG involves the use of two electrodes with mechanical motion of another triboelectric layer to generate charge, which can be applied through an electrode in a sample solution to ionize molecules for MS analysis.[25] TENG has shown improvements in ionization efficiency of lipids[26, 160] and anti-malarials[161] and metabolites.[27] There are also other factors that can make TENG an attractive ion source, such as the ability to analyze low volume (sub-nanoliter) samples[27] and differentially oxidize double bonds for lipids.[26, 160] While TENG has been shown to improve ionization efficiency of several classes of compounds, there has yet to be a systematic study to compare charge competition and ionization suppression effects for TENG and ESI.

Ionization suppression has previously been systematically studied for select metabolites using LC-MS with an ESI source by Mallet *et al*.[162] This study included raffinose, a neutral trisaccharide. Additives were chosen based on results of the study by Mallet *et al.*[162] in order to determine the differential effects of ionization suppression with additives between TENG and ESI. Formic acid and ammonium hydroxide were chosen to show the impact of acids and bases on carbohydrate ionization for TENG and ESI, and ammonium formate and ammonium bicarbonate to approximate the effects of buffers on carbohydrate ionization with these two different sources. Formic acid, ammonium formate, and ammonium bicarbonate suppressed the raffinose signal, while ammonium hydroxide enhanced it. Herein, a study was undertaken to systematically analyze the ionization efficiency and ionization suppression for a panel of five carbohydrates: glucose, isomaltose, isomaltotriose, maltotetraose, and maltopentaose.

## A.3. Experimental

### *A.3.1. Reagents and Materials*

Glucose, ammonium formate, ammonium bicarbonate, and ammonium hydroxide (28% solution) were obtained from Sigma Aldrich (St. Louis, MO). Isomaltose was purchased from TCI (Philadelphia, PA). Isomaltotriose and formic acid were obtained from VWR (Radnor, PA). Maltotetraose and maltopentaose were purchased from Carbosynth (San Diego, CA). Stock solutions (1 mM) were created for each of each carbohydrate and salt in 50/50 water/methanol. Formic acid and ammonium hydroxide stock solutions were prepared at 10% concentration in 50/50 water/methanol. For analysis, the carbohydrates were diluted to 10 µM each. Variable concentrations of salts were used from 10-200 µM, and 0.01%-0.5% formic acid or ammonium hydroxide were used.

### *A.3.2. TENG Ionization*

All experiments were performed in negative mode on a Synapt G2 HDMS (Waters Corp., Wilmslow, UK). A large-area sliding freestanding TENG was used to apply electricity to an ESI ion source identical to that described previously except for the emitters used.[27] The TENG sliding electrode was made of Nylon (12 × 12 cm), whereas the two stationary electrodes were made of fluorinated ethylene propylene (FEP, 24 × 12 cm). ESI glass emitter tips (GlassTip, New Objective, i.d. 1.0 mm, o.d. 2.0 mm) were employed in all cases. The ESI emitters were mounted on an *x*, *y*, *z* manual linear stage (Thorlabs, Newton, NJ) to control their position with respect to the mass spectrometer inlet. Unless specified otherwise, the emitter tip was held 8–10 mm away from the inlet. A 0.25 mm diameter platinum wire was inserted into the emitters to provide electric contact with the sample solution. A linear motor (LinMot USA, Inc.) was used to operate the movable TENG slider electrode in all experiments. The TENG pulse settings were determined empirically to maximize the signal obtained while minimizing signal between pulses. A 5 second pulse period was used for TENG with a 1.5 second MS scan. This setup can be seen in Figure A.1.

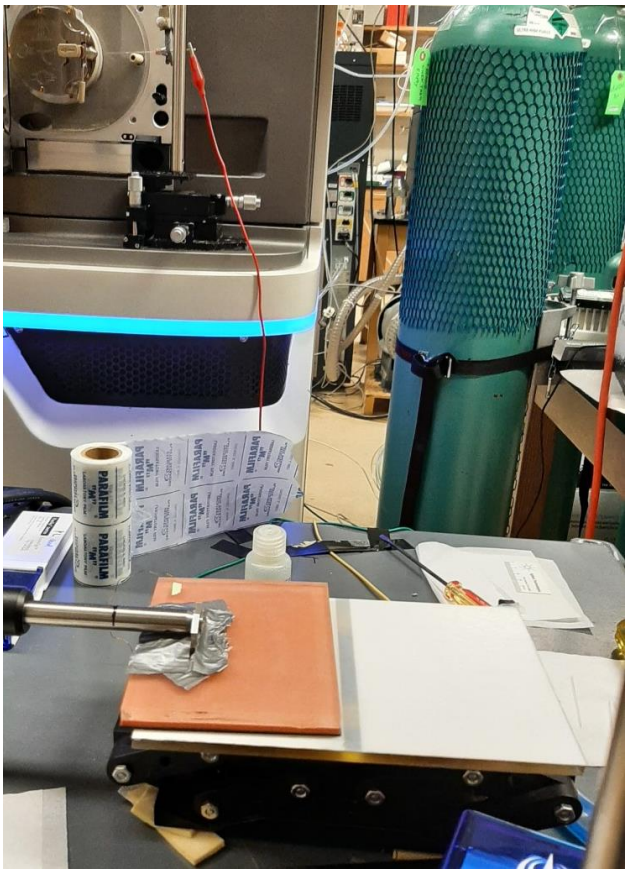


**Figure A.1.** A photograph of the TENG ionization source connected to an electrospray emitter.

## A.4. Results and Discussion

### *A.4.1. Comparison of TENG and ESI*

The structures for the analytes in this study can be seen in Figure A.2. These include glucose as well as four glucose oligomers of various lengths from dimer to pentamer: isomaltose (glucopyranosyl-α-(1→6)glucose), isomaltotriose (diglucopyranosyl- α-(1→6)glucose), maltotetraose (triglucopyranosyl- α-(1→4)glucose), and maltopentaose (tetraglucopyranosyl- α-(1→4)glucose).

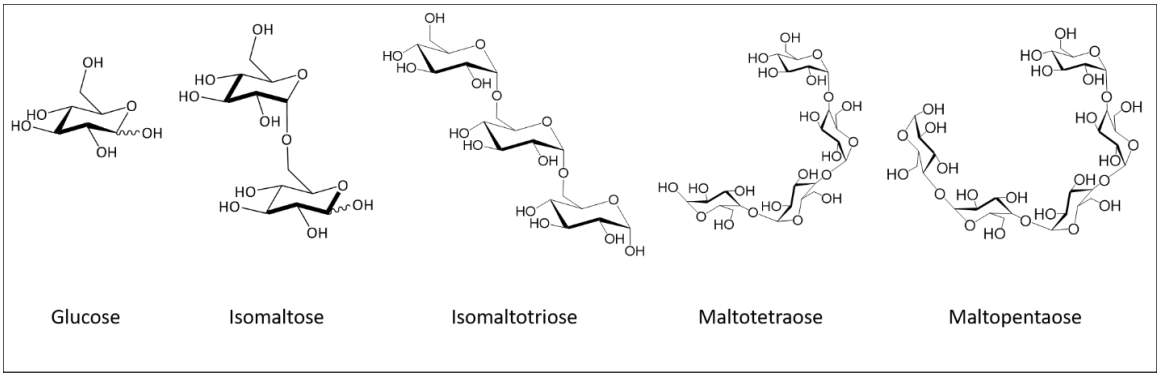


**Figure A.2.** Structures of the carbohydrates utilized in this study.

A mixture of these five carbohydrates was analyzed by both TENG and ESI to determine the abundances for the $[M-H]^-$ ion of each one. When these results were compared, TENG consistently showed higher abundances than ESI across four different experiments, as shown in Table A.1. The effect seemed to be somewhat stronger for the smaller sugars, with glucose showing the highest change at a 2.3 times ratio for the TENG *vs.* ESI abundance. This decreases to 2 times for isomaltose and then to 1.7 times for the remaining three larger oligosaccharides.

**Table A.1.** Comparison of the signal of TENG ionization *vs.* ESI for mixtures of five carbohydrates (10 µM each) over the course of four experiments performed on four different days.

| | Glucose | Isomaltose | Isomaltotriose | Maltotetraose | Maltopentaose |
|---|---|---|---|---|---|
| **TENG/ESI Ratio** | 2.3 ± 0.8 | 2.0 ± 0.7 | 1.7 ± 0.6 | 1.7 ± 0.6 | 1.7 ± 0.5 |

### *A.4.2. Impacts of Additives on TENG and ESI MS*

Since TENG showed promise to increase sensitivity over ESI, it was investigated whether this effect was consistent when additives were present in solution. The additives used include formic acid, ammonium formate, ammonium bicarbonate, and ammonium hydroxide. While Table A.1 shows that TENG consistently had higher signal for all five carbohydrates with no additive

present, there were variable results when additives were included, as shown in Table A.2. Generally, TENG and ESI did not show significantly different abundances for any of the carbohydrates no matter the additive, but ammonium hydroxide seemed to suppress TENG signal more than ESI. The other three additives still showed higher abundances for TENG, but the differences between the methods were decreased.

**Table A.2.** Comparison of the signal of TENG ionization *vs.* ESI for mixtures of five carbohydrates (10 µM each) over the course of four experiments at various concentrations of each additive (10-200 µM salts or 0.01-0.5% formic acid or ammonium hydroxide).

| TENG/ESI Ratio | Glucose | Isomaltose | Isomaltotriose | Maltotetraose | Maltopentaose |
|---|---|---|---|---|---|
| **Ammonium hydroxide** | 0.9 ± 0.4 | 0.9 ± 0.3 | 0.9 ± 0.3 | 0.9 ± 0.4 | 1.0 ± 0.5 |
| **Formic acid** | 1.0 ± 0.4 | 1.2 ± 0.6 | 1.5 ± 1.0 | 1.5 ± 1.1 | 1.6 ± 1.4 |
| **Ammonium formate** | 1.2 ± 0.5 | 1.2 ± 0.3 | 1.2 ± 0.2 | 1.1 ± 0.2 | 1.1 ± 0.2 |
| **Ammonium bicarbonate** | 1.9 ± 1.3 | 1.6 ± 1.0 | 1.6 ± 1.2 | 1.4 ± 1.1 | 1.4 ± 0.9 |

In order to further study the impact of each individual additive, the pattern of the abundance of each carbohydrate at different concentration was assessed. There appeared to be inconsistencies in most of the observed patterns, which have been attributed to the emitters used having too high of a tolerance. For example, in Figure A.3a, there appears to be an increase in abundance from 0 to 0.5% ammonium hydroxide that levels off around 0.1% of the additive. However, 0.01% ammonium hydroxide has lower abundance than 0% and thus deviates from this pattern. Similarly, for the ESI analog of the same additive, Figure A.3e shows an increase of abundance with increasing ammonium hydroxide concentration with the exception of the point at 0.1% ammonium

hydroxide. Ammonium bicarbonate and ammonium formate generally did not seem to impact the abundance for either TENG or ES ionization, as shown in Figure A.3b,c,f, and g. For formic acid, it appeared to increase the TENG abundance for maltopentaose in Figure A.3d with the notable exception of 0.5% formic acid. This may have been a true effect of this rather high concentration of formic acid or an effect of an emitter defect. Figure A.3h for ESI of maltopentaose with formic acid does not show a clear pattern.

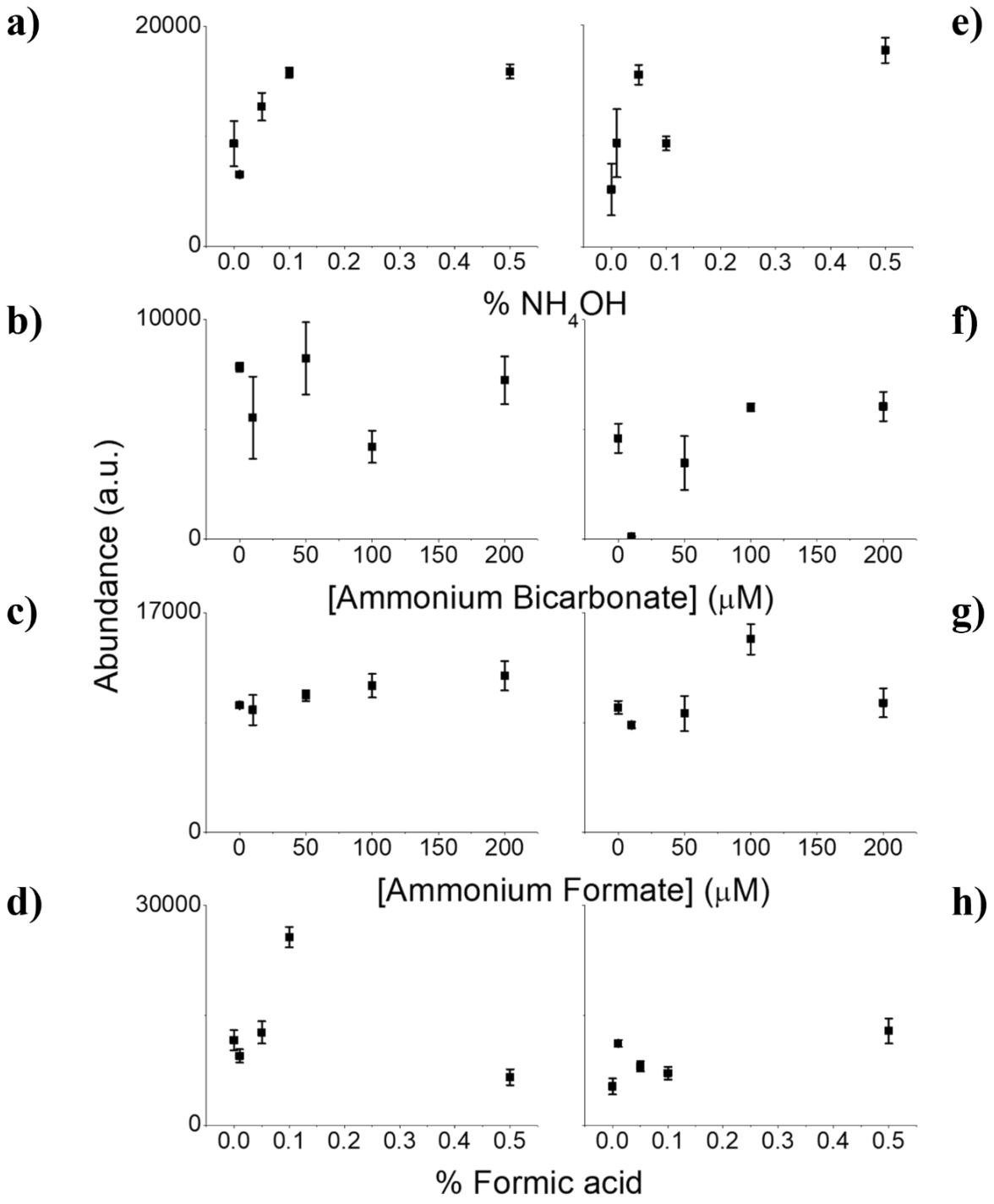


**Figure A.3.** Abundance for maltopentaose as measured by TENG ionization MS (a-d) and ESI (e-h) with the following additives: ammonium hydroxide (a,e), ammonium bicarbonate (b,f), ammonium formate (c,g), and formic acid (d,h).

## A.5. Conclusions

TENG has demonstrated to ionize small carbohydrates more efficiently than ESI in the presence of no additives. However, this effect was not consistent in experiments involving additives. The increase in signal for TENG compared to ESI was reduced with the addition of any of the additives used. Notably, TENG showed lower abundances for each carbohydrate for ammonium hydroxide. Certain additives appeared to demonstrate a pattern with increased additive concentration, but there were inconsistencies caused by issues with the emitters used. Future experiments repeating these with smaller emitters and subsequently using TENG IM-MS with shift reagents such as 3C5NBA, L-malic acid, and NMDA would yield interesting results to determine the utility for TENG for carbohydrate mixture analysis.

## REFERENCES


1. Abbott, D. W.; Ficko-Blean, E.; van Bueren, A. L.; Rogowski, A.; Cartmell, A.; Coutinho, P. M.; Henrissat, B.; Gilbert, H. J.; Boraston, A. B., Analysis of the Structural and Functional Diversity of Plant Cell Wall Specific Family 6 Carbohydrate Binding Modules. *Biochemistry* **2009,** *48* (43), 10395-10404.
2. Fry, S. C., Feruloylated pectins from the primary cell wall: their structure and possible functions. *Planta* **1983,** *157* (2), 111-123.
3. de la Fuente, J. M.; Penadés, S., Understanding carbohydrate-carbohydrate Interactions by means of glyconanotechnology. *Glycoconjugate Journal* **2004,** *21* (3), 149-163.
4. Gabius, H.-J.; Siebert, H.-C.; André, S.; Jiménez-Barbero, J.; Rüdiger, H., Chemical Biology of the Sugar Code. *ChemBioChem* **2004,** *5* (6), 740-764.
5. Krogh, A.; Lindhard, J., The Relative Value of Fat and Carbohydrate as Sources of Muscular Energy: With Appendices on the Correlation between Standard Metabolism and the Respiratory Quotient during Rest and Work. *Biochemical Journal* **1920,** *14* (3-4), 290-363.
6. de Figueiredo, P.; Terra, B.; Anand, J. K.; Hikita, T.; Sadilek, M.; Monks, D. E.; Lenskiy, A.; Hakomori, S.; Nester, E. W., A catalytic carbohydrate contributes to bacterial antibiotic resistance. *Extremophiles* **2007,** *11* (1), 133-43.
7. Dennis, J. W.; Granovsky, M.; Warren, C. E., Protein glycosylation in development and disease. *Bioessays* **1999,** *21* (5), 412-21.
8. Gamblin, D. P.; Scanlan, E. M.; Davis, B. G., Glycoprotein Synthesis: An Update. *Chemical Reviews* **2009,** *109* (1), 131-163.
9. Morrison, K. A.; Bendiak, B. K.; Clowers, B. H., Enhanced Mixture Separations of Metal Adducted Tetrasaccharides Using Frequency Encoded Ion Mobility Separations and Tandem Mass Spectrometry. *J Am Soc Mass Spectrom* **2017,** *28* (4), 664-677.
10. Morrison, K. A.; Clowers, B. H., Differential Fragmentation of Mobility-Selected Glycans via Ultraviolet Photodissociation and Ion Mobility-Mass Spectrometry. *Journal of the American Society for Mass Spectrometry* **2017,** *28* (6), 1236-1241.
11. Huang, Y.; Dodds, E. D., Ion mobility studies of carbohydrates as group i adducts: Isomer specific collisional cross section dependence on metal ion radius. *Analytical Chemistry* **2013,** *85* (20), 9728-9735.
12. Huang, Y.; Dodds, E. D., Discrimination of isomeric carbohydrates as the electron transfer products of group II cation adducts by ion mobility spectrometry and tandem mass spectrometry. *Analytical Chemistry* **2015,** *87* (11), 5664-5668.
13. Koizumi, K.; Okada, Y.; Fukuda, M., High-performance liquid chromatography of mono- and oligo-saccharides on a graphitized carbon column. *Carbohydrate Research* **1991,** *215* (1), 67-80.
14. Zhou, S.; Huang, Y.; Dong, X.; Peng, W.; Veillon, L.; Kitagawa, D. A. S.; Aquino, A. J. A.; Mechref, Y., Isomeric Separation of Permethylated Glycans by Porous Graphitic Carbon (PGC)-LC-MS/MS at High Temperatures. *Analytical Chemistry* **2017,** *89* (12), 6590-6597.
15. Guile, G. R.; Rudd, P. M.; Wing, D. R.; Prime, S. B.; Dwek, R. A., A rapid high-resolution high-performance liquid chromatographic method for separating glycan mixtures and analyzing oligosaccharide profiles. *Anal Biochem* **1996,** *240* (2), 210-26.

16. Azenha, C. S.; Coimbra, M. A.; Moreira, A. S.; Domingues, P.; Domingues, M. R., Differentiation of isomeric beta-(1-4) hexose disaccharides by positive electrospray tandem mass spectrometry. *J Mass Spectrom* **2013,** *48* (5), 548-52.
17. Kuki, Á.; Szabó, K. E.; Nagy, L.; Zsuga, M.; Kéki, S., Rapid identification of disaccharides by tandem mass spectrometry. *Journal of Mass Spectrometry* **2013,** *48* (12), 1276-1280.
18. Min, J. Z.; Nagai, K.; Shi, Q.; Zhou, W.; Todoroki, K.; Inoue, K.; Lee, Y.-I.; Toyo'oka, T., Highly sensitive derivatization reagents possessing positively charged structures for the determination of oligosaccharides in glycoproteins by high-performance liquid chromatography electrospray ionization tandem mass spectrometry. *J. Chromatogr. A* **2016,** *1465*, 79-89.
19. Harvey, D. J., Structural determination of N-linked glycans by matrix-assisted laser desorption/ionization and electrospray ionization mass spectrometry. *Proteomics* **2005,** *5* (7), 1774-1786.
20. Kailemia, M. J.; Ruhaak, L. R.; Lebrilla, C. B.; Amster, I. J., Oligosaccharide analysis by mass spectrometry: a review of recent developments. *Anal. Chem.* **2014,** *86* (1), 196-212.
21. Yang, B.; Solakyildirim, K.; Chang, Y.; Linhardt, R. J., Hyphenated techniques for the analysis of heparin and heparan sulfate. *Anal Bioanal Chem* **2011,** *399* (2), 541-57.
22. Zhou, W.; Håkansson, K., Structural Characterization of Carbohydrates by Fourier Transform Tandem Mass Spectrometry. *Current proteomics* **2011,** *8* (4), 297-308.
23. Thacker, J. B.; Schug, K. A., Use of a Continuous Stirred Tank Reactor for the Determination of Electrospray Response Factors and Its Application to Underivatized Sugars Under Various Solvent Parameters. *Journal of The American Society for Mass Spectrometry* **2019,** *30* (3), 439-447.
24. Suzuki, H.; Yamagaki, T.; Tachibana, K., Optimization of Matrix and Amount of Ammonium Chloride Additive for Effective Ionization of Neutral Oligosaccharides as Chloride Ion Adducts in Negative-Mode MALDI-TOF Mass Spectrometry. *Journal of the Mass Spectrometry Society of Japan* **2005,** *53* (4), 227-229.
25. Li, A.; Zi, Y.; Guo, H.; Wang, Z. L.; Fernández, F. M., Triboelectric nanogenerators for sensitive nano-coulomb molecular mass spectrometry. *Nature Nanotechnology* **2017,** *12*, 481.
26. Bouza, M.; Li, Y.; Wu, C.; Guo, H.; Wang, Z. L.; Fernández, F. M., Large-Area Triboelectric Nanogenerator Mass Spectrometry: Expanded Coverage, Double-Bond Pinpointing, and Supercharging. *Journal of the American Society for Mass Spectrometry* **2020,** *31* (3), 727-734.
27. Li, Y.; Bouza, M.; Wu, C.; Guo, H.; Huang, D.; Doron, G.; Temenoff, J. S.; Stecenko, A. A.; Wang, Z. L.; Fernández, F. M., Sub-nanoliter metabolomics via mass spectrometry to characterize volume-limited samples. *Nature Communications* **2020,** *11* (1), 5625.
28. Cohen, M. J.; Karasek, F. W., Plasma Chromatography™—A New Dimension for Gas Chromatography and Mass Spectrometry. *Journal of Chromatographic Science* **1970,** *8* (6), 330-337.
29. Kirk, A. T.; Allers, M.; Cochems, P.; Langejuergen, J.; Zimmermann, S., A compact high resolution ion mobility spectrometer for fast trace gas analysis. *Analyst* **2013,** *138* (18), 5200-5207.
30. Clowers, B. H.; Siems, W. F.; Hill, H. H.; Massick, S. M., Hadamard transform ion mobility spectrometry. *Analytical Chemistry* **2006,** *78* (1), 44-51.
31. Tummalacherla, M.; Garimella, S. V. B.; Prost, S. A.; Ibrahim, Y. M., Toward artifact-free data in Hadamard transform-based double multiplexing of ion mobility-Orbitrap mass spectrometry. *Analyst* **2017,** *142* (10), 1735-1745.
32. Szumlas, A. W.; Ray, S. J.; Hieftje, G. M., Hadamard transform ion mobility spectrometry. *Analytical Chemistry* **2006,** *78* (13), 4474-4481.

33. Prost, S. A.; Crowell, K. L.; Baker, E. S.; Ibrahim, Y. M.; Clowers, B. H.; Monroe, M. E.; Anderson, G. A.; Smith, R. D.; Payne, S. H., Detecting and Removing Data Artifacts in Hadamard Transform Ion Mobility-Mass Spectrometry Measurements. *Journal of The American Society for Mass Spectrometry* **2014,** *25* (12), 2020-2027.
34. Zare, R. N.; Fernández, F. M.; Kimmel, J. R., Hadamard Transform Time-of-Flight Mass Spectrometry: More Signal, More of the Time. *Angewandte Chemie International Edition* **2003,** *42* (1), 30-35.
35. Kwasnik, M.; Caramore, J.; Fernández, F. M., Digitally-multiplexed nanoelectrospray ionization atmospheric pressure drift tube ion mobility spectrometry. *Analytical Chemistry* **2009,** *81* (4), 1587-1594.
36. Knorr, F. J.; Eatherton, R. L.; Siems, W. F.; Hill, H. H., Fourier Transform Ion Mobility Spectrometry. *Analytical Chemistry* **1985,** *57* (2), 402-406.
37. Clowers, B. H.; Siems, W. F.; Yu, Z.; Davis, A. L., A two-phase approach to fourier transform ion mobility time-of-flight mass spectrometry. *Analyst* **2015,** *140* (20), 6862-6870.
38. Morrison, K. A.; Siems, W. F.; Clowers, B. H., Augmenting Ion Trap Mass Spectrometers Using a Frequency Modulated Drift Tube Ion Mobility Spectrometer. *Analytical Chemistry* **2016,** *88* (6), 3121-3129.
39. Poltash, M. L.; McCabe, J. W.; Shirzadeh, M.; Laganowsky, A.; Clowers, B. H.; Russell, D. H., Fourier Transform-Ion Mobility-Orbitrap Mass Spectrometer: A Next-Generation Instrument for Native Mass Spectrometry. *Anal Chem* **2018,** *90* (17), 10472-10478.
40. Pringle, S. D.; Giles, K.; Wildgoose, J. L.; Williams, J. P.; Slade, S. E.; Thalassinos, K.; Bateman, R. H.; Bowers, M. T.; Scrivens, J. H., An investigation of the mobility separation of some peptide and protein ions using a new hybrid quadrupole/travelling wave IMS/oa-ToF instrument. *International Journal of Mass Spectrometry* **2007,** *261* (1), 1-12.
41. Giles, K.; Pringle, S. D.; Worthington, K. R.; Little, D.; Wildgoose, J. L.; Bateman, R. H., Applications of a travelling wave-based radio-frequency-only stacked ring ion guide. *Rapid Communications in Mass Spectrometry* **2004,** *18* (20), 2401-2414.
42. Ruotolo, B. T.; Benesch, J. L. P.; Sandercock, A. M.; Hyung, S. J.; Robinson, C. V., Ion mobility-mass spectrometry analysis of large protein complexes. *Nature Protocols* **2008,** *3* (7), 1139-1152.
43. Smith, D. P.; Knapman, T. W.; Campuzano, I.; Malham, R. W.; Berryman, J. T.; Radford, S. E.; Ashcroft, A. E., Deciphering Drift Time Measurements from Travelling Wave Ion Mobility Spectrometry-Mass Spectrometry Studies. *European Journal of Mass Spectrometry* **2009,** *15* (2), 113-130.
44. Thalassinos, K.; Grabenauer, M.; Slade, S. E.; Hilton, G. R.; Bowers, M. T.; Scrivens, J. H., Characterization of phosphorylated peptides using traveling wave-based and drift cell ion mobility mass spectrometry. *Analytical Chemistry* **2009,** *81* (1), 248-254.
45. Bush, M. F.; Hall, Z.; Giles, K.; Hoyes, J.; Robinson, C. V.; Ruotolo, B. T., Collision cross sections of proteins and their complexes: A calibration framework and database for gas-phase structural biology. *Analytical Chemistry* **2010,** *82* (22), 9557-9565.
46. Dodds, J. N.; May, J. C.; McLean, J. A., Correlating Resolving Power, Resolution, and Collision Cross Section: Unifying Cross-Platform Assessment of Separation Efficiency in Ion Mobility Spectrometry. *Analytical Chemistry* **2017,** *89* (22), 12176-12184.
47. Kevin Giles, J. U., Jason Wildgoose, Martin R. Green, Keith Richardson, David Langridge, Nick Tomczyk In *Design and performance of a second-generation cyclic ion mobility enabled Q-ToF*, 65th ASMS Conference, Indianapolis, IN, Indianapolis, IN, 2017.

48. Giles, K.; Ujma, J.; Wildgoose, J.; Pringle, S.; Richardson, K.; Langridge, D.; Green, M., A Cyclic Ion Mobility-Mass Spectrometry System. *Anal Chem* **2019**.
49. Ujma, J.; Ropartz, D.; Giles, K.; Richardson, K.; Langridge, D.; Wildgoose, J.; Green, M.; Pringle, S., Cyclic Ion Mobility Mass Spectrometry Distinguishes Anomers and Open-Ring Forms of Pentasaccharides. *Journal of The American Society for Mass Spectrometry* **2019,** *30* (6), 1028-1037.
50. Ropartz, D.; Fanuel, M.; Ujma, J.; Palmer, M.; Giles, K.; Rogniaux, H., Structure Determination of Large Isomeric Oligosaccharides of Natural Origin through Multipass and Multistage Cyclic Traveling-Wave Ion Mobility Mass Spectrometry. *Analytical Chemistry* **2019,** *91* (18), 12030-12037.
51. Eldrid, C.; Ujma, J.; Kalfas, S.; Tomczyk, N.; Giles, K.; Morris, M.; Thalassinos, K., Gas Phase Stability of Protein Ions in a Cyclic Ion Mobility Spectrometry Traveling Wave Device. *Analytical Chemistry* **2019,** *91* (12), 7554-7561.
52. Yang, H.; Shi, L.; Zhuang, X.; Su, R.; Wan, D.; Song, F.; Li, J.; Liu, S., Identification of structurally closely related monosaccharide and disaccharide isomers by PMP labeling in conjunction with IM-MS/MS. *Scientific Reports* **2016,** *6*.
53. Li, L.; McKenna, K. R.; Li, Z.; Yadav, M.; Krishnamurthy, R.; Liotta, C. L.; Fernandez, F. M., Rapid resolution of carbohydrate isomers via multi-site derivatization ion mobility-mass spectrometry. *Analyst* **2018,** *143* (4), 949-955.
54. Williams, J. P.; Grabenauer, M.; Holland, R. J.; Carpenter, C. J.; Wormald, M. R.; Giles, K.; Harvey, D. J.; Bateman, R. H.; Scrivens, J. H.; Bowers, M. T., Characterization of simple isomeric oligosaccharides and the rapid separation of glycan mixtures by ion mobility mass spectrometry. *International Journal of Mass Spectrometry* **2010,** *298* (1), 119-127.
55. Li, H.; Bendiak, B.; Siems, W. F.; Gang, D. R.; Hill, H. H., Ion Mobility Mass Spectrometry Analysis of Isomeric Disaccharide Precursor, Product and Cluster Ions. *Rapid communications in mass spectrometry : RCM* **2013,** *27* (23), 2699-2709.
56. McKenna, K. R.; Li, L.; Baker, A. G.; Ujma, J.; Krishnamurthy, R.; Liotta, C. L.; Fernández, F. M., Carbohydrate isomer resolution via multi-site derivatization cyclic ion mobility-mass spectrometry. *Analyst* **2019,** *144* (24), 7220-7226.
57. Gaye, M. M.; Nagy, G.; Clemmer, D. E.; Pohl, N. L. B., Multidimensional Analysis of 16 Glucose Isomers by Ion Mobility Spectrometry. *Analytical Chemistry* **2016,** *88* (4), 2335-2344.
58. Miller, S. L., A production of amino acids under possible primitive earth conditions. *Science* **1953,** *117* (3046), 528-529.
59. Martins, Z.; Alexander, C. M. O. D.; Orzechowska, G. E.; Fogel, M. L.; Ehrenfreund, P., Indigenous amino acids in primitive CR meteorites. *Meteoritics & Planetary Science* **2007,** *42* (12), 2125-2136.
60. Zhao, M.; Bada, J. L., Extraterrestrial amino acids in Cretaceous/Tertiary boundary sediments at Stevns Klint, Denmark. *Nature* **1989,** *339* (6224), 463-465.
61. Majors, R. E., Historical Developments in HPLC and UHPLC Column

Technology: The Past 25 Years. *LCGC North America* **2015,** *33*, 818-840.
62. Glavin, D. P.; Dworkin, J. P., Enrichment of the amino acid l-isovaline by aqueous alteration on CI and CM meteorite parent bodies. *Proc. Natl. Acad. Sci. U. S. A.* **2009,** *106* (14), 5487-5492.
63. Callahan, M. P.; Burton, A. S.; Elsila, J. E.; Baker, E. M.; Smith, K. E.; Glavin, D. P.; Dworkin, J. P., A search for amino acids and nucleobases in the Martian meteorite Roberts Massif

04262 using liquid chromatography-mass spectrometry. *Meteoritics & Planetary Science* **2013,** *48* (5), 786-795.
64. Johnson, A. P.; Cleaves, H. J.; Dworkin, J. P.; Glavin, D. P.; Lazcano, A.; Bada, J. L., The Miller Volcanic Spark Discharge Experiment. *Science (New York, N.Y.)* **2008,** *322* (5900), 404-404.
65. Forsythe, J. G.; Yu, S.-S.; Mamajanov, I.; Grover, M. A.; Krishnamurthy, R.; Fernández, F. M.; Hud, N. V., Ester-Mediated Amide Bond Formation Driven by Wet–Dry Cycles: A Possible Path to Polypeptides on the Prebiotic Earth. *Angewandte Chemie International Edition* **2015,** *54* (34), 9871-9875.
66. Li, Z.; Li, L.; McKenna, K. R.; Schmidt, M.; Pollet, P.; Gelbaum, L.; Fernández, F. M.; Krishnamurthy, R.; Liotta, C. L., The Oligomerization of Glucose Under Plausible Prebiotic Conditions. *Origins of Life and Evolution of Biospheres* **2019,** *49* (4), 225-240.
67. Varki, A., Cummings, R., Esko, J., Freeze, H., Stanley, P., Bertozzi, C., Hart, G., Etzler, M. , Essentials of Glycobiology. . *Essentials of Glycobiology. Cold Spring Harbor Laboratories Press, New York. ISBN 978-0-87969-770-9.*
68. Biology of plants By Peter H. Raven, R. F. E., Susan E. Eichhorn, Biology of plants. 2005.
69. McMurry, J.; Begley, T., *The Organic Chemistry of Biological Pathways* Roberts and Company Publishers: Englewood, Colorado, 2005; p 512.
70. Schramm, G.; Grötsch, H.; Pollmann, W., Non-Enzymatic Synthesis of Polysaccharides, Nucleosides and Nucleic Acids and the Origin of Self-Reproducing Systems. *Angew. Chem. Int. Ed.* **1962,** *1* (1), 1-7.
71. Stern, R.; Jedrzejas, M. J., Carbohydrate Polymers at the Center of Life's Origins: The Importance of Molecular Processivity. *Chem. Rev.* **2008,** *108* (12), 5061-5085.
72. Schwartz, A. W., Origins of the RNA world. In *The Molecular Origin of Life*, Brack, A., Ed. Cambridge University Press: Cambridge, UK, 1998; pp 237-254.
73. Butlerow, A., Formation synthetique d'une substance sucree. *Compt. Rend. Acad. Sci.* **1861,** *53*, 145 - 147.
74. Cleaves, H. J., The prebiotic geochemistry of formaldehyde. *Precambrian Res.* **2008,** *164* (3-4), 111-118.
75. Eschenmoser, A., Etiology of Potentially Primordial Biomolecular Structures: From Vitamin B12 to the Nucleic Acids and an Inquiry into the Chemistry of Life's Origin: A Retrospective. *Angew. Chem. Int. Ed.* **2011,** *50* (52), 12412-12472.
76. Weber, A. L., Prebiotic sugar synthesis: hexose and hydroxy acid synthesis from glyceraldehyde catalyzed by iron(III) hydroxide oxide. *Journal of Molecular Evolution* **1992,** *35* (1), 1-6.
77. Mizuno, T.; Weiss, A. H., *Adv. Carbohydr. Chem. Biochem.* **1974,** *29*, 173.
78. Reid, C.; Orgel, L. E., Synthesis of sugars in potentially prebiotic conditions. *Nature* **1967,** *216* (5114), 455.
79. Sagi, V. N.; Punna, V.; Hu, F.; Meher, G.; Krishnamurthy, R., Exploratory Experiments on the Chemistry of the "Glyoxylate Scenario": Formation of Ketosugars from Dihydroxyfumarate. *J Am Chem Soc* **2012,** *134* (7), 3577-3589.
80. Kim, H.-J.; Ricardo, A.; Illangkoon, H. I.; Kim, M. J.; Carrigan, M. A.; Frye, F.; Benner, S. A., Synthesis of Carbohydrates in Mineral-Guided Prebiotic Cycles. *J Am Chem Soc* **2011,** *133* (24), 9457-9468.
81. Ross, D. S.; Deamer, D., Dry/Wet Cycling and the Thermodynamics and Kinetics of Prebiotic Polymer Synthesis. *Life* **2016,** *6* (3).

82. Weiss, A. H.; Socha, R. F.; Likholobov, V. A.; Sakharov, M. M., Formose sugars from formaldehyde. *Appl. Catal.* **1981,** *1* (5), 237-246.
83. Brack, A.; Spach, G., Enantiomer Enrichment in Early Peptides. *Origins Life Evol. Biosphere* **1981,** *11* (1-2), 135-142.
84. Mamajanov, I.; MacDonald, P. J.; Ying, J. Y.; Duncanson, D. M.; Dowdy, G. R.; Walker, C. A.; Engelhart, A. E.; Fernandez, F. M.; Grover, M. A.; Hud, N. V.; Schork, F. J., Ester Formation and Hydrolysis during Wet-Dry Cycles: Generation of Far-from-Equilibrium Polymers in a Model Prebiotic Reaction. *Macromolecules* **2014,** *47* (4), 1334-1343.
85. Forsythe, J. G.; Yu, S. S.; Mamajanov, I.; Grover, M. A.; Krishnamurthy, R.; Fernandez, F. M.; Hud, N. V., Ester-Mediated Amide Bond Formation Driven by Wet-Dry Cycles: A Possible Path to Polypeptides on the Prebiotic Earth. *Angew. Chem. Int. Ed.* **2015,** *54* (34), 9871-9875.
86. Stern, R. J., M., Carbohydrate Polymers at the Center of Life's Origins: The Importance of Molecular Processivity. *Chem. Rev.* **2008,** *108*, 5061–5085.
87. Hofmann, J.; Hahm, H. S.; Seeberger, P. H.; Pagel, K., Identification of carbohydrate anomers using ion mobility-mass spectrometry. *Nature* **2015,** *526* (7572), 241-4.
88. Lanucara, F.; Holman, S. W.; Gray, C. J.; Eyers, C. E., The power of ion mobility-mass spectrometry for structural characterization and the study of conformational dynamics. *Nat Chem* **2014,** *6* (4), 281-94.
89. Fenn, L. S.; McLean, J. A., Structural resolution of carbohydrate positional and structural isomers based on gas-phase ion mobility-mass spectrometry. *Phys Chem Chem Phys* **2011,** *13* (6), 2196-205.
90. Abu B. Kanu, M. M. G., Herbert H. Hill, Jr., Predicting Optimal Resolving Power for Ambient Pressure Ion Mobility Spectrometry. *Anal. Chem.* **2008,** *80*, 6610-6619.
91. Mariano, A. V.; Su, W.; Guharay, S. K., Effect of space charge on resolving power and ion loss in ion mobility spectrometry. *Anal Chem* **2009,** *81* (9), 3385-91.
92. Sakakura, M.; Takayama, M., In-source decay and fragmentation characteristics of peptides using 5-aminosalicylic acid as a matrix in matrix-assisted laser desorption/ionization mass spectrometry. *J Am Soc Mass Spectrom* **2010,** *21* (6), 979-88.
93. Watson, J. D.; Crick, F. H. C., Molecular Structure of Nucleic Acids: A Structure for Deoxyribose Nucleic Acid. *Nature* **1953,** *171*, 737.
94. Huang, Y.; Dodds, E. D., Ion mobility studies of carbohydrates as group I adducts: isomer specific collisional cross section dependence on metal ion radius. *Anal Chem* **2013,** *85* (20), 9728-35.
95. Huang, Y.; Dodds, E. D., Discrimination of Isomeric Carbohydrates as the Electron Transfer Products of Group II Cation Adducts by Ion Mobility Spectrometry and Tandem Mass Spectrometry. *Anal Chem* **2015,** *87* (11), 5664-8.
96. Dwivedi, P.; Bendiak, B.; Clowers, B. H.; Hill, H. H., Jr., Rapid resolution of carbohydrate isomers by electrospray ionization ambient pressure ion mobility spectrometry-time-of-flight mass spectrometry (ESI-APIMS-TOFMS). *J Am Soc Mass Spectrom* **2007,** *18* (7), 1163-75.
97. Gabryelski, W.; Froese, K. L., Rapid and sensitive differentiation of anomers, linkage, and position isomers of disaccharides using High-Field Asymmetric Waveform Ion Mobility Spectrometry (FAIMS). *Journal of the American Society for Mass Spectrometry* **2003,** *14* (3), 265-277.

98. Yang, H.; Shi, L.; Zhuang, X.; Su, R.; Wan, D.; Song, F.; Li, J.; Liu, S., Identification of structurally closely related monosaccharide and disaccharide isomers by PMP labeling in conjunction with IM-MS/MS. *Sci Rep* **2016,** *6*, 28079.
99. Fenn, L. S., McLean, J. A., Enhanced carbohydrate structural selectivity in ion mobility-mass spectrometry analyses by boronic acid derivatization. *Chem. Commun.* **2008,** *43*, 5505-5507.
100. Eggleston, G.; Vercellotti, J. R., Degradation of Sucrose, Glucose and Fructose in Concentrated Aqueous Solutions Under Constant pH Conditions at Elevated Temperature. *Journal of Carbohydrate Chemistry* **2000,** *19* (9), 1305-1318.
101. Giles, K.; Wildgoose, J. L.; Pringle, S.; Langridge, D. J.; Nixon, P.; Garside, J.; Carney, P., *Characterising A T-Wave Enabled Multi-pass Cyclic Ion Mobility Separator* **2015**.
102. Mulla, H. R. A., Nicholas J.; Basu, Amit, 3-Methoxycarbonyl-5-nitrophenyl boronic acid: high affinity diol recognition at neutral pH. *Bioorganic & Medicinal Chemistry Letters* **2004,** *14* (1), 25-27.
103. Chiaki Miyamoto, K. S., Satoshi Iwatsuki, Masahiko Inamo, Hideo D. Takagi Koji Ishihara, Kinetic Evidence for High Reactivity of 3-Nitrophenylboronic Acid Compared to Its Conjugate Boronate Ion in Reactions with Ethylene and

Propylene Glycols. *Inorganic Chemistry* **2008,** *47*, 1417-1419.
104. Waldemar Hoffmann, J. H., Kevin Pagel, Energy-Resolved Ion Mobility-Mass Spectrometry-A Concept to Improve the Separation of Isomeric Carbohydrates. *Journal of the American Society for Mass Spectrometry* **2014,** *25*, 471-479.
105. Boutegrabet, L.; Kanawati, B.; Gebefugi, I.; Peyron, D.; Cayot, P.; Gougeon, R. D.; Schmitt-Kopplin, P., Attachment of chloride anion to sugars: mechanistic investigation and discovery of a new dopant for efficient sugar ionization/detection in mass spectrometers. *Chemistry* **2012,** *18* (41), 13059-67.
106. Jiang, Y.; Cole, R. B., Oligosaccharide analysis using anion attachment in negative mode electrospray mass spectrometry. *J Am Soc Mass Spectrom* **2005,** *16* (1), 60-70.
107. Zhu, M.; Bendiak, B.; Clowers, B.; Hill, H. H., Jr., Ion mobility-mass spectrometry analysis of isomeric carbohydrate precursor ions. *Anal Bioanal Chem* **2009,** *394* (7), 1853-67.
108. Breslow, R.; Dong, S. D., Biomimetic Reactions Catalyzed by Cyclodextrins and Their Derivatives. *Chem. Rev.* **1998,** *98* (5), 1997-2012.
109. Riske, F.; Hayes, M.; Lazarus, G. Use of polysaccharides for promotion of enzymatic activity. 2006.
110. Allscher, T.; Klüfers, P.; Mayer, P., Carbohydrate-Metal Complexes : Structural Chemistry of Stable Solution Species. In *Glycoscience – Chemistry and Chemical Biology*, Fraser-Reid, B. O.; Tatsuta, K.; Thiem, J., Eds. Springer-Verlag Berlin Heidelberg: New York, 2008.
111. Hart, J. L.; Harris, Z. M.; Testa, S. M., Analyzing and Predicting the Thermodynamic Effects of the Metabolite Trehalose on Nucleic Acids. *Biopolymers* **2010,** *93* (12), 1085-1092.
112. Seo, Y. J.; Schenauer, M. R.; Leary, J. A., Biologically relevant metal-cation binding induces conformational changes in heparin oligosaccharides as measured by ion mobility mass spectrometry. *Int. J. Mass Spectrom.* **2011,** *303* (2-3), 191-198.
113. Lazcano, A.; Miller, S. L., The Origin and Early Evolution of Life: Prebiotic Chemistry, the Pre-RNA World, and Time. *Cell* **1996,** *85* (6), 793-798.
114. Fox, S. W.; Harada, K., Thermal Copolymerization of Amino Acids to a Product Resembling Protein. *Science* **1958,** *128* (3333), 1214.

115. Oró, J., Mechanism of Synthesis of Adenine from Hydrogen Cyanide under Possible Primitive Earth Conditions. *Nature* **1961,** *191*, 1193-1194.
116. Weber, A. L., Prebiotic sugar synthesis: Hexose and hydroxy acid synthesis from glyceraldehyde catalyzed by iron(III) hydroxide oxide. *J. Mol. Evol.* **1992,** *35* (1), 1-6.
117. Tolstoguzov, V., Thermodynamic considerations on polysaccharide functions. Polysaccharides came first. *Carbohydrate Polymers* **2003,** *54* (3), 371-380.
118. Dell, A.; Morris, H. R.; Easton, R. L.; Panico, M.; Patankar, M.; Oehninger, S.; Koistinen, R.; Koistinen, H.; Seppala, M.; Clark, G. F., Structural analysis of the oligosaccharides derived from glycodelin, a human glycoprotein with potent immunosuppressive and contraceptive activities. *Journal of Biological Chemistry* **1995,** *270* (41), 24116-24126.
119. Mottram, D. S.; Wedzicha, B. L.; Dodson, A. T., Food chemistry: Acrylamide is formed in the Maillard reaction. *Nature* **2002,** *419* (6906), 448-449.
120. Schramm, G.; Grötsch, H.; Pollmann, W., Non-Enzymatic Synthesis of Polysaccharides, Nucleosides and Nucleic Acids and the Origin of Self-Reproducing Systems. *Angewandte Chemie International Edition in English* **1962,** *1* (1), 1-7.
121. Stern, R.; Jedrzejas, M. J., Carbohydrate polymers at the center of life's origins: the importance of molecular processivity. *Chem Rev* **2008,** *108* (12), 5061-85.
122. Xing, X.; Hsieh, Y. S. Y.; Yap, K.; Ang, M. E.; Lahnstein, J.; Tucker, M. R.; Burton, R. A.; Bulone, V., Isolation and structural elucidation by 2D NMR of planteose, a major oligosaccharide in the mucilage of chia (Salvia hispanica L.) seeds. *Carbohydrate Polymers* **2017,** *175* (Supplement C), 231-240.
123. Agrawal, P. K., NMR Spectroscopy in the structural elucidation of oligosaccharides and glycosides. *Phytochemistry* **1992,** *31* (10), 3307-3330.
124. Armstrong, G. S.; Mandelshtam, V. A.; Shaka, A. J.; Bendiak, B., Rapid high-resolution four-dimensional NMR spectroscopy using the filter diagonalization method and its advantages for detailed structural elucidation of oligosaccharides. *Journal of Magnetic Resonance* **2005,** *173* (1), 160-168.
125. Stadlmann, J.; Weber, A.; Pabst, M.; Anderle, H.; Kunert, R.; J. Ehrlich, H.; Peter Schwarz, H.; Altmann, F., A close look at human IgG sialylation and subclass distribution after lectin fractionation. *PROTEOMICS* **2009,** *9* (17), 4143-4153.
126. Robinson, L. N.; Artpradit, C.; Raman, R.; Shriver, Z. H.; Ruchirawat, M.; Sasisekharan, R., Harnessing glycomics technologies: Integrating structure with function for glycan characterization. *ELECTROPHORESIS* **2012,** *33* (5), 797-814.
127. Mantovani, V.; Galeotti, F.; Maccari, F.; Volpi, N., Recent advances in capillary electrophoresis separation of monosaccharides, oligosaccharides, and polysaccharides. *ELECTROPHORESIS* **2018,** *39* (1), 179-189.
128. Siems, W. F.; Wu, C.; Tarver, E. E.; Hill, H. H., Jr.; Larsen, P. R.; McMinn, D. G., Measuring the Resolving Power of Ion Mobility Spectrometers. *Analytical Chemistry* **1994,** *66* (23), 4195-4201.
129. Clemmer, D. E.; Jarrold, M. F., Ion Mobility Measurements and their Applications to Clusters and Biomolecules. *Journal of Mass Spectrometry* **1997,** *32* (6), 577-592.
130. Forsythe, J. G.; Petrov, A. S.; Walker, C. A.; Allen, S. J.; Pellissier, J. S.; Bush, M. F.; Hud, N. V.; Fernandez, F. M., Collision cross section calibrants for negative ion mode traveling wave ion mobility-mass spectrometry. *Analyst* **2015,** *140* (20), 6853-61.
131. Hess, D.; Klufers, P., Phenylboronic acid esters of the common 2-deoxy-aldoses. *Carbohydr Res* **2011,** *346* (13), 1752-9.

132. Meiland, M.; Heinze, T.; Guenther, W.; Liebert, T., Seven-membered ring boronates at trans-diol moieties of carbohydrates. *Tetrahedron Letters* **2009,** *50* (4), 469-472.
133. Koeniger, S. L.; Clemmer, D. E., Resolution and Structural Transitions of Elongated States of Ubiquitin. *Journal of the American Society for Mass Spectrometry* **2007,** *18* (2), 322-331.
134. Allen, S. J.; Giles, K.; Gilbert, T.; Bush, M. F., Ion mobility mass spectrometry of peptide, protein, and protein complex ions using a radio-frequency confining drift cell. *Analyst* **2016,** *141* (3), 884-891.
135. Bush, M. F.; Campuzano, I. D. G.; Robinson, C. V., Ion Mobility Mass Spectrometry of Peptide Ions: Effects of Drift Gas and Calibration Strategies. *Analytical Chemistry* **2012,** *84* (16), 7124-7130.
136. Zheng, X.; Zhang, X.; Schocker, N. S.; Renslow, R. S.; Orton, D. J.; Khamsi, J.; Ashmus, R. A.; Almeida, I. C.; Tang, K.; Costello, C. E.; Smith, R. D.; Michael, K.; Baker, E. S., Enhancing glycan isomer separations with metal ions and positive and negative polarity ion mobility spectrometry-mass spectrometry analyses. *Analytical and Bioanalytical Chemistry* **2017,** *409* (2), 467-476.
137. Pence, H. E.; Williams, A., ChemSpider: An Online Chemical Information Resource. *Journal of Chemical Education* **2010,** *87* (11), 1123-1124.
138. Hanwell, M. D.; Curtis, D. E.; Lonie, D. C.; Vandermeersch, T.; Zurek, E.; Hutchison, G. R., Avogadro: an advanced semantic chemical editor, visualization, and analysis platform. *Journal of cheminformatics* **2012,** *4* (1), 17-17.
139. Valiev, M.; Bylaska, E. J.; Govind, N.; Kowalski, K.; Straatsma, T. P.; Van Dam, H. J. J.; Wang, D.; Nieplocha, J.; Apra, E.; Windus, T. L.; de Jong, W. A., NWChem: A comprehensive and scalable open-source solution for large scale molecular simulations. *Computer Physics Communications* **2010,** *181* (9), 1477-1489.
140. Becke, A. D., Density-functional thermochemistry. III. The role of exact exchange. *The Journal of Chemical Physics* **1993,** *98* (7), 5648-5652.
141. Francl, M. M.; Pietro, W. J.; Hehre, W. J.; Binkley, J. S.; Gordon, M. S.; DeFrees, D. J.; Pople, J. A., Self-consistent molecular orbital methods. XXIII. A polarization-type basis set for second-row elements. *The Journal of Chemical Physics* **1982,** *77* (7), 3654-3665.
142. Keelor, J. D.; Zambrzycki, S.; Li, A.; Clowers, B. H.; Fernández, F. M., Atmospheric Pressure Drift Tube Ion Mobility–Orbitrap Mass Spectrometry: Initial Performance Characterization. *Analytical Chemistry* **2017,** *89* (21), 11301-11309.
143. Li, H.; Bendiak, B.; Siems, W. F.; Gang, D. R.; Hill Jr, H. H., Ion mobility mass spectrometry analysis of isomeric disaccharide precursor, product and cluster ions. *Rapid Communications in Mass Spectrometry* **2013,** *27* (23), 2699-2709.
144. Butlerow, A., Formation synthétique d'une substance sucrée. *CR Acad. Sci* **1861,** *53*, 145-147.
145. Cleaves, H. J., The prebiotic geochemistry of formaldehyde. *Precambrian Research* **2008,** *164* (3), 111-118.
146. Sagi, V. N.; Punna, V.; Hu, F.; Meher, G.; Krishnamurthy, R., Exploratory experiments on the chemistry of the "glyoxylate scenario": formation of ketosugars from dihydroxyfumarate. *Journal of the American Chemical Society* **2012,** *134* (7), 3577-3589.
147. Laine, R. A., Invited Commentary: A calculation of all possible oligosaccharide isomers both branched and linear yields 1.05 × 1012 structures for a reducing hexasaccharide: the Isomer Barrier to development of single-method saccharide sequencing or synthesis systems. *Glycobiology* **1994,** *4* (6), 759-767.

148. Mårtensson, S.; Levery, S. B.; Fang, T. T.; Bendiak, B., Neutral core oligosaccharides of bovine submaxillary mucin. *European Journal of Biochemistry* **1998,** *258* (2), 603-622.
149. Klein, A.; Lamblin, G.; Lhermitte, M.; Roussel, P.; Breg, J.; Van Halbeek, H.; Vliegenthart, J. F. G., Primary structure of neutral oligosaccharides derived from respiratory-mucus glycoproteins of a patient suffering from bronchiectasis, determined by combination of 500-MHz 1H-NMR spectroscopy and quantitative sugar analysis. *European Journal of Biochemistry* **1988,** *171* (3), 631-642.
150. Takasaki, S.; Kobata, A., Asparagine-linked sugar chains of fetuin: occurrence of tetrasialyl triantennary sugar chains containing the Gal.beta.1 .fwdarw. 3GlcNAc sequence. *Biochemistry* **1986,** *25* (19), 5709-5715.
151. McKenna, K. R.; Li, L.; Krishnamurthy, R.; Liotta, C. L.; Fernández, F. M., Organic acid shift reagents for the discrimination of carbohydrate isobars by ion mobility-mass spectrometry. *Analyst* **2020,** *145* (24), 8008-8015.
152. Tadjimukhamedov, F. K.; Puton, J.; Stone, J. A.; Eiceman, G. A., A study of the performance of an ion shutter for drift tubes in atmospheric pressure ion mobility spectrometry: computer models and experimental findings. *Rev. Sci. Instrum.* **2009,** *80* (10), 103103.
153. Maizel, A. C.; Remucal, C. K., The effect of advanced secondary municipal wastewater treatment on the molecular composition of dissolved organic matter. *Water Research* **2017,** *122*, 42-52.
154. Cho, E.; Riches, E.; Palmer, M.; Giles, K.; Ujma, J.; Kim, S., Isolation of Crude Oil Peaks Differing by m/z ∼0.1 via Tandem Mass Spectrometry Using a Cyclic Ion Mobility-Mass Spectrometer. *Analytical Chemistry* **2019,** *91* (22), 14268-14274.
155. Bohrer, B. C.; Clemmer, D. E., Biologically-Inspired Peptide Reagents for Enhancing IMS-MS Analysis of Carbohydrates. *Journal of The American Society for Mass Spectrometry* **2011,** *22* (9), 1602-1609.
156. Liu, W.; Zhang, X.; Siems, W. F.; Hill, H. H.; Yin, D., Rapid profiling and identification of anthocyanins in fruits with Hadamard transform ion mobility mass spectrometry. *Food Chemistry* **2015,** *177*, 225-232.
157. Higton, D.; Palmer, M. E.; Vissers, J. P. C.; Mullin, L. G.; Plumb, R. S.; Wilson, I. D., Use of Cyclic Ion Mobility Spectrometry (cIM)-Mass Spectrometry to Study the Intramolecular Transacylation of Diclofenac Acyl Glucuronide. *Analytical Chemistry* **2021,** *93* (20), 7413-7421.
158. Ollivier, S.; Tarquis, L.; Fanuel, M.; Li, A.; Durand, J.; Laville, E.; Potocki-Veronese, G.; Ropartz, D.; Rogniaux, H., Anomeric Retention of Carbohydrates in Multistage Cyclic Ion Mobility (IMSn): De Novo Structural Elucidation of Enzymatically Produced Mannosides. *Analytical Chemistry* **2021,** *93* (15), 6254-6261.
159. William R. Alley, J.; Novotny, M. V., Structural Glycomic Analyses at High Sensitivity: A Decade of Progress. *Annual Review of Analytical Chemistry* **2013,** *6* (1), 237-265.
160. Bouza, M.; Li, Y.; Wang, A. C.; Wang, Z. L.; Fernández, F. M., Triboelectric Nanogenerator Ion Mobility–Mass Spectrometry for In-Depth Lipid Annotation. *Analytical Chemistry* **2021,** *93* (13), 5468-5475.
161. Bernier, M. C.; Li, A.; Winalski, L.; Zi, Y.; Li, Y.; Caillet, C.; Newton, P.; Wang, Z. L.; Fernández, F. M., Triboelectric nanogenerator (TENG) mass spectrometry of falsified antimalarials. *Rapid Communications in Mass Spectrometry* **2018,** *32* (18), 1585-1590.
162. Mallet, C. R.; Lu, Z.; Mazzeo, J. R., A study of ion suppression effects in electrospray ionization from mobile phase additives and solid-phase extracts. *Rapid Communications in Mass Spectrometry* **2004,** *18* (1), 49-58.